PB 218-781

SALT WATER CONING BENEATH FRESH WATER WELLS

Brij M. Sahni

Colorado State University
Fort Collins, Colorado

April 1972

SALT WATER CONING BENEATH FRESH WATER WELLS

Water Management Technical Report No. 18

by

Brij Mohan Sahni

Published under support of

United States Agency for International Development
Contract No. AID/csd-2162
Water Management Research
in Arid and Sub-Humid Lands of the
Less Developed Countries

Colorado State University
Fort Collins, Colorado
April 1972

AED71-72BMS29

Reports published previously in this series are listed below. Copies can be obtained by contacting Mrs. Mary Fox, Engineering Research Center, Colorado State University, Fort Collins, Colorado 80521. The prices noted are effective as long as supplies last. After the supply of reports is exhausted, xerox copies can be provided at 10 cents per page.

No.	Title	Author	No. of Pages	Cost
1	Bibliography with Annotations on Water Diversion, Conveyance, and Application for Irrigation and Drainage, CER69-70KM3, Sept. '69	K. Mahmood A. G. Mercer E. V. Richardson	165	$3.00
2	Organization of Water Management for Agricultural Production in West Pakistan (a Progress Report) ID70-71-1, May 1970	P. O. Foss J. A. Straayer R. Dildine A. Dwyer R. Schmidt	148	$3.00
3	Dye Dilution Method of Discharge Measurement, CER70-71WSL-EVR47, January 1971	W. S. Liang E. V. Richardson	36	$3.00
4	Water Management in West Pakistan, MISC-T-70-71RFS43 May, 1970	Robert Schmidt	167	$3.00
5	The Economics of Water Use, An Inquiry into the Economic Behavior of Farmers in West Pakistan, MISC-D-70-71DW44 March, 1971	Debebe Worku	176	$3.00
6	Pakistan Government and Administration: A Comprehensive Bibliography, ID70-71GNJ17, March, 1971	Garth N. Jones	114	$3.00
7	The Effect of Data Limitations on the Application of Systems Analysis to Water Resources Planning in Developing Countries, CED70-71LG35, May, 1971	Luis E. Garcia-Martinez	225	$3.00

No.	Title	Author	No. of Pages	Cost
8	The Problem of Under-Irrigation in West Pakistan: Research Studies and Needs, ID 70-71GNJ-RLA19	G . N. Jones R. L. Anderson	53	$3.00
9	Check-Drop-Energy Dissipator Structures in Irrigation Systems, AER 70-71, GVS-VTS-WRW4, May 1971	G. V. Skogerboe V. T. Somorey W. R. Walker	180	$3.00
10	Maximum Water Delivery in Irrigation	J. H. Duke, Jr.	213	$3.00
11	Flow in Sand-Bed Channels	K. Mahmood	292	$3.00
12	Effect of Settlement on Flume Ratings	T. Y. Wu	98	$3.00
13	The Problem of Water Scheduling in West Pakistan: Research Studies and Needs, ID 71-72GNJ8, November 1971	G. N. Jones	39	$3.00
14	Monastery Model of Development: Towards a Strategy of Large Scale Planned Change, ID 71-72GNJ9, November 1971	G. N. Jones	77	$3.00
15	Width Constrictions in Open Channels	J. W. Hugh Barrett	106	$3.00
16	Cutthroat Flume Discharge Relations	Ray S. Bennett	133	$3.00
17	Culverts as Flow Measuring Devices	Va-son Boonkird	104	$3.00

ABSTRACT

SALT WATER CONING BENEATH FRESH WATER WELLS

The purpose of this research is to investigate the phenomenon of salt water coning below a discharge well partially penetrating an aquifer in which fresh water is underlain by saline water. The first portion of this report is concerned with the evaluation of techniques presently available for analyzing the performance of such wells. Both theoretical considerations as well as experimental results have shown that some of the assumptions used in the analytical techniques available are not valid while others are acceptable only under limited conditions.

The study also presents a mathematical model which is developed for evaluating the performance of a skimming well under a wide range of field situations. The practical utility of the results in deciding the optimum discharge from a skimming well is discussed. It is shown that for given aquifer conditions and well geometry the maximum steady-state production of uncontaminated fresh water is obtained at shallower well penetrations and closer well spacings than that predicted by the theory previously available.

Brij Mohan Sahni
Agricultural Engineering Department
Colorado State University
Fort Collins, Colorado 80521

April, 1972

ACKNOWLEDGMENTS

The author wishes to express his sincere appreciation to his major professor, Dr. A. T. Corey, and to other members of his graduate committee, Drs. A. Klute, D. F. Heermann, and D. B. McWhorter, for their guidance and suggestions throughout this study.

Thanks are due to Messrs. H. R. Duke, D. B. Sapik and V. P. Singh for their valuable discussions at various stages of this work. The time and ideas contributed by Dr. S. Melvin and Mr. J. Brookman for the laboratory work is gratefully acknowledged.

The assistance of Mr. Robert Chandler in data collection and computations is highly appreciated. Thanks are due to Mrs. Diane English for typing the rough drafts and the final manuscript of this report.

The author also wishes to express his heartfelt gratefulness to his parents whose blessings have been a constant source of encouragement throughout this study.

Financial support for this study from USAID and GOI is gratefully acknowledged.

TABLE OF CONTENTS

TABLE OF CONTENTS (continued)

LIST OF TABLES

LIST OF TABLES (Continued)

LIST OF FIGURES

LIST OF FIGURES (continued)

LIST OF SYMBOLS

Symbol	Definition	Physical Dimensions
A	Coefficient of flow between grids (i, j) and (i, j-1)	L^2T^{-1}
B	Coefficient of flow between grids (i, j) and (i, j+1)	L^2T^{-1}
B_o	Recharge factor in Wang's formula	none
C	Coefficient of flow between grids (i-1, j) and (i, j)	L^2T^{-1}
$\hat{C}$	Amount of critical coning beneath the well	L
D	Coefficient of flow between grids (i+1, j) and (i, j)	L^2T^{-1}
$\hat{D}$	Critical drawdown at the well	L
$\dot{D}$	$= \rho_f \hat{D} / \Delta\rho\, H_e$, dimensionless critical drawdown	none
E	$= -(A+B+C+D)$	L^2T^{-1}
f	Porosity	none
g	Acceleration due to gravity	LT^{-2}
H	Hydraulic head (neglecting velocity head), and is equal to ϕ. It is also equal to the elevation z of the point in question if the original position of the interface were taken as the datum.	L
H_e	Head value at the radius of influence of the well. This is also equal to the fresh-water thickness prior to pumping.	L

Symbol	Definition	Physical Dimensions
K	Hydraulic conductivity of the medium to the fluid in question	LT^{-1}
k	Intrinsic permeability	L^2
k_s	Pore-shape factor, a numerical constant	none
$\dot{L}$	$= r_e/H_e$, dimensionless radius of influence of the well	none
m	Slope of the line representing interface on a dimensionless potential drop vs. depth plot	none
MAXIT	Maximum number of iterations	none
p	Fluid pressure	$ML^{-1}T^{-2}$
P_b	Bubbling pressure, that value of P_c at which the non-wetting phase first becomes continuous in a desaturation process	$ML^{-1}T^{-2}$
P_c	Capillary pressure $= P_{nw} - P_w$	$ML^{-1}T^{-2}$
P_{nw}	Pressure of the non-wetting fluid	$ML^{-1}T^{-2}$
P_w	Pressure of the wetting fluid	$ML^{-1}T^{-2}$
PW	Depth of penetration of the well below the initial position of the free surface	L
Q	Discharge	L^3T^{-1}
$\dot{Q}$	$= \frac{Q\rho_f}{H_e^2 K\Delta\rho}$, dimensionless critical discharge	none
q	Volume flux	LT^{-1}
r	Radial distance from the axis of the well	L

Symbol	Definition	Physical Dimensions
r_e	Radius of influence of the well	L
r_w	Radius of the well	L
$\dot{r}$	$= r_e/r_w$	none
S	Specific surface	L^{-1}
$\dot{S}$	$= \frac{Q}{H_e^2 K \hat{D}}$, dimensionless critical specific capacity	none
T	Tortuosity	none
w	$= \bar{z}/2H_e$	none
x	$= PW/2H_e$	none
z	Elevation above original interface	L
$\bar{z}$	Depth below the position of the free surface prior to pumping and is equal to $H_e - z$	L
$\dot{\bar{z}}$	$= \bar{z}/H_e$, dimensionless depth	none
α	Degree of well penetration $= PW/H_e$	none
β	$= \pi\alpha/2$	none
γ	Well slimness $= r_w/H_e$	none
ζ	Elevation of a point on the interface	L
ρ_f	Density of fresh water	ML^{-3}
ρ_s	Density of saline water	ML^{-3}
$\Delta\rho$	Density difference of the two fluids	ML^{-3}
ϕ	Force potential on unit weight basis	L

INTRODUCTION

Ground water is needed for irrigation and other purposes in many places where the supply of surface water is inadequate. In many coastal and several inland areas, including some of the world's most important agricultural lands, fresh water in the aquifer is underlain by saline water. The situation is similar in some respects to a typical petroleum reservoir where oil is underlain by water. However, unlike a petroleum reservoir, a distinct interface does not exist between the two fluids. This is because the fluids are miscible and there is only a slight difference in their densities. In fact, fresh water and salt water are separated by a zone of dispersion with density decreasing with elevation. It is not economical to install wells for pumping fresh water from aquifers in which the fresh water zone has only a very small thickness. The concern of this study, therefore, has been those aquifers in which the dispersed layer is only a small fraction of the total thickness of the fresh water zone. In such cases the intermediate "layer" can be considered, for all practical purposes, as a boundary surface and is, therefore, referred to as an "interface" in this study.

The fresh water-salt water interface is not static but moves in response to motion of both fresh and saline water. When it is desired to pump fresh water, the well should be so installed as to

"skim" the fresh water from above the saline water with a minimum of mixing, either within the well or within the aquifer itself.

When a well is pumped, the reduced head towards the well causes an upconing or mounding of the interface under the well. In order to get maximum yield, it would be desirable to place the well deeper into the fresh water zone. However, the bottom of the well screen must be at a minimum height above the interface to avoid contamination with saline water when the coning takes place. The saline water should not be allowed to enter the well for, once it mixes with the fresh water, the well will produce water of poor quality.

Where the saline water occurs at a considerable depth, it may be possible to install deep wells to produce sufficient water of good quality which could be used for irrigation. In places where the saline water is already near the surface, deep wells cannot be installed without producing saline water. Disposing of the saline water so produced is a major problem. Obtaining an equivalent amount of water from relatively shallow wells requires many additional pumping plants and is a comparatively inefficient and uneconomical operation.

In addition to its function as a source of water for irrigation, pumping is often needed to lower water tables. If the water table rises close to the surface, for example, following a prolonged period of irrigation or rain, pumping can lower the water table and thus

prevent water logging and soil salinity. If the saline water is close to the surface, the depth of the water table becomes even more critical. One possible solution in such a condition is the installation of horizontal relief drains below the water table, but the cost of their installation needs to be considered which, for example, in non-cohesive soils may be too high to be practical. As an alternate method, groups of several shallow skimming wells can be installed, each group being operated by a single centrifugal pump.

This research is part of a study to determine the performance of vertical skimming wells as a means of pumping fresh water from a free-surface aquifer with maximum efficiency and minimum disturbance of underlying saline water. The objectives of this research were:

1) To construct a physical model to study the physics of the phenomenon of coning below a fresh water skimming well.

2) To develop a methematical model to predict the maximum safe yield for given aquifer conditions and well geometry, and the corresponding amount of coning of the interface below the well.

3) To study the validity of the available analytic solutions to the coning problem and the assumptions involved therein.

Ideally, it is desirable to have a physical model which would be a replica of the prototype system in every physical sense, but on a smaller scale convenient for laboratory use. However, when it is not practical to design such a model, it becomes necessary to have one which has physical similarity in all important respects to the prototype in question. With this in mind, a laboratory model was designed to gain a better understanding of coning problems and to provide quantitative data which could be utilized for the verification of the mathematical model. Since the boundary conditions were too complicated to allow an exact analytic solution to the problem, the second objective was realized by computer simulation. Finally, the results obtained from this numerical model were compared with the experimental results and also with those obtained by using the methods of earlier investigators, namely, Muskat, Wang, and Bennett, et al..

The numerical model developed in this research is sufficiently general to predict the behavior of prototypes with aquifer conditions and well geometries different from those existing in the physical model. It could be modified to simulate many additional situations.

REVIEW OF LITERATURE

The earliest ideas about water coning were developed by investigators in the petroleum industry. These investigators were concerned with water coning under oil wells. In recent years, several authors have tried to apply those ideas to ground water reservoirs in which fresh water is underlain by saline water. The petroleum literature which is applicable to the present study is reviewed first.

Research on water coning problems in petroleum reservoirs falls into three main categories, that is, theoretical analysis, physical and analog model studies, and numerical model studies. The earliest mathematical models were reported by Muskat and Wyckoff (21) and Muskat (24). They provided the first physical explanation for the problem of water coning beneath an oil well. They realized that the problem was too complex to make an exact theoretical analysis possible. However, they demonstrated that with certain approximations an analytical solution for the flow system (before the water has broken through the well and during the time it lies statically beneath the oil zone), could be obtained.

It was assumed that the potential distribution in the flow region was the same as if the second fluid were absent. Formulas for the latter case were obtained by analyzing the analogous problem of

electrical potential distribution in a large cylindrical disc with partially penetrating electrodes (23). A detailed account of these theoretical developments are given in a text by Muskat (22). These mathematical models were later modified and extended by several authors to incorporate various situations of interest in petroleum reservoirs.

It is fruitful to distinguish two phenomena, namely, 'coning' and bottom-water drive, which are responsible for the formation of the cone beneath an oil well. These are two different mechanisms. Henley, et al. (13) and Stephen (34) have explained the difference. In the so called coning, the underlying aquifer is relatively inactive and the cone is formed beneath the producing well by the pressure gradients associated with the flow of oil into the well. In a bottom-water drive, the driving force for oil production is provided by a vertical upward flow of the underlying water. Thus, while the oil-water interface during 'coning' will be parallel to the adjacent streamlines in the oil zone, during bottom-water drive it will be perpendicular to them. It is the water coning problem and the pro-- duction performance of the bottom-water drive which has been the subject of most of the recent research in petroleum reservoirs.

Rapaport (27) and Geertsma, et al. (12) studied the scaling laws for use in interpretation of experimental work on design and operation of water-oil flow system. Their results formed the basis

of many laboratory studies. Some of the recent physical model studies of coning problems in petroleum reservoirs are those of Caudle (7), Henley, et al. (13), Khan (16), Stephen (34), and Soengkowo (32). A pie-shaped model was generally used for such experimental studies. It was shown (13) that the role of interfacial forces was negligible in the gross fluid movement in a reservoir where the two fluid phases were under very large pressure gradients. Therefore, no effort was made to scale capillary forces in the physical models. Mutually miscible analog fluids with different viscosities were used to represent oil and water.

The analogy between the flow through porous media and electric current through electric conductors has been used to obtain a solution to Laplace's equation with the help of analog models. Several analog studies have been reported in petroleum literature (2, 3, 5, 21, 25). Fluid flow in cylindrical coordinates has been simulated with the help of a network of resistors and analog computers with proper boundary conditions. Capacitors were included in the network if unsteady flow problems were to be simulated.

A rigorous analytic solution describing multidimensional flow systems with fluids of different densities and viscosities is not available at the present time. In such cases approximate numerical methods have been used wherein the complex partial differential equation describing flow was transformed into a set of algebraic

equations which can be handled by available solution techniques. Recently, MacDonald and Coats (19) and Letkeman and Ridings (17) presented numerical models related to some coning problems in petroleum reservoirs.

Control of water coning in oil wells has been one of the subjects of recent research. Several methods have been proposed to prevent or suppress water coning (15, 29, 30, 38). Smith (29) and Smith and Pirson (30) studied (both experimentally and analytically) the effect of fluid injection as a means of partially or completely suppressing the water cone. The effect of several factors on the net water-oil ratio produced was determined. These factors are: the position and length of the completion interval, the point of fluid injection, the viscosity of the injected fluid and the relative benefit of the use of impermeable barriers or cement "pancakes".

Both Hele-Shaw and radial or pie-shaped models were employed for the experimental work. It was observed that a radial system was most difficult to treat either in the laboratory or analytically. The positioning of impermeable barriers or pancakes was relatively quite difficult in a radial model. This could not be done without substantially altering the packing of the sand which often made it difficult to get reproducible results. Studies conducted using the Hele-Shaw model did not have this disadvantage. However, a radial model had the advantage of providing information relative to a three dimensional flow problem. The use of two-dimensional models

provided only qualitative conclusions regarding water coning in a radial system. Some of the important conclusions drawn from the above studies were as follows:

1. The water-oil ratio for a given oil producing rate could be reduced by the injection of fluid. It is important from a practical point of view that the injection fluid could be either oil or water. However, more benefit is derived if the injection fluid is more viscous than the reservoir oil, or if a zone of reduced permeability exists in the vicinity of the point of injection.

2. For maximum efficiency in water cone suppression, the optimum point of fluid injection is the point closest to the bottom of the producing interval.

3. Under test conditions, little benefit is derived through the use of impermeable barriers.

It should be interesting to study, on similar lines, the suppression of a cone beneath a fresh water well in an aquifer which is underlain by saline water.

The published literature contains relatively little on the subject of growth of the cone and the time it takes to reach an incipient breakthrough position. A study of this aspect of water coning could undoubtedly be very useful in scheduling pumping at an appropriate interval while getting maximum efficiency in production and keeping the cone below a desired safe level. Sobocinski and Cornelius (31) established a correlation between dimensionless cone height and

dimensionless time for predicting the behavior of a water cone as it builds from the static water-oil contact to breakthrough conditions. They realized that simplifying assumptions and use of a one cone model with one set of fluids and boundary conditions could not supply enough data for a completely generalized correlation. While their correlation was good at intermediate values of dimensionless cone height, it was not good at the low values and high values. Nevertheless, Sobocinski and Cornelius' work did provide a means to estimate the rate at which the apex of the cone rises toward a well.

To summarize, the main purpose of the studies of water coning in oil wells has been to investigate the effects of coning on the oil-to-water ratio. An ideal situation would be one where water coning can be completely suppressed or controlled and a relatively large production of oil can be obtained without producing water. This, however, does not seem practical under field conditions. Since oil and water are immiscible, petroleum geologists and engineers have not been concerned about the production of water together with oil as long as the ratio of oil-to-water production is such as to insure an economical production of oil. On the other hand, in a fresh water-salt water aquifer, since the two fluids are miscible, it is desirable to prevent the brine from entering the well.

A good account of the existence, nature, shape, slope, and depth of a fresh water-saline water interface can be found in Hubbert's

paper on the theory of ground-water motion (14) and also in later texts by Todd (35), Walton (36), and Polubarinova-Kochina (26). The physics of salt-water coning beneath a fresh-water well is similar to that of brine coning beneath an oil well. Theories for oil wells given by Muskat and some other authors, which have been discussed above, have been applied to fresh water wells also. In recent years, some work has been reported which is directly related to problems associated with a fresh water-salt water interface.

Wang (37) presented an approximate theory of a partially penetrating well designed for pumping fresh water from an aquifer underlain by saline water. The purpose of this study was to relate the well discharge to well spacing, well penetration, well radius, thickness of aquifer and densities of the fluids, and to determine the maximum production of fresh water without entrainment of saline water as a function of well geometry and aquifer conditions. The theoretical analysis employed by Wang used Muskat's (22) treatment of a partially penetrating well combined with the Ghyben-Herzberg approach (18, 35) to make it applicable to 'skimming wells'.

The graphical procedure developed by Muskat (22) to analyze the water coning problem beneath an oil well has been adapted by Bennett, et al. (1) to study the upconing of saline water beneath a fresh water well. Muskat employed the analytic expressions for the potential distribution about a partially penetrating well in a confined aquifer of uniform thickness as well as the results of experiments on

a pressed carbon electric analog. The head distribution in the fresh water zone required in the analysis of Bennett, et al. was obtained from an electric analog model for steady-state axisymmetrical flow to a partially penetrating well. This model was made up of a network of electric resistances, similar to the one employed by Stallman (33) in his electric analog study of three-dimensional flow to wells. It was also equipped with a system of switches by means of which the lower portion of the network of resistors could be adjusted by trial-and-error to obtain a lower boundary which would simulate the fresh water-saline water interface for a given set of conditions.

The underlying principle in the above study was that if the boundary conditions in the electric analog model conform to the boundary conditions in the hydraulic prototype, the hydraulic head distribution could be calculated from the voltage measurements made at the network junctions. Initially, the model was set up to represent uniform thickness of the fresh water zone. From the graphical analysis of the potential distribution so obtained, the highest position of the stable interface was determined, assuming that the head distribution did not change due to coning. The resistors below this location were switched off and the experiment repeated. This was done until the lower boundary of the analog model and the interface position obtained from graphical analysis were in close agreement.

Several authors have studied fresh water-saline water interface problems in a two-dimensional domain. Charmonman (8) made a theoretical analysis of the pattern of fresh water flow in a coastal aquifer. The problem investigated was that of two interfaces, namely, the upper boundary of the flow region between air and fresh water and the lower boundary between the fresh water and salt water. The following simplifying assumptions were made:

1. the aquifer was two-dimensional, isotropic, and homogeneous,
2. fresh water flow was steady,
3. the underlying saline water was stationary, and,
4. the interfaces between air and fresh water and fresh water and saline water were sharp surfaces of separation.

Laplace's equations with the known boundary conditions for steady flow of fresh water in an unconfined aquifer were solved using the complex potential plane.

The exact solutions of simple situations in an unconfined aquifer were compared with the approximate solutions obtained by considering the problem as that of a confined aquifer. The approximate solutions were found to be satisfactory for practical purposes. According to Charmonman, if the ratio of the specific gravities of saline water and fresh water was taken as 1.025, the upper interface

location would be in error by an amount less than 1.3% and the lower interface and the outflow face would be in error by an amount less than 2.6%. Charmonman (9) also studied the effectiveness of an artificial fresh water barrier for preventing salt water from intruding inland and presented a numerical solution to the complex free surface problems (10).

Dagan and Bear (11) employed the method of small perturbation, often used in the theory of surface waves, to determine the shape of the rising interface in connection with the withdrawal of fresh water by a coastal collector operating a short distance above the interface. A coastal collector is an array of shallow wells used for exploitation of fresh ground water in coastal aquifers and controlling sea water intrusion into it. The assumptions underlying their theoretical approach were that the medium was homogeneous, nondeformable, and that the two fluids were incompressible and separated by an abrupt interface.

A velocity potential satisfying Laplace equation was defined in the flow region of each fluid. Because of the non-linear nature of the boundary conditions along the interface, a linearized approximate solution based on the method of small perturbations was developed. It was assumed that the potential in each fluid could be expressed as a sum of power series of small parameter. In their analytical treatment, a first order linearized solution was derived. However,

their method is applicable to second and higher order linearizations as well. This method is applicable to unsteady flow where the interface undergoes a sufficiently small displacement at a certain instant of time relative to some average interface position.

Approximate solutions were obtained for a continuous drain and for a point sink. The validity of these approximate theoretical solutions was examined with the help of sand box experiments, and it was observed that the range of validity of these solutions was for displacements which (at the crest of the upconing surface) reach a value not greater than 1/3 the initial distance between the interface and the sink.

The validity of the analytic studies of the interface upconing beneath collector wells was checked by field experiments by Schmorak and Mercado (28). It was found that the theoretical results were in agreement with field results up to some critical rise of the interface, which seemed to be approximately half the distance between the bottom of the well and the undisturbed interface. Also, the pattern of the dispersion zone was studied with the help of field data and it was concluded that the linear approximation of the dispersion pattern, used in the analytic approach of Dagan and Bear, was acceptable for all practical engineering purposes. Therefore, the abrupt interface referred to in these studies could be considered as the average position of the transition zone between the fresh water and salt water, that is, position of relative salinity of 50%.

Very recently Youngs (40, 41) has presented an exact approach to the theoretical analysis of some interface problems using his method of analysis of horizontal seepage. The method has been applied to calculate the maximum pumping rate of fresh water from wells located in coastal aquifers and to give optimum conditions for installation of such wells. The problem considered by Youngs was one of two-dimensional flow. It was, therefore, possible to arrive at an exact solution by solving Laplace's equation by the method of conformal transformation, a technique which cannot be employed for three dimensional flow problems.

THEORETICAL BACK GROUND

The theory described here is intended to apply to the case of fresh water overlying saline water in an aquifer. The two fluids are miscible and at their contant, they tend to mix by molecular diffusion and macroscopic dispersion. Therefore, they are not separated by an oil-water type of interface, they do not constitute distinct fluid phases, and there is no pressure discontinuity where they are in contact. However, for the sake of simplicity, it is assumed that fresh water and salt water are separated by an abrupt interface and have distinct and uniform densities (Figure 1).

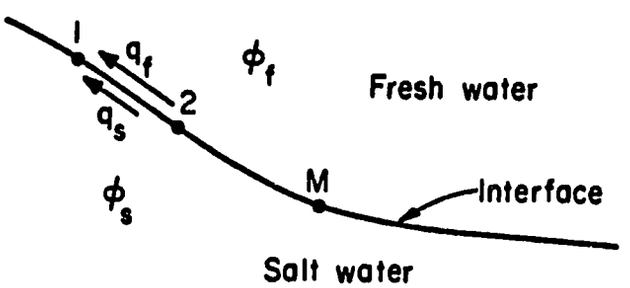

Figure 1. A fresh water-salt water interface.

A potential ϕ can be defined for each of these fluids as follows:

$$\phi_f = \frac{\rho_f}{\rho_f g} + z \qquad (1)$$

and

$$\phi_s = \frac{p_s}{\rho_s g} + z \tag{2}$$

where p is the pressure, ρ is the density, z is the elevation of the point in question measured above some arbitrary datum, and the subscripts f and s denote fresh water and salt water respectively.

Since it is assumed that no pressure discontinuity exists across the interface, at any point M on the interface $p_f = p_s = p_i$, the pressure at the interface. Denoting the elevation of M by ζ and eliminating p_i from (1) and (2) results in

$$\left(\phi_{if} - \zeta\right) \rho_f g = \left(\phi_{is} - \zeta\right) \rho_s g \tag{3}$$

where the suffix i refers to the interface.

Solving for ζ gives

$$\zeta = \frac{\rho_s}{\rho_s - \rho_f} \phi_{is} - \frac{\rho_f}{\rho_s - \rho_f} \phi_{if} \tag{4}$$

or, writing $\Delta\rho = \rho_s - \rho_f$

$$\zeta = \frac{\rho_s}{\Delta\rho} \phi_{is} - \frac{\rho_f}{\Delta\rho} \phi_{if} \tag{5}$$

Equation (5) can be used to describe the interface, if the potentials ϕ_{is} and ϕ_{if} are known at a number of points along the interface. If both potentials vary along the interface, that is, if flow exists in both fluids, the location and shape of the interface depends on the velocity components along the interface in both fluids.

Differentiating equation (5) with respect to S, distance measured along the interface, we get the slope of the interface at the point in question

$$\sin \delta = \frac{\partial \zeta}{\partial S} = \frac{\rho_s}{\Delta \rho} \frac{\partial \phi_{is}}{\partial S} - \frac{\rho_f}{\Delta \rho} \frac{\partial \phi_{if}}{\partial S} \quad . \tag{6}$$

The flux q is given by Darcy's equation which, for isotropic media gives

$$\frac{\partial \phi_{is}}{\partial S} = - \frac{1}{K} q_s \tag{7}$$

and

$$\frac{\partial \phi_{if}}{\partial S} = - \frac{1}{K} q_f \tag{8}$$

where K is the conductivity coefficient having the dimensions of velocity. Therefore, equation (6) can be written as

$$\sin \delta = \frac{\partial \zeta}{\partial S} = \frac{1}{K} \left[- \frac{\rho_s}{\Delta \rho} q_s + \frac{\rho_f}{\Delta \rho} q_f \right] \quad . \tag{9}$$

If the salt water zone is static, the potential is constant throughout this zone. Then using equation (5), the elevation difference between any two points 1 and 2 on the interface is given by

$$\zeta_2 - \zeta_1 = \frac{\rho_f}{\Delta \rho} \left(\phi_{if1} - \phi_{if2} \right) \quad . \tag{10}$$

Also, in this case, equation (9) reduces to

$$\sin \delta = \frac{\rho_f}{\Delta \rho} \frac{q_f}{K} \quad . \tag{11}$$

The case of a partially penetrating well used for pumping fresh water from an aquifer is considered next. The bottom portion of the aquifer is saturated with brine as is illustrated in Figure 2. The

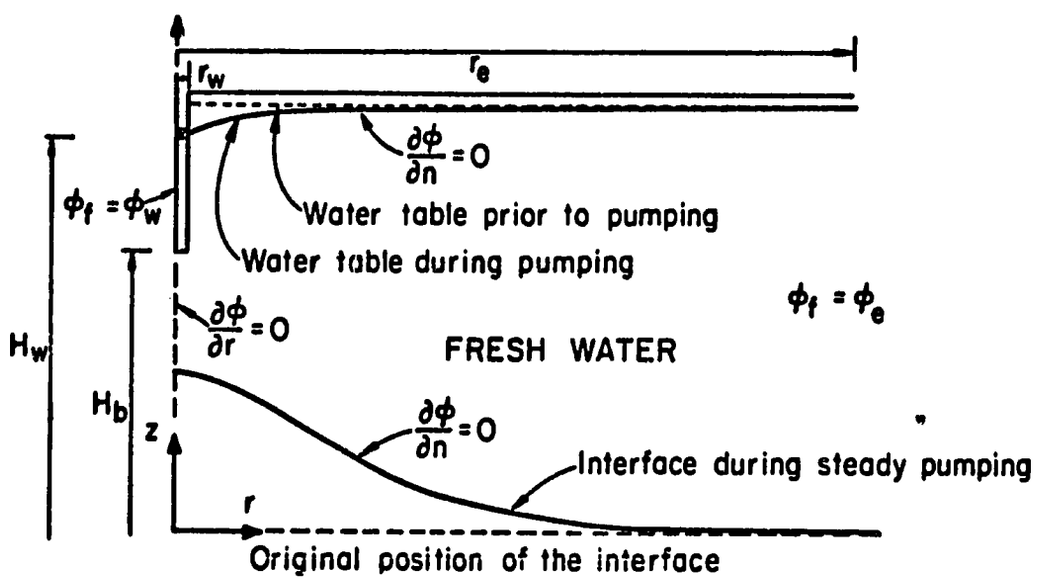

Figure 2. Salt water coning below a fresh water well.

thickness of the fresh water zone prior to pumping is H_e. It is assumed that the well has been pumped until it reaches a steady state. The potential in the well is ϕ_w. At a distance greater than the radius of influence r_e from the well, where the flow becomes strictly radial with no vertical components, the fresh water potential along any vertical line is a constant designated as ϕ_e. When flow takes place, in response to a drop in fresh water potential toward the well, the interface, tends to mound beneath the well to a height such that it will be in hydrodynamic equilibrium. The brine will then be static and the flow will take place

only in the fresh water zone. Also, since there is no flux across the interface, the latter is the lowest stream surface in the fresh water zone and is analogous to an impervious boundary. When the cone becomes stable, the location and shape of the interface at any point is a function only of the fresh water-velocity along the interface at that point. Because of symmetry of the radial flow, the apex of the upconed interface beneath the well is a stagnation point. The apex of a stable cone, therefore, must be flat.

If the original position of the interface prior to pumping (or its position at the effective radius during pumping) is taken as the datum for measuring elevations, and noting that at $\zeta = 0$, $\phi_{if} = \phi_e$, the elevation of the interface at any point can be written from equation (10) as

$$\zeta = \frac{\rho_f}{\Delta\rho} \left(\phi_e - \phi_{if}\right) \quad . \tag{12}$$

The elevation of the apex of the cone is given by

$$\zeta_{(r=0)} = \frac{\rho_f}{\Delta\rho} \left[\phi_e - \left(\phi_{if}\right)_{r=0} \right] \quad . \tag{13}$$

If the second term within the brackets in equation (13) is replaced by the well potential ϕ_w, the result is

$$\zeta_{(r=0)} = \frac{\rho_f}{\Delta\rho} \left[\phi_e - \phi_w \right] \quad . \tag{14}$$

This is the well known Ghyben-Herzberg relation. A comparison of equations (13) and (14) shows that the potential $(\phi_{if})_{r=0}$ vertically below the well is greater than the potential ϕ_w in the well, otherwise there cannot be any flow into the well from below. Therefore, $\zeta_{(r=0)}$ calculated from equation (14) is greater than that calculated from equation (13). Thus, for the same drawdown, the Ghyben-Herzberg relation overestimates the height of the cone. Similarly, equation (14) places the interface at a greater depth than would be predicted by equation (13).

The difference in the two equations (13) and (14) arises due to the fact that the Ghyben-Herzberg relation was arrived at by using the Dupuit-Forchheimer approximation, which implies that the potential does not change along any vertical line in the entire flow region. This assumption is valid only near the effective radius or where the vertical flow components are very small. The latter condition can be achieved, for example, at very small discharge rates, and deeper well penetrations. The theoretical analysis in the present work is based on equation (13).

In order to use equation (13) to determine the location of the interface, one needs to know the densities of the fluids, the fresh water thickness prior to pumping, and the distribution of the fresh water potentials along any vertical surface. In order to obtain the potential distribution analytically, one needs to solve the flow

equation

$$\frac{1}{r}\frac{\partial}{\partial r}\left(r\frac{\partial \phi}{\partial r}\right) + \frac{\partial^2 \phi}{\partial z^2} = 0 \qquad (15)$$

with the boundary conditions

$$\left.\begin{aligned} &\phi = \phi_e && \text{at } r = r_e \\ &\phi = \phi_w && \text{at } r = r_w,\ H_b \leq z \leq H_w \\ &\frac{\partial \phi}{\partial r} = 0 && \text{at } r = 0,\ \zeta_{(r=0)} \leq z \leq H_b \\ &\frac{\partial \phi}{\partial n} = 0 && \text{along the free surface} \\ &\frac{\partial \phi}{\partial n} = 0 && \text{along the interface} \end{aligned}\right\} \qquad (16)$$

where $\partial/\partial n$ denotes the partial derivative with respect to distance along the normal drawn to the surface being considered at the point in question. The last three boundary conditions imply that the fresh water flow has only vertical components along the center line of the well between the bottom of the well and the interface, and there is no flux across the free surface and the interface.

Thus, if it is desired to calculate the position of the interface by an exact analytic method, equation (15) must be solved for the potential distribution using the boundary conditions (16). However, these boundary conditions in turn depend on the position of the interface. Therefore, it does not seem possible to obtain an exact analytic solution to the problem. Apparently, the best way to solve

this problem is to use numerical analysis. This technique will be described in detail in later sections.

It is useful to analyze the two approximate analytic approaches employed by Muskat (22) and Wang (37) to solve the coning problem beneath a partially penetrating well. Muskat's approach is discussed first.

A stable cone with brine in static equilibrium requires that any decrease in the fresh water potential at a point (r, z) along the interface, as a result of pumping, must be compensated for by an equal increase in the differential hydrostatic head. This condition can be expressed mathematically by the equation

$$\phi(r,z) = \phi_e - \frac{\Delta\rho}{\rho_f} z \quad . \tag{17}$$

Subtracting ϕ_w from each side of equation (17) gives

$$\phi(r,z) - \phi_w = (\phi_e - \phi_w) - \frac{\Delta\rho}{\rho_f} z \quad . \tag{18}$$

Dividing through by $(\phi_e - \phi_w)$ yields

$$\frac{\phi(r,z) - \phi_w}{\phi_e - \phi_w} = 1 - \frac{\Delta\rho}{\rho_f(\Delta\phi)_e} z \tag{19}$$

or,

$$\frac{\Delta\phi(r,z)}{(\Delta\phi)_e} = 1 - \left[\frac{\Delta\rho H_e}{\rho_f(\Delta\phi)_e}\right]\frac{z}{H_e} \tag{20}$$

where, $$\Delta\phi(r,z) = \phi(r,z) - \phi_w \tag{21}$$

and $$(\Delta\phi)_e = \phi_e - \phi_w \qquad (22)$$

Equation (20) is the dimensionless form of equation (17).

Every point on the interface must satisfy equation (20). The parameters ϕ_e, ϕ_w, H_e, $\Delta\rho$, ρ_f are known in particular situations. Therefore, if the fresh water potential $\phi(r, z)$ can be determined, the elevation of the interface at a distance r from the well axis can be calculated by solving equation (20) for z. Equation (20) can also be solved graphically as suggested by Muskat. The underlying principle of Muskat's approach is as follows: When the potential distribution at a particular value of r is known as a function of z, both sides of equation (20) can be calculated for various values of z. If these values of the expressions on both sides of this equation are plotted on the same graph against z or z/H_e, the points of intersection of the two curves give the desired solutions. Obviously, the right hand side of the equation plots as a straight line with a slope equal to $\{\Delta\rho H_e/\rho_f(\Delta\phi)_e\}$. This is the graph of equation (20) and represents the interface. Using the same approach for different values of r, a composite picture of the interface can be obtained.

Since there was no method available to obtain the exact potential distribution required in the above analysis, Muskat found it necessary to neglect the effect of the cone on this distribution. This is equivalent to assuming that the potential distribution in the above case is the same as if the lower boundary of the aquifer was an

impermeable bed instead of an interface. With this assumption, he computed the potential distribution for the water coning case from his formula for a well partially penetrating a confined aquifer saturated with only one fluid. Muskat accepted the solution obtained because it was not possible to obtain a new potential distribution considering the lower boundary to be at the calculated location.

Another important point to be considered is the phenomenon of instability of the cone. As the well-discharge is increased, the drawdown is increased and therefore, a greater cone height is expected. The question arises as to whether this drawdown-cone height relationship holds for all values of drawdown; that is, will the condition of static equilibrium of the brine always exist irrespective of the potential distribution? Muskat predicted that the cone should in fact become unstable long before it reached the bottom of the well.

Considering the potential at the interface ϕ_{if} as a function of both the well potential (for given ϕ_e) and the elevation of the interface ζ, the condition for static equilibrium of the brine cone, i.e., equation (12), can be rewritten as

$$\zeta = \frac{\rho_f}{\Delta\rho} \left[\phi_e - \phi_{if} \left(\phi_w, \zeta \right) \right] \quad . \qquad (23)$$

If the drawdown is increased by lowering the well potential by an amount $\Delta\phi_w$, the corresponding increase in the elevation of the

interface at the point in question is given by

$$\Delta\zeta = -\frac{\rho_f}{\Delta\rho}\left[\left(\frac{\partial\phi_{if}}{\partial\phi_w}\right)_\zeta \Delta\phi_w + \left(\frac{\partial\phi_{if}}{\partial\zeta}\right)_{\phi_w} \Delta\zeta\right] \quad . \tag{24}$$

In equation (24), the first term in the brackets gives the change in potential $\Delta\phi_{if}$ due to change in the well potential and the second term gives the contribution to $\Delta\phi_{if}$ due to change in position of the interface.

Solving (24) for $\Delta\zeta$ gives

$$\Delta\zeta\left[1 + \frac{\rho_f}{\Delta\rho}\left(\frac{\partial\phi_{if}}{\partial\zeta}\right)_{\phi_w}\right] = -\frac{\rho_f}{\Delta\rho}\left(\frac{\partial\phi_{if}}{\partial\phi_w}\right)_\zeta \Delta\phi_w$$

or,

$$\Delta\zeta = \frac{-\frac{\rho_f}{\Delta\rho}\left(\frac{\partial\phi_{if}}{\partial\phi_w}\right)_\zeta \Delta\phi_w}{1 + \frac{\rho_f}{\Delta\rho}\left(\frac{\partial\phi_{if}}{\partial\zeta}\right)_{\phi_w}} \tag{25}$$

For a given value of ϕ_e, a decrease in ϕ_w leads to a decrease in ϕ_{if}. Therefore, $(\partial\phi_{if}/\partial\phi_w)_\zeta$ is a positive quantity and $\Delta\phi_w$ is negative so that the numerator on the right hand side of equation (25) is positive. Since a rise in the interface causes more convergence and hence decreases ϕ_{if}, $(\partial\phi_{if}/\partial\zeta)_{\phi_w}$ is a negative quantity. As the drawdown in the well is continuously increased, the absolute value of this term increases until it is numerically equal to one. In that case, the denominator is zero and $\Delta\zeta$ is undefined. Physically this means that the brine begins to flow and the well starts producing brine. A stable cone does not exist when this condition is present.

The phenomenon of instability predicted by Muskat can also be explained as follows: since as pointed out before, there is no pressure discontinuity across the fresh water-saline water interface,

$$\frac{\partial p_f}{\partial S} = \frac{\partial p_s}{\partial S} \tag{26}$$

along the interface.

Each of these terms can be considered as a combination of two terms, namely, one due to gravity alone and the other due to flux q along the interface in the respective fluids. Equation (26), therefore, can be written as

$$\left(\frac{\partial p_f}{\partial S}\right)_G + \left(\frac{\partial p_f}{\partial S}\right)_{q_f} = \left(\frac{\partial p_s}{\partial S}\right)_G + \left(\frac{\partial p_s}{\partial S}\right)_{q_s} \tag{27}$$

where the suffix G denotes the contribution due to gravity alone and the suffixes q_f and q_s denote contributions due to the flux along the interface in the fresh water and saline water respectively.

Rewriting equation (27) results in

$$\left(\frac{\partial p_f}{\partial S}\right)_{q_f} - \left(\frac{\partial p_s}{\partial S}\right)_{q_s} = \left(\frac{\partial p_s}{\partial S}\right)_G - \left(\frac{\partial p_f}{\partial S}\right)_G \quad . \tag{28}$$

The right hand side of this equation is equal to $\Delta\rho g \sin\delta$, the differential hydrostatic pressure gradients along the interface. Here, g is the acceleration due to gravity and δ, as before, is the angle that the interface makes with the horizontal at the point in question.

Since the angle δ can vary only from 0 to $\pi/2$,

$$\left(\frac{\partial p_f}{\partial S}\right)_{q_f} - \left(\frac{\partial p_s}{\partial S}\right)_{q_s} \geq \Delta\rho g \quad . \qquad (29)$$

From equation (29) it is clear that for static equilibrium of the cone, $(\partial p_s/\partial S)_{q_s}$ must be zero and $(\partial p_f/\partial S)_{q_f}$ cannot exceed the value $\Delta\rho g$. However, when the pumping rate is such that $(\partial p_f/\partial S)_{q_f}$ exceeds this value, $(\partial p_s/\partial S)_{q_s}$ must have a value greater than zero so that equation (29) still holds. In other words, the brine is no longer static. Hence, for a stable equilibrium of the cone, the upward pressure-gradient force due to flow in fresh water must be less than or equal to the quantity $\Delta\rho g$.

Carrying the above explanation further, it is noted that in the situation where $\sin\delta = 1$, the apex of the cone can no longer remain flat which is a requirement if the cone were to be stable with brine in static equilibrium. Furthermore, the value of $\sin\delta$ is about 0.71 when $\delta = 45^{\circ}$. Therefore, when the slope of the interface becomes 45°, a relatively small increment in $(\partial p_f/\partial S)_{q_f}$ is sufficient to bring the cone to the critical condition. In other words, the cone tends to become vertical rather abruptly. Also, since the maximum velocity of fresh water flow along the interface (that is the limiting stream line) is at its point of inflexion, the abrupt rise in the cone should take place at that point.

Alternately, considering the fluxes q_f and q_s along the interface instead of the pressure gradients, the conditions that lead to instability can also be understood as follows. As explained before, if no flow occurs in the underlying saline water, that is, if the cone is in static equilibrium, the equation (9) describing the interface reduces to equation (11). As the production rate is increased, q_f increases and the cone becomes steeper. The maximum value that q_f can theoretically have with no flow in the brine is equal to $\Delta\rho K/\rho_f$ when $\sin\delta = 1$. Should q_f exceed this value, since $\sin\delta$ cannot exceed unity, equation (9) requires that q_s be greater than zero. Physically, this implies that for given aquifer conditions and well geometry, there exists a production rate above which the cone cannot remain in stable equilibrium.

In order to determine the maximum fresh water yield without producing brine for given aquifer properties and the well geometry, it is necessary to know the critical drawdown and the position of the highest stable cone.

Another analytic solution is given by Wang. This approach starts with the assumption that the maximum safe yield, that is, the critical discharge, is for a drawdown corresponding to which the apex of the brine-cone just reaches the bottom of the well. The critical drawdown was obtained by using the Ghyben-Herzberg relation corresponding to a cone height equal to the height of the well-bottom above the original position of the interface. The discharge

corresponding to this critical drawdown was computed by using Kozeny's formula (a simpler version of Muskat's formula) for discharge for a partially penetrating aquifer in a confined aquifer of uniform thickness and saturated with one fluid. This formula does not deal with the problem of an interface.

Thus Wang's approach differs from Muskat's in three respects:

1. Muskat's original work was related to water coning beneath an oil well. Wang was interested in salt water coning beneath a fresh water well in an unconfined aquifer but she used the discharge formula which was derived for the case of a confined aquifer.
2. Instead of using the potential distribution for the case of a partially penetrating well, the potential was assumed to be constant along any vertical line. With this assumption equation (13) becomes the Ghyben-Herzberg relation. Wang's method is thus essentially the Ghyben-Herzberg approach.
3. Because of the fact that Wang neglected vertical components of flow, her analysis does not predict the phenomenon of instability of the cone. Perhaps that is why she considered the highest cone to be at the bottom of the well.

PHYSICAL MODEL AND EXPERIMENTAL PROCEDURE

Scaling of the Model

Ideally a model should be constructed so that the flow phenomena in the model are identical in terms of scaled variables to the corresponding phenomena in the prototype. When it is not possible to construct a model which, in every sense, is similar to the prototype, it is sufficient to build a model which is similar to the prototype with regard to the most important variables. When the scaled forms of all the important variables and dimensions which describe the geometry and control the conditions of flow have identical values in the model and the prototype, the flow phenomena observed in the model can be applied to evaluate the performance of the prototype.

Simulation of a given set of field conditions was not attempted in the physical model used in this study. The purpose of using this physical model was (1) to understand the physics of coning problems, (2) to check the validity of the existing theoretical models, and (3) to check the validity of the numerical model which was developed as part of this research. It was, therefore, not necessary to simulate an actual field situation in the model. It was sufficient to apply the existing theories to a few hypothetical prototypes and compare the results with those obtained by studying identical situations experimentally with the help of a physical model.

All pertinent variables were taken into consideration while designing the model and care was taken not to include any factors in the model which might make the phenomenon different from that in the field. For example, since the effect of capillary forces and the thickness of the dispersion zone were considered to be negligible in the field situation, an attempt was made to insure that this was the case for the model also. Thus, although simulation of particular field conditions was not attempted in the model, the model was realistic in the sense that it could represent some field situations.

The scaling factors for designing the model were selected from Wang's equation for maximum fresh-water discharge from a skimming well. Although this equation is based on questionable assumptions, it does give an insight into some of the important variables that need to be scaled. Wang's equation, in the notation used here, is:

$$Q_{max} = \left[\frac{2\pi H_e^2 K}{\ell n(r_e/r_w) - B_o}\right]\left(\frac{\rho_s - \rho_f}{\rho_f}\right)\alpha(1-\alpha)\cdot\left[1 + 7\left(\frac{r_w}{2\alpha H_e}\right)^{\frac{1}{2}}\cos\frac{\pi\alpha}{2}\right] \qquad (30)$$

where

Q_{max} is the maximum discharge without entrainment of salt,

$\alpha = PW/H_e$,

B_o is a numerical constant and is equal to 0 for lateral recharge and $\frac{1}{2}$ for vertical recharge.

Introducing the dimensionless variable $\gamma = r_w/H_e$, called "well-slimness", and writing $\beta = \pi\alpha/2$ equation (30) can be written as

$$W_{\beta,\gamma} \equiv \beta\left(\frac{\pi}{2}-\beta\right)\left[1 + 7\left(\frac{\pi\gamma}{4\beta}\right)^{\frac{1}{2}}\cos\beta\right] = \frac{\pi[\ell n(r_e/r_w)-\bar{B}_o]Q_{max}}{8KH_e^2(\rho_s - \rho_f)/\rho_f} \quad . \quad (31)$$

Here, $W_{\beta,\gamma}$ is a dimensionless variable called "well number" by Wang and is a function of

(1) degree of well-penetration (β or α), and

(2) well-slimness γ.

In a single-well leboratory model built with some suitable fixed length and with constant head maintained at its exterior boundary, the effective drainage radius r_e is equal to the radius of the exterior boundary of the model. In the case of multi-well reservoirs, the external boundary of the model reprsents the effective drainage radius of the well being studied. If a square array of producing wells of equal radius and degree of penetration is simulated in the model, the well spacing L can be related to a dimensionless parameter $\dot{r} = r_e/r_w$ as follows: The drainage area A of each well with effective radius r_e is given by

$$A = \pi r_e^2 = L^2$$

so that

$$r_e = L/\sqrt{\pi}$$

and

$$\dot{r} = \frac{r_e}{r_w} = \frac{L}{\sqrt{\pi}\, r_w} \tag{32}$$

In the pie-shaped model used in this study, the radius of the well and the radius of the outer boundary (where a constant head was maintained) were fixed. This model is considered adequate to study multi-well reservoirs in which the wells have a scaled effective drainage radius $\dot{r}$ at lease equal to the $\dot{r}$ value in the model.

According to equation (31) the dimensionless discharge in a hypothetical prototype computed from Wang's theory and that determined experimentally in a model simulating the same prototype could be equal only if the following parameters have the same value in both model and prototype:

(1) recharge factor B_o ,

(2) well penetration α ,

(3) well slimness γ ,

(4) well-spacing $\dot{r}$.

Since it was not intended to study the transient case, that is, the rate of growth of the brine cone, the time variable was not scaled.

Choice of Porous Medium

Since capillary forces in the field situation are considered to have negligible effect, an attempt was made to insure that this was

the case for the model also. It is difficult to satisfy the requirement for negligible capillary phenomena in designing a laboratory model of practical size. It was necessary to select a material to simulate the aquifer such that the capillary fringe in the model would be only a small fraction of the total thickness of the fresh-water zone. After running several tests with different kinds of materials, it was decided that the simulating material should have an average grain size of at least 2 mm. Since the present study relates to homogeneous and isotropic aquifers, it was decided to use spherical glass beads[1] about 2.5 mm size.

The glass beads used as the aquifer material in the model, in contrast to soils and sands, could easily be packed to practically the same density in each run. Therefore, it was possible to obtain reproducible results. Another reason for the selection of glass beads as the aquifer material in the model was that their smooth surfaces made it easy to wash them after each experiment. Thus, the same glass beads could be used in all the experiments.

Choice of Fluids

The two fluids in the prototype are fresh water and saline water, which are miscible. As explained before, in actual field conditions a zone of dispersion exists at the contact of the two fluids.

[1] The glass beads used in this study were Industrial Glass Beads Type V-110 (product #12330) manufactured by Potters Bros., Inc., 600 Industrial Road, Carlstadt, New Jersey 07072.

This zone, however, may often be a small fraction of the total thickness of the aquifer and therefore, as a simplification in analysis, could be considered as an abrupt interface. When tap water and water with some salt dissolved in it were used in a test model, it was observed that the dispersion zone was a disproportionately large fraction of the total thickness of fresh-water aquifer. Also, because of complete miscibility of the two fluids, this zone of separation was not well defined.

It was also necessary that the amount of mounding of the brine, in response to the production of the well, be a realistic fraction of the total height of the model. A very coarse material was used for the aquifer in the model. Therefore, if fresh water and saline water had been used, the drawdown in the well would have been very small to keep the mound within realistic limits. However, it was not possible to measure a very small drawdown with the desired accuracy. Further, from equation (12) it is observed that the cone height can be reduced by using two fluids with a larger density contrast.

The above reasons, therefore, led to the choice of two immiscible fluids having a density difference much greater than that for fresh water and saline water. Fresh water was simulated by Soltrol "C"[2] and saline water by tap water containing a dye called

---

[2]Soltrol "C" is a special core test fluid manufactured by the Special Products Division of Phillips Petroleum Co., Bartlesville, Okla. Some of its physical properties are given in Appendix E.

Pontacyl[3]. This dye is water soluble and is insoluble in soltrol. A very small amount of this dye gave a brilliant pink color to water which made visual observation of the interface at various stages of coning quite easy. With this choice of simulating fluids and with careful packing of glass beads in the model it was possible to obtain a well-defined interface between the two fluids.

Equipment and Experimental Set-Up

Ideally, in order to minimize the wall effects on flow, it would be desirable to construct a very large cylindrical model. However, a large model is uneconomical to build, impractical from the point of view of simulating all boundary conditions, and difficult to operate. Since the present work deals with axisymmetrical flow toward a well in a homogeneous and isotropic medium, it was sufficient to construct only a sector of a cylindrical model. The model used in this study has radial walls forming an angle of 15° which represents 1/24 of a complete cylinder. The radial length of the sector was four feet. Toward the outflow end of the model a brass screen of 50 mesh size was placed at a distance of 0.96 inch from the center line of the cylinder where the gap between the two radial walls of the sector was 1/4 inch. This screen represented the screen of a well of

[3]Pontacyl is a product of E. I. duPont de Nemours Co., Wilmington, Del. It was been used as dye in some sediment transport studies. Its chemical formula is $C_{27}H_{29}N_2O_4S_2Na$.

radius 2.38 cm with its axis along the center line of the cylinder. Figure 3 shows the discharge end of the model and figures 4(a) and 4(b) give details of the recharge end. A sketch of the assembly used in the experimental study is shown in figure 5.

The model was made of plexiglass, so that the position of the interface and free surface could be clearly seen. At the inflow end the model was 12.72 inches wide. The total height of the model was two feet. The portion of the model containing the beads was separated at its inflow end from a reservoir by a wall which was perforated uniformly by sixty-three 1/4 inch holes with 2-inch separations. The purpose of this reservoir was to maintain a constant head at the inflow boundary of the model. The liquid level in the reservoir was maintained constant by an overflow tap in the outer wall of the reservoir at a depth of three inches from the top. Perforations at the inner wall insured a uniform distribution of liquid against the outer end of the sector. These holes were covered with a screen to prevent glass beads from falling into the reservoir.

Preliminary tests showed that, unless special precautions were taken in filling the model with glass beads and the simulating fluids, air bubbles were trapped in the pores. This destroys the homogeneity of the pores and causes local discontinuities in the flow channels. It was important to insure that the glass beads in the oil zone were wet with Soltrol only and those in the water zone with

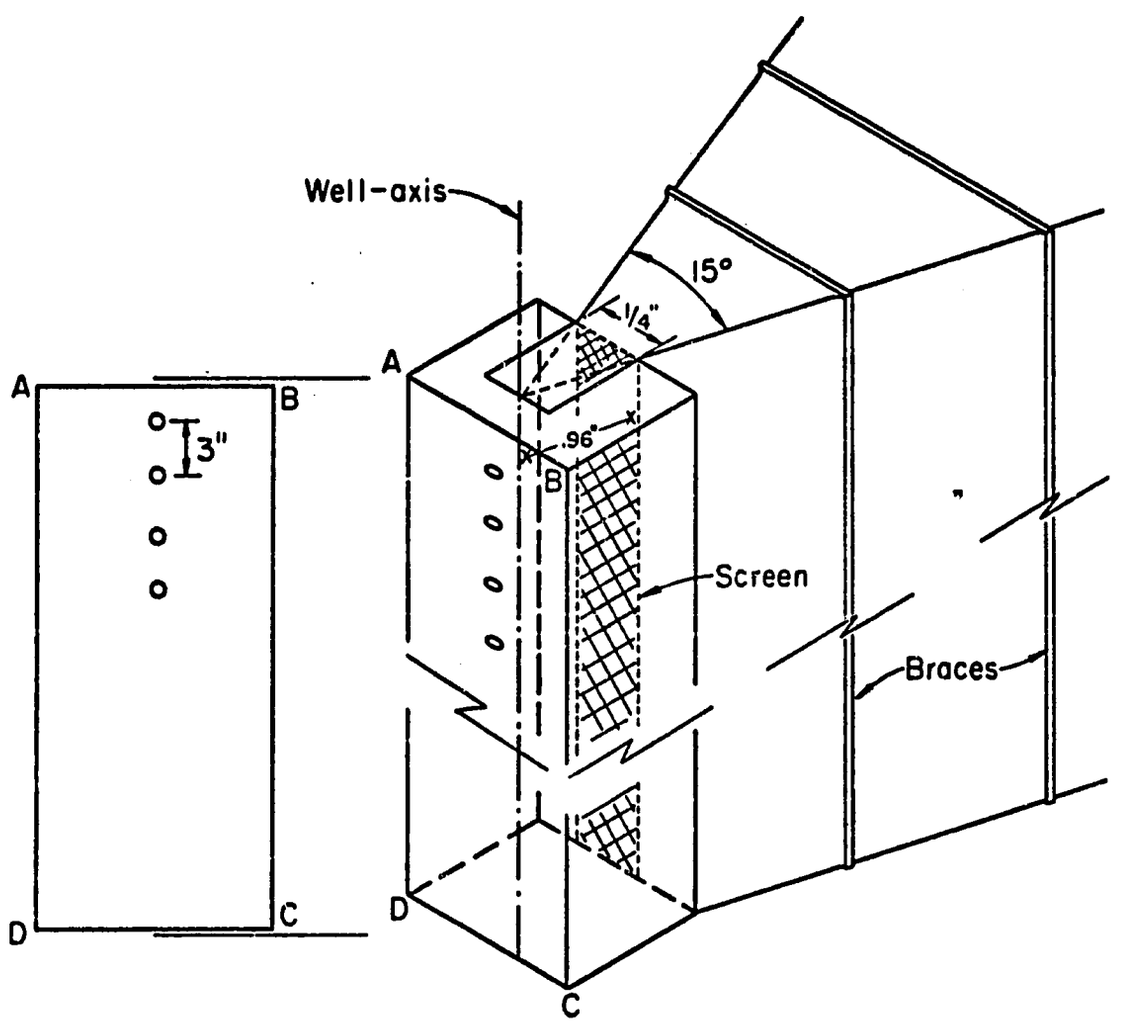

Figure 3. Discharge end of the laboratory model.

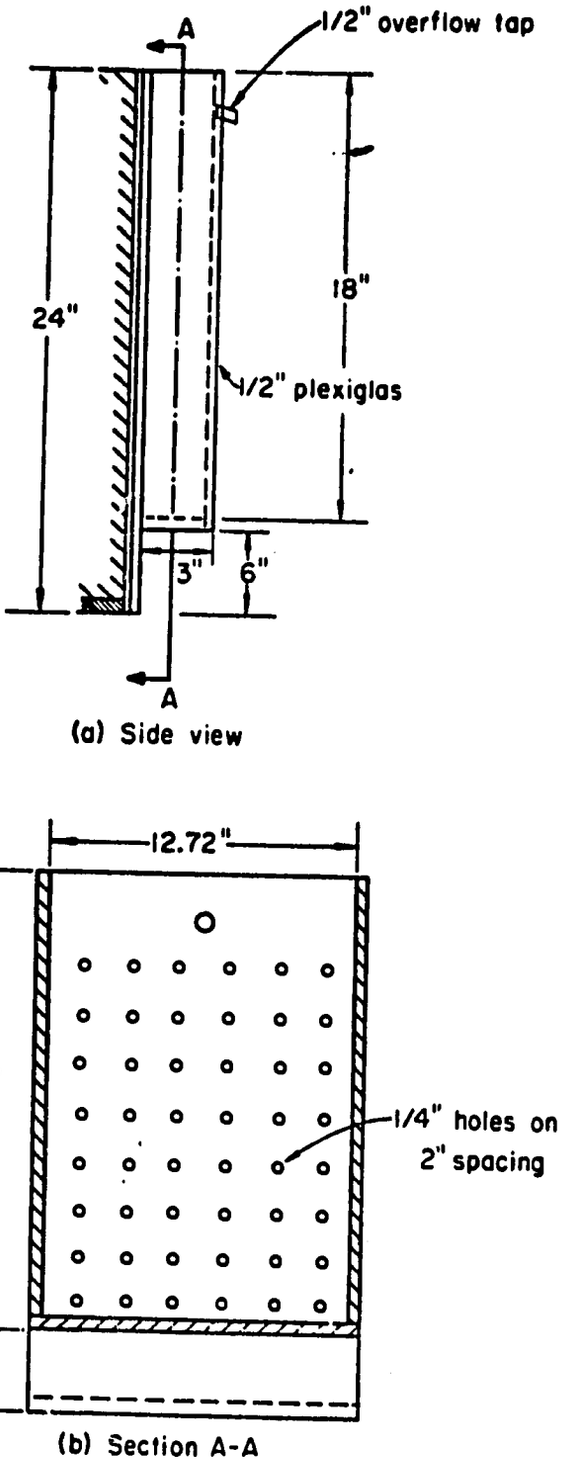

Figure 4. Recharge end of the model.

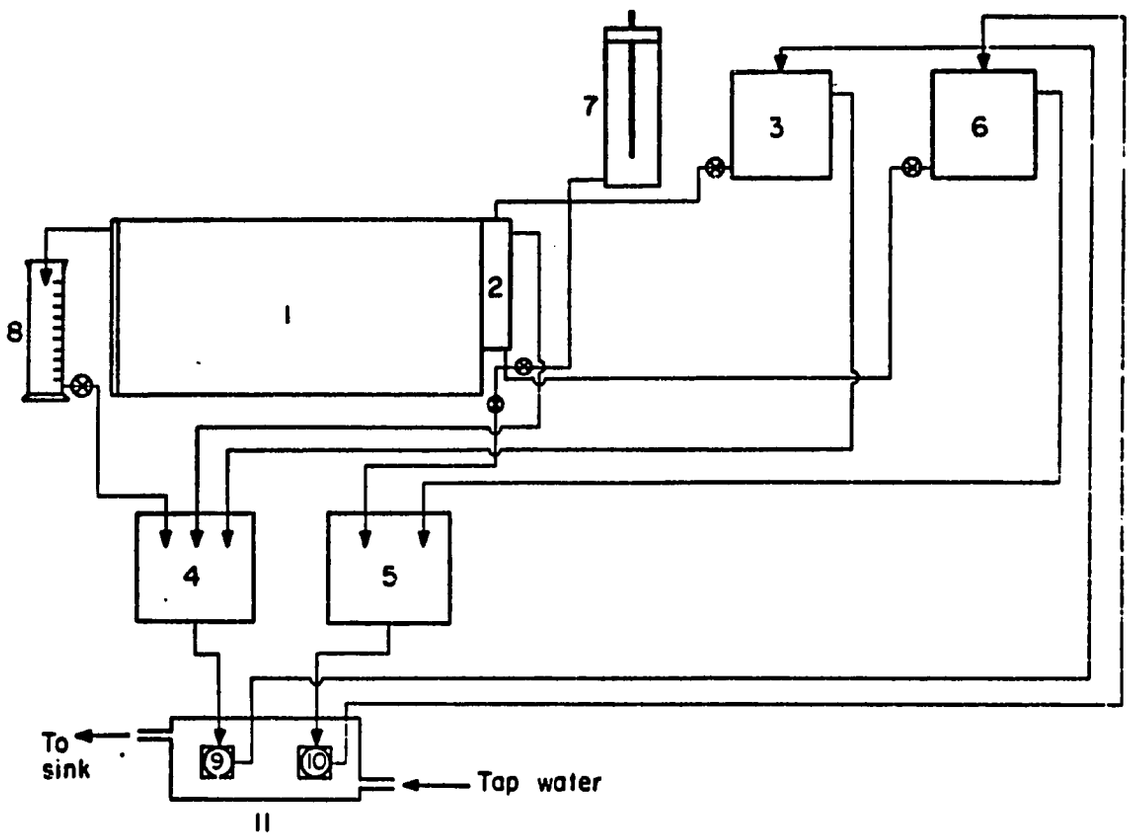

Legend:

1 Pie-shape model
2 Recharge reservoir
3 Overhead tank (oil)
4 Oil reservoir
5 Water reservoir
6 Overhead tank (water)
7 Mariotte siphon
8 Measuring jar
9 Pump for oil-circulation
10 Pump for water-circulation
11 Water-tank for cooling the pumps

Figure 5. Complete assembly of the experimental equipment.

water only. It was also found in the preliminary tests that the same precautions were required to obtain a well-defined interface. After trying various techniques to avoid these problems, the following procedure was finally adopted for filling the model.

Beads to be used in the oil zone in the model were first immersed in oil in a separate tank. Likewise, beads to be used in the water zone were immersed in dyed water in another tank to insure that they were wet with the respective fluids. Next, dyed water was allowed to flow slowly from the overhead tank into the model, and beads previously wet with water were slowly placed in the model while keeping the water level in the model just above the beads. This layer of beads was thoroughly mixed by stirring to eliminate air bubbles. The beads were packed by pressing with a flat metal piece from above and by tapping the side walls of the model with a rubber hammer. Each layer of beads was as uniformly packed as possible and freed of air bubbles before more beads were added. The procedure was repeated until the level of dyed water and the top of the layer of the beads in it reached the level which coincided with the initial position of the interface in a particular set of conditions being simulated in the physical model.

Next, a thin layer of oil was formed on top of the water-wet beads by adding oil slowly in very small quantities along the side wall of the model. It was necessary to take utmost care while adding

this first layer of oil in the model to insure that the surface of the layer of water-wet beads was not disturbed. After adding some oil, sufficient time was allowed for the oil to spread evenly over the water-wet beads. Then, oil-wet beads were placed in this oil layer in small quantities and evenly distributed throughout the model. The procedure was repeated layer after layer insuring that the beads were uniformly packed and that they were freed of air before more beads were added. The model was filled with beads to a height about two centimeters above the outflow tap.

The rectangular prism at the 'well-end' of the model was also filled with beads wet with the fluid they were to be in contact with at the start of the experiment. The top of the beads in this prism represented the bottom of the well in the prototype conditions being simulated in the model.

A closed system for circulating the fluids was set up in the experiment as follows. Oil from overhead tank 3 was allowed to flow into recharge reservoir 2 of the model at a rate somewhat higher than the expected discharge rate in the experiment. The excess fluid drained from the outflow tap and thus the free surface elevation at the exterior end was maintained at the level of the tap. This excess fluid was received in oil reservoir 4. From reservoir 4, oil was recirculated by a pump back into tank 3.

A three-way tap was connected to the bottom of reservoir 2. Through this tap the reservoir was connected to Mariotte siphon 7

containing dyed water used in the model, and to reservoir 5 containing the same dyed water. Thus, by opening one valve, small quantities of dyed water could be added to reservoir 2 from the Mariotte siphon, whereas by opening the other valve any excess water in recharge reservoir 2 could be drained into water reservoir 5 if needed. The level of the lower end of the tube open to the atmosphere in the Mariotte bottle could be adjusted by lowering or raising the latter with the help of a screw jack.

Most of the additional water required in upconing was fed to reservoir 2 from tank 6, but at later stages of the coning, it was fed in small quantities by opening the valve between the bottom of reservoir 2 and Mariotte siphon 7.

It was found convenient to fill the model with water by pumping it to overhead tank 6 from reservoir 5. Tank 6 was provided with an overflow outlet near the tap and a valve near the bottom to adjust flow into reservoir 2.

The pumps used in recirculation of the fluids were cooled by running tap water. It was thus possible to maintain the temperature of the fluids nearly constant throughout the experiment to insure that the fluid properties did not change during the experiment.

Production from the well was simulated in the model by siphoning oil with a tube (about 1/4-inch I.D.). The height of the fluid in the well and the production rate were varied with the help of a

screw clamp. After allowing sufficient time for the flow to reach an equilibrium following each adjustment of the flow rate, it was possible to maintain a steady flow in the model. Fluid drained from the model was collected in a large measuring jar (about 2 inches in diameter and of 2000 cc capacity), which was provided near its base with an outlet and a stop cock. When the measurements for discharge were not being made, the valve at the outlet of the jar was left open so that all the fluid drained from the well was continuously received by reservoir 4. For making measurements of the producing rate, the valve was closed, so that all the fluid drained by the well was collected in tne measuring jar. The flow rate was determined by noting the total volume collected in an increment of time. After the measurement, the stop cock was again opened and the fluid allowed to drain back into reservoir 4 as before. The fluid in reservoir 4 was continuously recirculated back into inflow tank 1 and from there into reservoir 2. This closed circulation had two advantages: (1) A steady-state condition of flow could be maintained for given levels in reservoir 2 and the well, and (2) accumulation of air bubbles in the medium in the model, which would occur if fresh oil were continuously supplied to the system, could be avoided.

Conductivity Measurement of Glass Beads

Since it was intended to study only steady-state flow of oil, with brine in static equilibrium, the conductivity of glass beads to

Soltrol only was determined experimentally. A constant head permeameter was used for the purpose. It was observed in preliminary tests that conductivity of these glass beads was very high with the result that the observed gradient of head was too small to insure desired accuracy with the apparatus being used. A much larger permeameter, therefore, was constructed from a steel pipe 7.803 cm in I.D. and 160 cm long. The head was measured at three points, 50 cm apart along its length. The experimental set up is shown in figure 6.

A lack of consistency in the results was noticed in the first measurements which was attributed to the following experimental problems:

1. In order to keep the head in the overhead tank constant, a closed circulation of Soltrol was maintained between the overhead tank and the permeameter with the help of a pump immersed in the reservoir tank. Heat supplied to the oil by the pump caused an increase in temperature of the oil and hence an observed increase in measured conductivity with time.
2. A non-linear head-loss along the length of the measuring column was indicated by manometers connected to taps equally spaced along the column. This was found to be due to a density gradient in the Soltrol caused by a

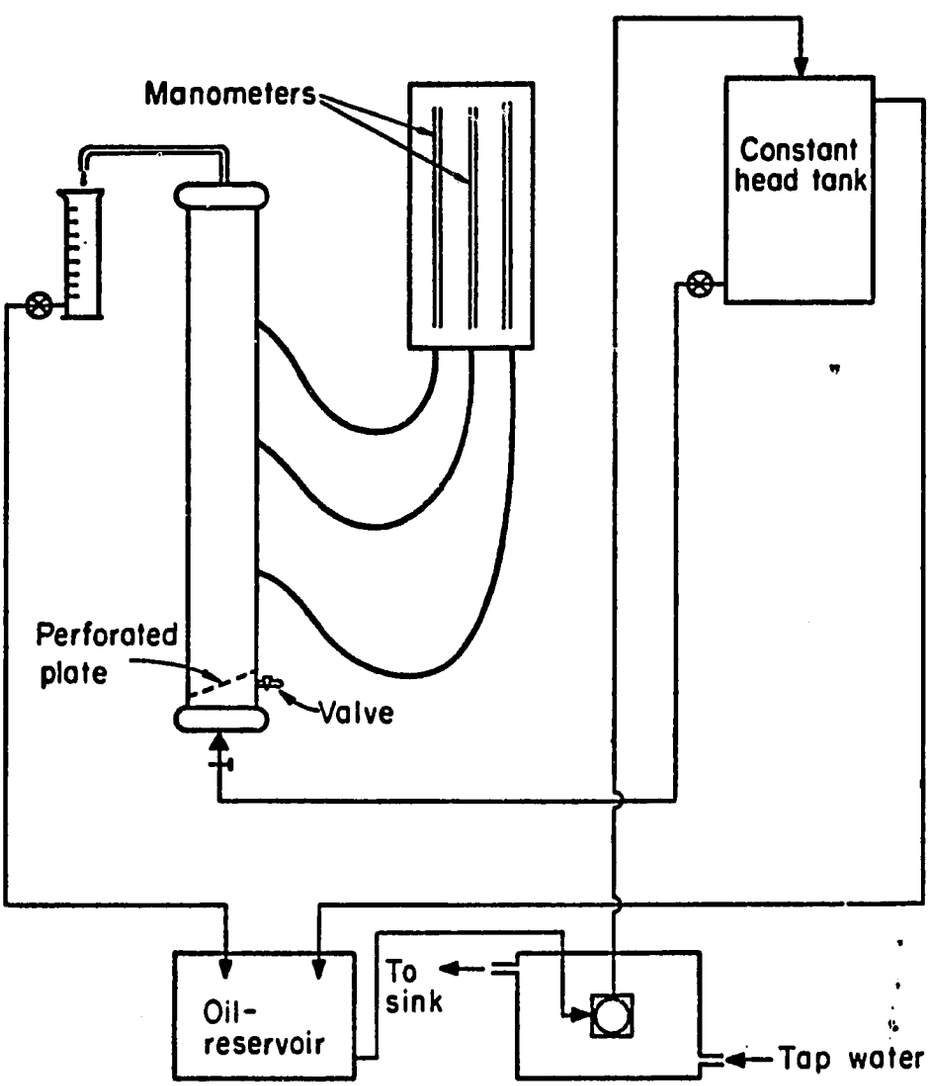

Figure 6. Experimental set up for measurement of conductivity.

temperature gradient between the inflow and outflow ends of the column.

3. Air became trapped at the base of the column causing a gradual reduction in flow rate.

These problems were largely overcome in subsequent measurements in the following way. Instead of immersing the pump in oil, it was immersed in water in a separate reservoir and cooled by running tap water. This permitted the temperature of Soltrol in circulation to remain constant at 23.5°C. An elliptical plate of plexiglass with vertical perforations (shown in Figure 7) was installed at an angle of 20° from horizontal inside the vertical column about 10 cm above the inflow end and was sealed to the inner surface of the pipe. The column

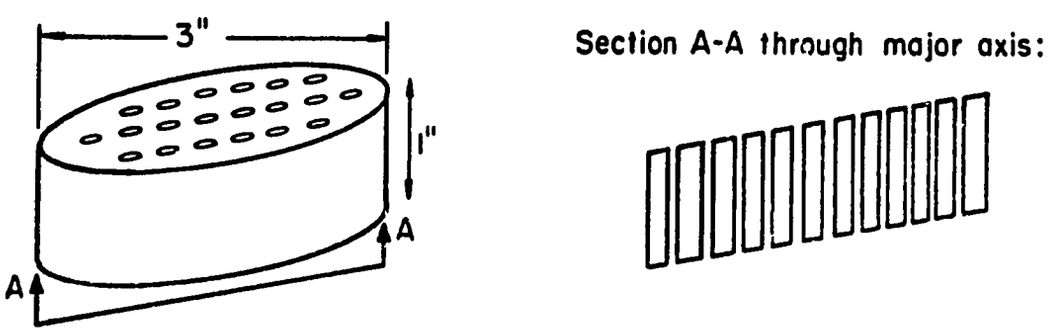

Figure 7. Perforated plate installed in the measuring column.

was packed with beads above this plate. Immediately below the highest point of the perforated plate, a valve was installed in the steel pipe to

permit periodic purging of air released from the solution before it entered the measuring column. Subsequent measurements resulted in consistent values of conductivity.

The permeability k of the beads also was calculated using the Kozeny-Carman equation

$$k = \frac{f^3}{S^2 k_s T} \tag{33}$$

in which f is the porosity, S the specific surface, k_s a numerical constant depending on the shape of pores, and T the tortuosity of the porous medium.

For spherical glass beads of almost uniform size, equation (33) can be rewritten as

$$k = \frac{f^3}{k_s T(1-f)^2} \left(\frac{\overline{V}_b}{\overline{A}_b} \right)^2 \tag{34}$$

where $\overline{V}_b$ and $\overline{A}_b$ are the average bead volume and the surface area respectively. Equation (34) can be further simplified and written as

$$k = \frac{f^3 D_m^2}{6k_s T(1-f)^2} \tag{35}$$

where D_m is the median bead diameter.

The porosity f of the porous medium used in the model was determined by the density method using several random samples in sufficiently large quantities. With each sample, observations were

repeated. Since there was no problem of reproducing the packing of the beads, a problem often encountered in dealing with soils, consistent results were obtained. The median diameter of the beads D_m was determined by a sieve analysis and the semilog plot of cumulative percentage of beads retained vs. bead size obtained. Finally, it is known from theoretical and experimental considerations (6, 39) that for the type of material used in the measurement, the shape factor k_s can be taken as 2.5 and the tortuosity as 2, so that the product $k_s T$ was 5 in this analysis.

Using the Kozeny-Carman equation the value of permeability of $5390\mu^2$ was obtained. This was in good agreement (3.9%) with the experimental value of $5190\mu^2$.

Experimental Procedure

The procedure for making an experimental run was as follows. First the values of the dimensionless parameters were selected for prototype conditions simulated in the model. Since the wall radius in the model was fixed, a well slimness parameter was obtained by selecting a proper thickness H_e of the oil zone, that is, the thickness of the flow region prior to pumping. With H_e fixed, a given well-penetration parameter was obtained by calculating the actual depth of penetration of the well using the calculated value of H_e. With both the radius of the well r_w and the position of the constant head boundary fixed, the important geometrical parameters were simulated in the physical model.

Once the model tank was filled with glass beads and fluids, a steady circulation of the fluids was maintained. A reference line was etched on the front wall of the model coinciding with the location of the original free surface. Since in all the experiments, irrespective of the position of the interface, the free surface position prior to pumping was the same, it was convenient to use this line as the reference line rather than the position of the interface. Depths below this reference line were marked in millimeters at a number of suitable distances from the well axis along the front wall and also along the well on the discharge-end plate.

The initial position of the interface and the free surface were noted. Then the production of oil was started at a slow rate. This induced a drawdown of the free surface toward the well in an approximately parabolic shape and an upconing of the interface below the well. In order to insure that the free surface at the recharge end never went below the level of the overflow outlet of reservoir 2, the rate of inflow of oil into reservoir 2 was adjusted so that it was slightly higher than the discharge rate. At the same time, care was taken that the inflow into the reservoir was not high enough to cause ponding at the surface which would result in a higher free surface location at the recharge end than the original position prior to pumping.

After allowing sufficient time for the flow system to reach a steady state, several measurements were made for calculating

discharge. The locations of both the free surface as well as the interface were recorded at several radial distances from the well axis. The readings were taken at much closer intervals in the vicinity of the well. This was helpful in making a detailed study of the effects of convergence near the well on the free liquid surface and on production rates.

Next, the discharge was increased and after the flow system had again reached equilibrium under the new conditions, the new discharge was measured and the locations of the free surface and interface were recorded.

Whenever the discharge was increased, the interface rose to a higher position and the cone in the vicinity of the well became steeper. In the later stages, as the critical condition was approached, only a slight increase in production rate would raise the cone near the well by a significant amount. The experiment was continued until the cone became almost vertical near the well. Any further increases in the production rate forced the cone to become unstable and eventually the well produced water along with oil. Just before this happened, the cone was considered as 'critical'. The discharge without producing water corresponding to this critical condition was measured. This completed the set of observations that were needed to analyze the performance of a partially penetrating well for a given set of aquifer conditions and well geometry. Similar experiments were made with several other sets of prototype conditions.

COMPUTER SIMULATION OF CONING PROBLEM

The intent of this research is to study the conditions under which brine cones, in response to steady pumping of fresh water, will remain in static equilibrium. The problem, therefore, reduces to one of steady-state flow occuring only in the upper fluid. Equations of flow need to be written only for the fresh water zone and solved with proper boundary conditions.

For simplicity, the following assumptions are made:

1. The aquifer is nondeformable, and is isotropic and homogeneous with regard to its hydraulic properties.
2. Fluids are incompressible.
3. Flow occurs only in the fresh water zone; it is steady and radially symmetrical about the producing well.
4. An abrupt interface separates the fresh water and saline water zones.
5. Darcy's law is applicable to the entire flow region.
6. An isothermal condition prevails throught the period of pumping, so that the fluid properties remain unchanged with time.

Cylindrical coordinates (r, θ, z) are the obvious choice to describe flow toward a well. With the assumption of radial symmetry, only radial coordinates and vertical coordinates appear in the flow

equation which can be derived by combining the mass balance equation and Darcy's law.

Flow Equation

The following derivation considers a small element of fluid in the frame of reference of the cylindrical coordinate system shown in Figure 8. The element has a vertical thickness Δz, a length Δr, and occupies the angular segment $\Delta\theta$.

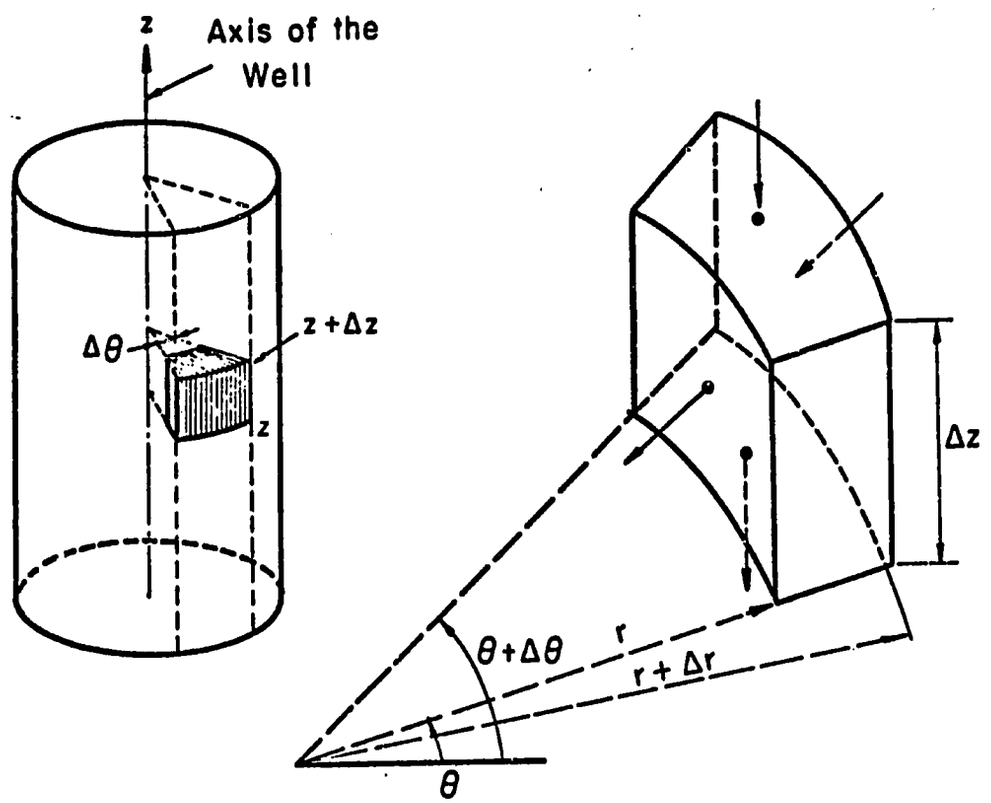

Figure 8. Fluid element considered for derivation of flow equation.

Because of radial symmetry, flow occurs only in z and r directions. The average cross-sectional area of this differential fluid element perpendicular to flow in the r direction is designated as A_r and that perpendicular to the flow in the z direction as A_z. The mass balance of this

element at steady state requires that the net gain in mass within the element is zero in any time increment; that is, the total amount going into the element must equal that leaving the element. Therefore, considering first only flow in the r direction and taking the center of mass of the element at (r_o, θ_o, z_o), the rate of increment of mass (RIM) is given by

$$(RIM)_r = (\rho\, Q_r)\Big|_{r_o+\Delta r/2} - (\rho\, Q_r)\Big|_{r_o-\Delta r/2} \tag{36}$$

where ρ and Q_r are, respectively, the fluid density and flow rate in the radial direction. Considering the mass flow function as continuously differentiable, each of the terms on the left hand side of equation (36) is expanded about the center of mass of the differential element by a Taylor series as follows:

$$(\rho\, Q_r)\Big|_{r_o+\Delta r/2} = (\rho\, Q_r)\Big|_{r_o} + \frac{\partial}{\partial r}\left[(\rho\, Q_r)\Big|_{r_o}\right]\cdot\frac{\Delta r}{2} + \frac{1}{2!}\frac{\partial^2}{\partial r^2}\left[(\rho\, Q_r)\Big|_{r_o}\right]\cdot\left(\frac{\Delta r}{2}\right)^2 + \text{---}\,, \tag{37}$$

and

$$(\rho\, Q_r)\Big|_{r_o-\Delta r/2} = (\rho\, Q_r)\Big|_{r_o} - \frac{\partial}{\partial r}\left[(\rho\, Q_r)\Big|_{r_o}\right]\cdot\frac{\Delta r}{2} - \frac{1}{2!}\frac{\partial^2}{\partial r^2}\left[(\rho\, Q_r)\Big|_{r_o}\right]\cdot\left(\frac{\Delta r}{2}\right)^2 \text{----}\,. \tag{38}$$

In the limiting case where Δr is very small, the second and higher order terms in equations (37) and (38) can be neglected. Using equations (37) and (38), equation (36) is written as

$$(RIM)_r = \frac{\partial}{\partial r}\left[(\rho\ Q_r)\Big|_{r_o}\right]\cdot \Delta r \quad . \tag{39}$$

Similarly, considering flow in the vertical direction, rate of increment of mass in the z direction is written as

$$(RIM)_z = \frac{\partial}{\partial z}\left[(\rho\ Q_z)\Big|_{z_o}\right]\cdot \Delta z \quad . \tag{40}$$

The complete mass balance equation is

$$\frac{\partial}{\partial r}\left[(\rho\ Q_r)\Big|_{r_o, z_o}\right]\cdot \Delta r + \frac{\partial}{\partial z}\left[(\rho\ Q_z)\Big|_{r_o, r_z}\right]\cdot \Delta z = 0 \quad . \tag{41}$$

Since the fluid is assumed to be incompresible, the density ρ is the same at all points. Therefore, equation (41) is written as

$$\frac{\partial}{\partial r}(Q_r)_{r_o, r_z}\cdot \Delta r + \frac{\partial}{\partial z}(Q_z)_{r_o, z_o}\cdot \Delta z = 0 \quad . \tag{42}$$

Also, by Darcy's law

$$Q_r = - K_r A_r \frac{\partial H}{\partial r} \quad , \tag{43}$$

and

$$Q_z = - K_z A_z \frac{\partial H}{\partial z} \quad . \tag{44}$$

Substituting Q_r and Q_z from (43) and (44), equation (42) is rewritten as

$$\frac{\partial}{\partial r}\left(K_r A_r \frac{\partial H}{\partial r}\right)\Delta r + \frac{\partial}{\partial z}\left(K_z A_z \frac{\partial H}{\partial z}\right)\Delta z = 0 \qquad (45)$$

where the suffix r_o, z_o has been omitted. It is implied that the equation refers to the center of mass of the fluid element in question. This is the flow equation applicable to the system under consideration. The conductivity is the same at all points and in all directions in a homogeneous and isotropic medium as assumed in the study.

Finite Difference Form of Flow Equation

In order to solve equation (45) with given boundary conditions by a finite difference method it is necessary to write the flow equation in a discretized form. The entire flow region in a vertical plane is divided into a convenient grid system with grid blocks small enough to ensure the desired accuracy of the results and large enough to keep the total number of grid blocks within a practical limit. For each of these grid blocks a flow equation is written in the discretized form. Thus the original problem of solving the complex second-order non-linear equation is reduced to one of solving a set of simultaneous linear algebraic equations.

The grid system used is illustrated in Figure 9 where a typical central block (isolated from the boundaries) is shown together with its four adjoining grids. Indices i and j denote, respectively, the

number of the row and column in which a particular grid element lies, and they refer to the center of the block.

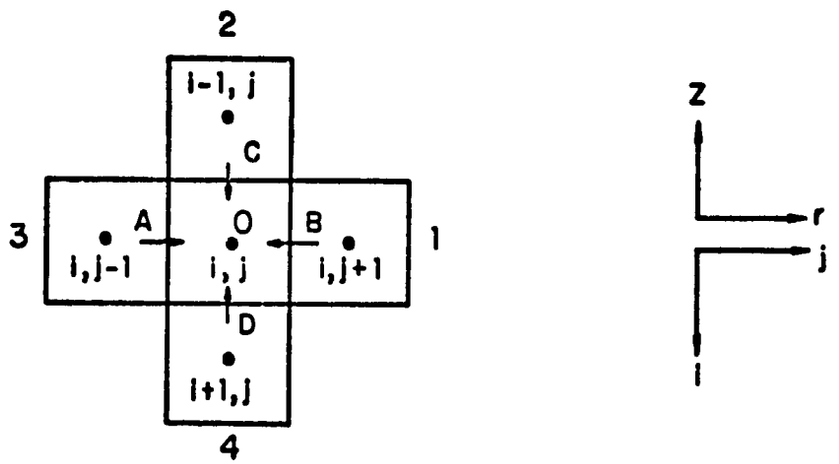

Figure 9. Grid system used for writing the finite difference form of the flow equation.

For convenience, the grid in question is labeled 0 and those adjacent to it are referred to as 1 through 4 in an anti-clockwise direction as shown in the figure.

The first term on the left hand side of equation (45) can be written in the discretized form as

$$\frac{\partial}{\partial r}\left(KA_r \frac{\partial H}{\partial r}\right) = \left[(KA_r)_{i,j-\frac{1}{2}} \frac{H_{i,j-1} - H_{i,j}}{\Delta r} + (KA_r)_{i,j+\frac{1}{2}} \frac{H_{i,j+1} - H_{i,j}}{\Delta r}\right] \frac{1}{\Delta r} \qquad (46)$$

and the second term as

$$\frac{\partial}{\partial z}\left(KA_z \frac{\partial H}{\partial z}\right) \approx \left[(KA_z)_{i-\frac{1}{2},j} \frac{H_{i-1,j}-H_{i,j}}{\Delta z} + (KA_z)_{i+\frac{1}{2},j} \frac{H_{i+1,j}-H_{i,j}}{\Delta z}\right] \frac{1}{\Delta z} \quad . \tag{47}$$

In writing these finite difference expressions for flow between two adjacent grid blocks, the values of conductivity and cross-sectional area to flow have been taken as those at a point midway between the two blocks.

Substitution of the right side of equations (46) and (47) into equation (45) results in

$$(A_r K)_{i,j-\frac{1}{2}} \frac{H_{i,j-1}-H_{i,j}}{\Delta r} + (A_r K)_{i,j+\frac{1}{2}} \frac{H_{i,j+1}-H_{i,j}}{\Delta r} + (A_z K)_{i-\frac{1}{2},j} \frac{H_{i-1,j}-H_{i,j}}{\Delta z} + (A_z K)_{i+\frac{1}{2},j} \frac{H_{i+1,j}-H_{i,j}}{\Delta z} = 0 \quad . \tag{48}$$

This can also be written as

$$A(H_{i,j-1}-H_{i,j}) + B(H_{i,j+1}-H_{i,j}) + C(H_{i-1,j}-H_{i,j}) + D(H_{i+1,j}-H_{i,j}) = 0 \tag{49}$$

where A, B, C, and D are the flow coefficients for the grid block (i,j) for the flow across the boundaries between blocks (i,j-1) and (i,j), (i,j) and (i,j+1), (i-1,j) and (i,j), and (i+1,j) and (i,j),

respectively. Rearranging the terms, equation (49) can be written as

$$AH_{i,j-1} + B H_{i,j+1} + CH_{i-1,j} + DH_{i+1,j} + EH_{i,j} = 0 \qquad (50)$$

where,

$$E = -(A + B + C + D) \quad . \qquad (51)$$

The next step is to obtain expressions for these flow coefficients in the finite difference form.

Flow coefficients A and B

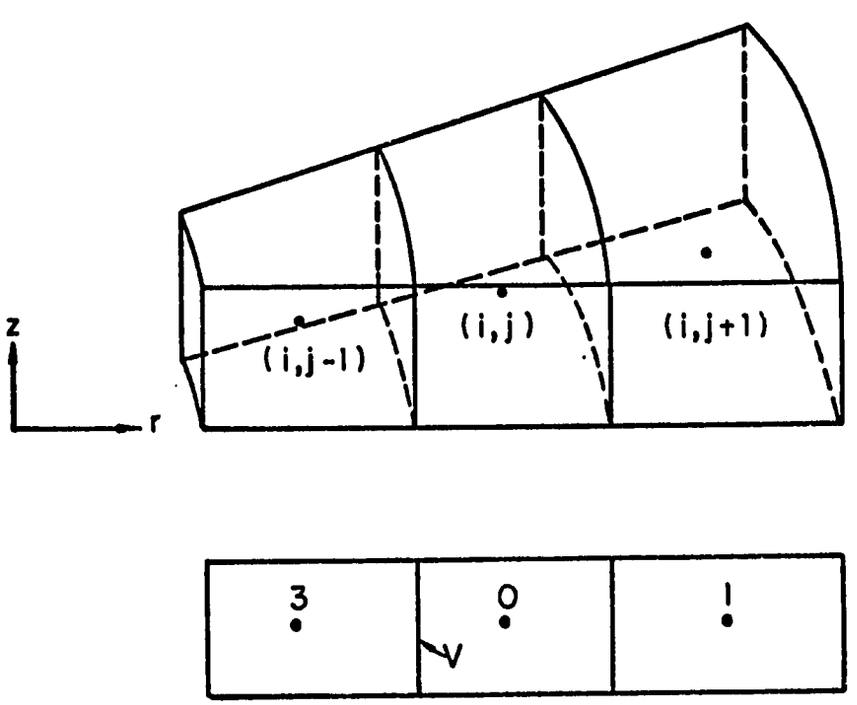

Figure 10. A typical grid (i, j) with its adjacent blocks in radial direction.

Figure 10 shows the grid block 0 and its two neighboring blocks 3 and 1. The vertical wall or face separating the grid blocks 3 and 0 is denoted by V. The flow in the r direction at any point is given by Darcy's law as

$$Q_r = - KA_r \frac{\partial H}{\partial r}$$

$$= - K2\pi r \Delta z_r \frac{\partial H}{\partial r}$$

or

$$\frac{\partial H}{\partial r} = - \frac{Q_r}{2\pi K r \Delta z_r} \quad . \tag{52}$$

Integrating differential equation (52), the flow between points 3 and V is given by

$$Q_{3-v} = - K_{i,j-\frac{1}{2}} 2\pi \, \Delta z_{i,j-\frac{1}{2}} \frac{H_v - H_3}{\ell n \frac{r_{i,j-\frac{1}{2}}}{r_{i,j-1}}} \quad . \tag{53}$$

Similarly, flow from point V and 0 is given by

$$Q_{v-o} = - K_{i,j-\frac{1}{2}} 2\pi \, \Delta z_{i,j-\frac{1}{2}} \frac{H_o - H_v}{\ell n \frac{r_{i,j}}{r_{i,j-\frac{1}{2}}}} \quad . \tag{54}$$

During the integration which leads to equations (53) and (54), conductivity and the vertical thickness of the grid block were treated as constants and equal to their respective values at the wall V.

Continuity requires that

$$Q_{3-v} = Q_{v-o} = Q_r \quad . \tag{55}$$

Therefore, solving for the head difference permits equations (53) and (54) to be written as

$$H_3 - H_v = Q_r \frac{\ell n \frac{r_{i,j-\frac{1}{2}}}{r_{i,j-1}}}{K_{i,j-\frac{1}{2}} 2\pi \Delta z_{i,j-\frac{1}{2}}} \tag{56}$$

and

$$H_v - H_o = Q_r \frac{\ell n \frac{r_{i,j}}{r_{i,j-\frac{1}{2}}}}{K_{i,j-\frac{1}{2}} 2\pi \Delta z_{i,j-\frac{1}{2}}} \tag{57}$$

Adding equations (56) and (57) gives

$$H_3 - H_o = Q_r \frac{\left[\ell n \frac{r_{i,j-\frac{1}{2}}}{r_{i,j-1}} + \ell n \frac{r_{i,j}}{r_{i,j-\frac{1}{2}}}\right]}{K_{i,j-\frac{1}{2}} 2\pi \Delta z_{i,j-\frac{1}{2}}}$$

$$= Q_r \frac{\ell n \left[\frac{r_{i,j-\frac{1}{2}}}{r_{i,j-1}} \cdot \frac{r_{i,j}}{r_{i,j-\frac{1}{2}}}\right]}{K_{i,j-\frac{1}{2}} 2\pi \Delta z_{i,j-\frac{1}{2}}}$$

$$= Q_r \frac{\ell n \frac{r_{i,j}}{r_{i,j-1}}}{K_{i,j-\frac{1}{2}} 2\pi \Delta z_{i,j-\frac{1}{2}}} \tag{58}$$

Comparison of equation (58) with the equation

$$Q_r = A\,(H_3 - H_o) \tag{59}$$

shows that the flow coefficient A for the flow between grid blocks 3 and 0 is given by

$$A = \frac{2\pi\,(K\Delta z)_{i,\,j-\frac{1}{2}}}{\ell n\,\frac{r_{i,j}}{r_{i,j-1}}} \tag{60}$$

Similarly, considering the radial flow between the grid blocks 0 and 1, it can be shown that the flow coefficient B is given by

$$B = \frac{2\pi\,(K\Delta z)_{i,\,j+\frac{1}{2}}}{\ell n\,\frac{r_{i,j+1}}{r_{i,j}}} \tag{61}$$

Coefficients C and D

For obtaining expressions for the flow coefficients C and D, flow in the vertical direction is considered in grid blocks 2, 0, and 4 as shown in Figure 11.

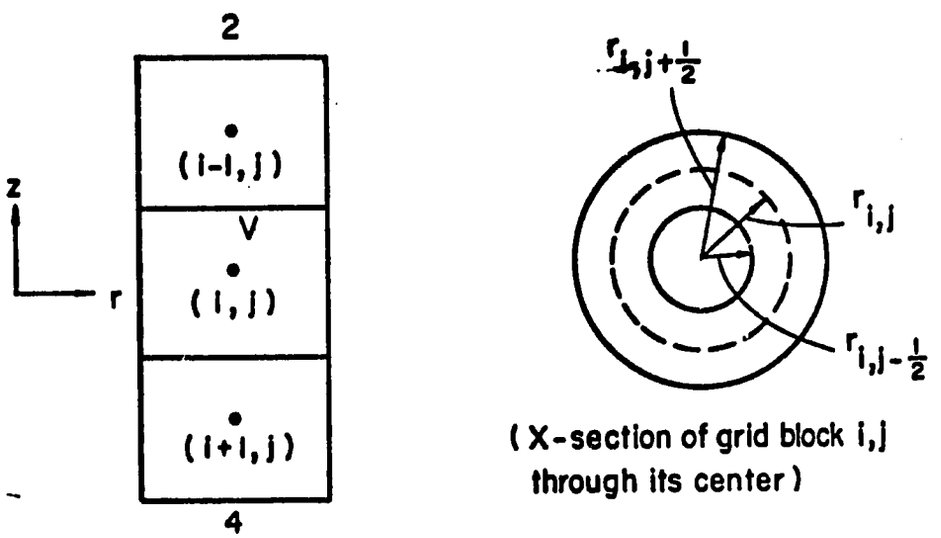

Figure 11. A typical grid (i, j) with its adjacent blocks in the vertical direction.

The flow in the vertical direction at any point is given by

$$Q_z = - KA_z \frac{\partial H}{\partial z} \quad . \tag{62}$$

Therefore, flow from the center of grid block 2 to the boundary V between the blocks 2 and 0 is

$$Q_{2-v} = \frac{K_{i-\frac{1}{2},j}\, \pi\left(r^2_{i,j+\frac{1}{2}} - r^2_{i,j-\frac{1}{2}}\right) \cdot \left(H_{i-1,j} - H_{i-\frac{1}{2},j}\right)}{\Delta z_{i-1,j}/2} \quad , \tag{63}$$

and that between boundary V and the point 0 is

$$Q_{v-o} = \frac{K_{i-\frac{1}{2},j}\, \pi\left(r^2_{i,j+\frac{1}{2}} - r^2_{i,j-\frac{1}{2}}\right) \cdot \left(H_{i-\frac{1}{2},j} - H_{i,j}\right)}{\Delta z_{i,j}/2} \quad . \tag{64}$$

Here, as before, the conductivity value is taken as that at the boundary between the grid blocks 2 and 0. Continuity requires that

$$Q_{2-v} = Q_{v-o} = Q_z \tag{65}$$

Therefore, equations (63) and (64), using (65), are written as

$$H_{i-1,j} - H_{i-\frac{1}{2},j} = \frac{Q_z \, \Delta z_{i-1,j}}{2\pi K_{i-\frac{1}{2},j} \left(r^2_{i,j+\frac{1}{2}} - r^2_{i,j-\frac{1}{2}} \right)} \tag{66}$$

and

$$H_{i-\frac{1}{2},j} - H_{i,j} = \frac{Q_z \, \Delta z_{i,j}}{2\pi K_{i-\frac{1}{2},j} \left(r^2_{i,j+\frac{1}{2}} - r^2_{i,j-\frac{1}{2}} \right)} \tag{67}$$

Adding equations (66) and (67) results in

$$H_{i-1,j} - H_{i,j} = \frac{Q_z \left(\Delta z_{i-1,j} + \Delta z_{i,j} \right)}{2\pi K_{i-\frac{1}{2},j} \left(r^2_{i,j+\frac{1}{2}} - r^2_{i,j-\frac{1}{2}} \right)}$$

or,

$$Q_z = \frac{\pi K_{i-\frac{1}{2},j} \left(r^2_{i,j+\frac{1}{2}} - r^2_{i,j-\frac{1}{2}} \right)}{\left(\Delta z_{i-1,j} + \Delta z_{i,j} \right)/2} \cdot \left(H_{i-1,j} - H_{i,j} \right) \tag{68}$$

Comparison of equation (68) with the equation

$$Q_z = C \left(H_{i-1,j} - H_{i,j} \right) \tag{69}$$

shows that the flow coefficient C is given by

$$C = \frac{\pi K_{i-\frac{1}{2},j}\left(r^2_{i,j+\frac{1}{2}} - r^2_{i,j-\frac{1}{2}}\right)}{\left(\Delta z_{i-1,j} + \Delta z_{i,j}\right)/2} \qquad (70)$$

Likewise, considering flow between grid blocks 0 and 4 it can be shown that the flow coefficient D is given by

$$D = \frac{\pi K_{i+\frac{1}{2},j}\left(r^2_{i,j+\frac{1}{2}} - r^2_{i,j-\frac{1}{2}}\right)}{\left(\Delta z_{i+1,j} + \Delta z_{i,j}\right)/2} \qquad (71)$$

Once the coefficients, A, B, C, and D are defined, the only remaining coefficient, E, in equation (50) is also defined using the relation (51). Thus, every term in the flow equation is defined in the finite difference form.

If all the blocks in the entire grid system have the same thickness Δz then the denominators on the right-hand side of equations (70) and (71) reduce to simply Δz. While simulating the conditions employed in the laboratory model, a constant thickness of 1 cm for all the grids is used. For studying the fresh water - saline water aquifers, since the drawdown is a relatively much smaller fraction of the coning, a grid system with variable thickness Δz is employed. In such cases, the upper 7 to 12 grid-rows are of smaller thickness than the rest of the rows in the model.

Grid System

The flow region in the mathematical model is bounded by the well axis on the left, by a vertical line at the radius of influence on the right, by the initial position of the interface (prior to pumping) at the bottom and by one extra row of grid blocks above the initial position of the free surface on top. This flow region is divided into NR number of rows and NC number of columns, so that the total number of grid blocks is NR x NC. The grid rows are numbered 2 through NR1 and likewise the grid columns are numbered 2 through NC1. For simplicity, the vertical thickness of all the grid blocks is taken to be the same and equal to Δz which is sufficiently small to ensure that the free surface and interface locations can be computed to a desired accuracy. Pressure gradients are much larger in the vicinity of the well than at points away from it. Therefore, more detailed information with regard to potential distribution and positions of the free surface and interface are required in the grid blocks in the vicinity of the well. This is accomplished by having narrower columns i.e., smaller grid spacings toward the well. Furthermore, since the pressure varies in a logarithmic manner with distance from the well axis, a logarithmic distribution of the radii from the well axis to the center of the grid blocks is employed. The grid system used in this study is illustrated in Figures 12(a) and 12(b).

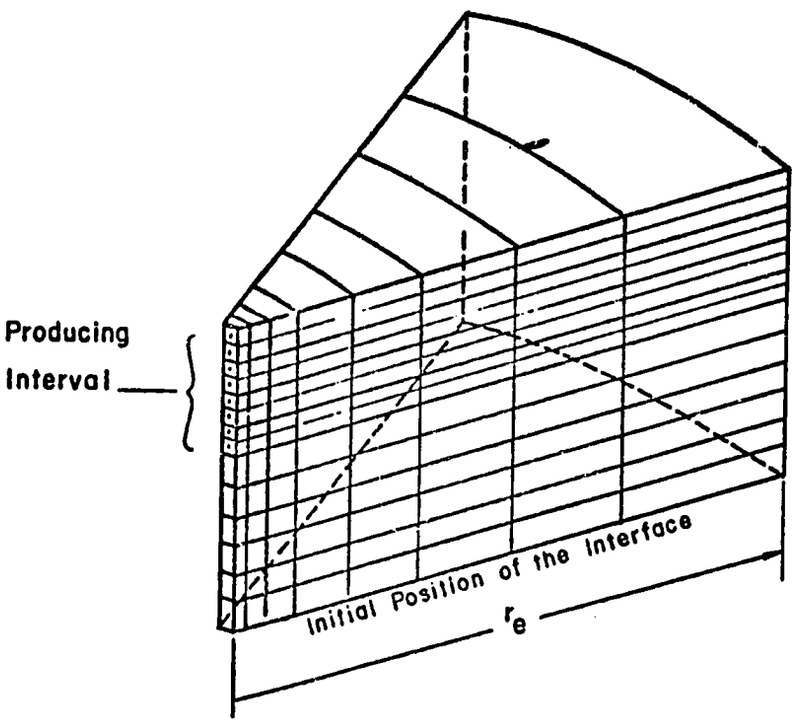

Figure 12(a). Grid system for axisymmetrical flow toward a well.

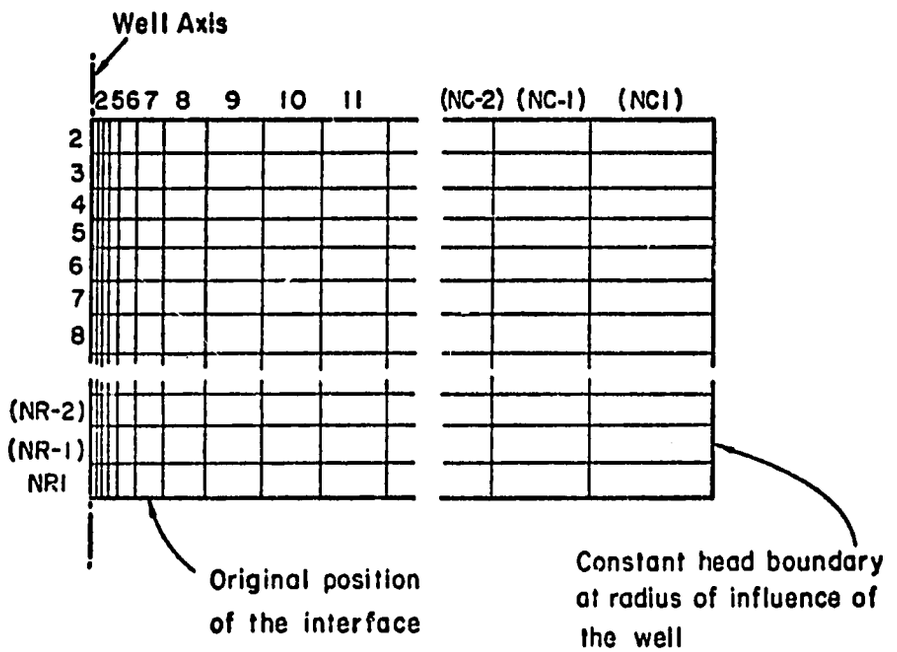

Figure 12(b). Grid system in a vertical section.

Simulation of Boundary Conditions

The boundary conditions as described in equation (16) that must be considered in solving the flow equations are of three kinds, namely,

1. Constant potential boundary,
2. No flow boundary,
3. Constant pressure boundary.

Boundary condition at the well - Neglecting the flow within the well, the potential inside the well and on the face of the well bore is constant. In the mathematical model this boundary condition is incorporated by setting the value of hydraulic head in all the grid blocks occupied by the well as H_w, the head in the well. This value is known for each set of conditions studied. Flow equations are not written for these grids.

Boundary condition beneath the well - As explained earlier, there can be no flow across the axis of the well and below the bottom of the well. Analytically this condition is given by $\partial\phi/\partial r = 0$ in equation (16). This particular boundary condition is incorporated in the computer simulation model by setting the flow coefficient A equal to zero in all grids in the first grid column which are bounded on the left by the well axis and lie between the bottom of the well and the interface.

Boundary condition at the exterior radius - At the exterior radius of the drainage area, the head remains unchanged by pumping. Therefore, to the right of all the grids in the last grid column within the flow region (toward the exterior end of the model), the head is known and equal to H_e, its value prior to pumping. For all these grids in the last column the product of the flow coefficient B and H_e is known. Therefore, this product is transferred to the right hand side of the flow equation (in the finite difference form) and the coefficient B is replaced by a zero in the coefficient matrix.

Boundary condition at the top of the aquifer - At the "free surface" the pressure is constant everywhere and equal to the atmospheric pressure. Also, there is no flow across the free surface. This condition is incorporated in the mathematical model by setting the flow coefficient C equal to zero for all the grids bounded from above by the free surface.

Boundary condition along the interface - As explained before, the interface behaves like an impermeable boundary and there is no flux across this boundary. This condition is simulated in the mathematical model by setting the flow coefficient D equal to zero in all the grids in the flow region along the interface.

Computer Program - It is explained in sections dealing with the theory that, in order to solve the flow equation for potential distribution, the boundary conditions must be known, but some of these

boundary conditions are in turn dependent on the potential distribution. Therefore, in the numerical solution of the coning problem, an iterative procedure is used. The program is written to include the flow above the water table. The procedure is outlined below.

1. First, a case is considered where there is no flow. The free surface and the interface are flat, and the head is the same at all points in the fresh water zone and therefore, is equal to the given head at the exterior radius of the model. Thus, the upper and lower boundaries of the model are completely defined to begin with. With given fresh water levels in the well and at the exterior radius of the model, the boundary conditions at these two ends of the model are defined. Also, other boundary conditions are simulated as explained in the last section. Each grid is assigned a conductivity value equal to the saturated conductivity. Flow coefficients are calculated for all the grid blocks and stored in the coefficient matrix called "T-matrix" in this program. This matrix is solved for head distribution, which is of course, quite different from the actual head distribution. Nevertheless, this distribution does form the basis of further computations. From the head values calculated above, fresh-water pressure in each grid and the first approximate location of the interface in each grid column are computed. The free surface is located as a surface at atmospheric pressure (referred to as zero in the model) by interpolation of pressure values in the top grids in each

column. Also, from the first computed head values, discharge is calculated. This completes the first cycle of computations.

2. Next, all the grids lying below the position of the interface computed in the first iteration are made "hydraulically dead" in the mathematical model by setting the conductivity value equal to zero in these grids. Using the most recently calculated pressure values, a new conductivity value for each grid above the interface is computed from the Brooks and Corey formula (4)

$$\left.\begin{aligned} K &= K_s && \text{for} && P_c \leq P_b \\ K &= K_s(P_b/P_c)^{\eta} && \text{for} && P_c > P_b \end{aligned}\right\} \qquad (72)$$

where,

K is the effective conductivity of the medium to the wetting fluid,

K_s is the conductivity of the medium when it is fully saturated by the wetting fluid,

P_c is the capillary pressure, and equal to the pressure of the non-wetting phase (P_{nw}) minus that of wetting phase (P_w),

P_b is that capillary pressure at which the non-wetting phase first becomes continuous in a desaturation process, and

η is a constant depending on the pore-size distribution.

Since P_{nw} is zero in the case considered here, the second part of the equation (72) is written as

$$K = K_s (P_b/-P_w)^{\eta} \quad \text{for} \quad -P_w > P_b \quad .$$

Therefore, by entering P_b as a negative quantity in the input data, the formula for calculating conductivities becomes

$$\begin{aligned} K &= K_s && \text{for} \quad P \geq P_b \\ K &= K_s (P_b/P)^{\eta} && \text{for} \quad P < P_b \end{aligned} \tag{72a}$$

where, P refers to the fresh-water pressure in the grid in question.

Thus, new conductivity values are obtained for all the "useable" grids. A grid is referred to as a useable grid if it participates in the flow. Only such grids, therefore, have the flow equations. New boundary conditions, to be used in the next iteration, are defined with regard to the position of the free surface and the calculated interface. All other boundary conditions remain the same.

3. With these conductivity values new flow coefficients are computed for the useable grids and stored in the T-matrix. All the subsequent steps in the first iteration are repeated in the second iteration.

4. This iteration process is repeated until the solution converges. Two possible criteria for this convergence can be used: 1) the difference between head values calculated in a particular cycle and those for the same grids calculated in the previous iteration, or 2) the difference between discharge computed in two successive iterations. The change DIFQ in the computed value of the discharge

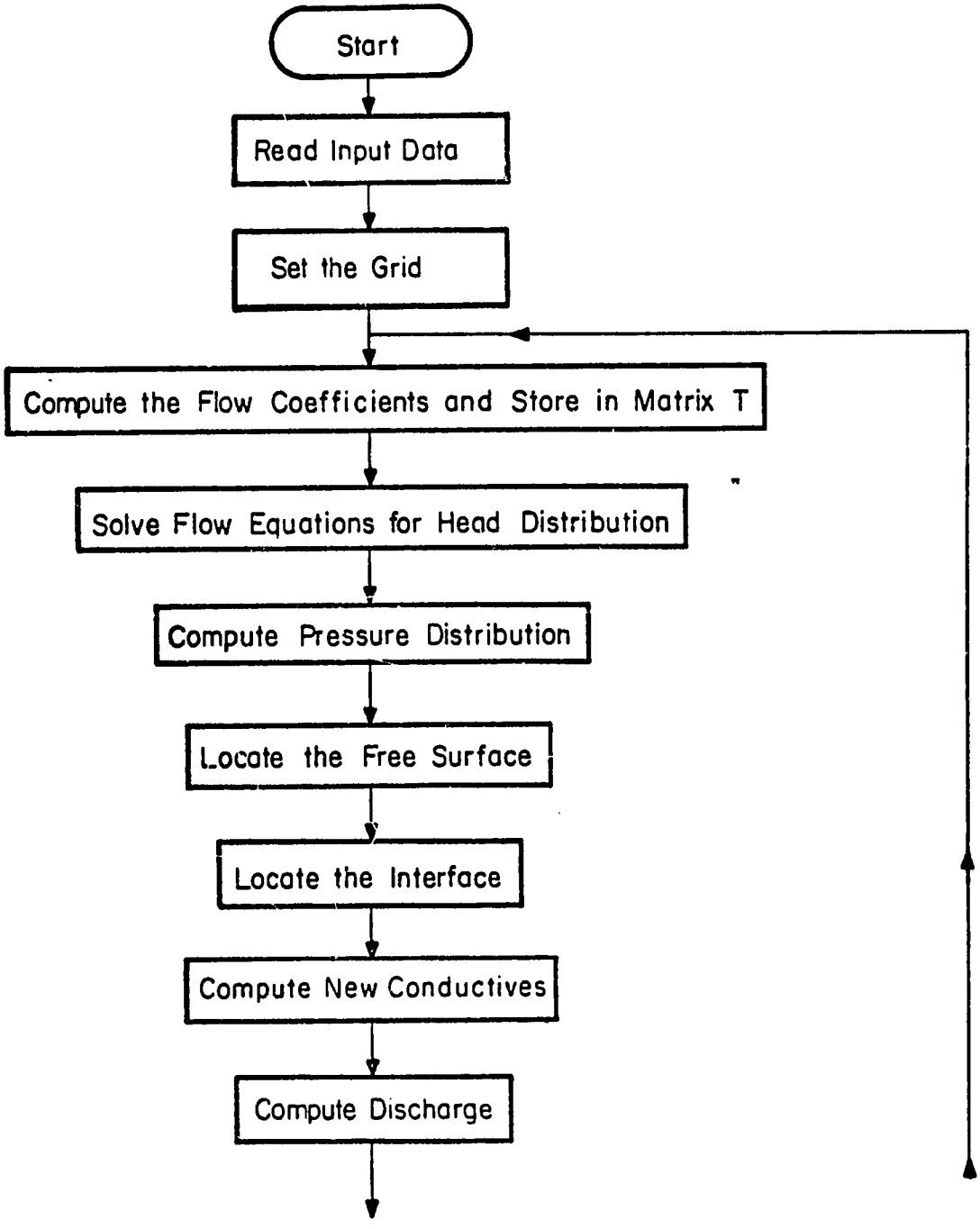

Figure 13. Flow chart illustrating important steps in program CONING.

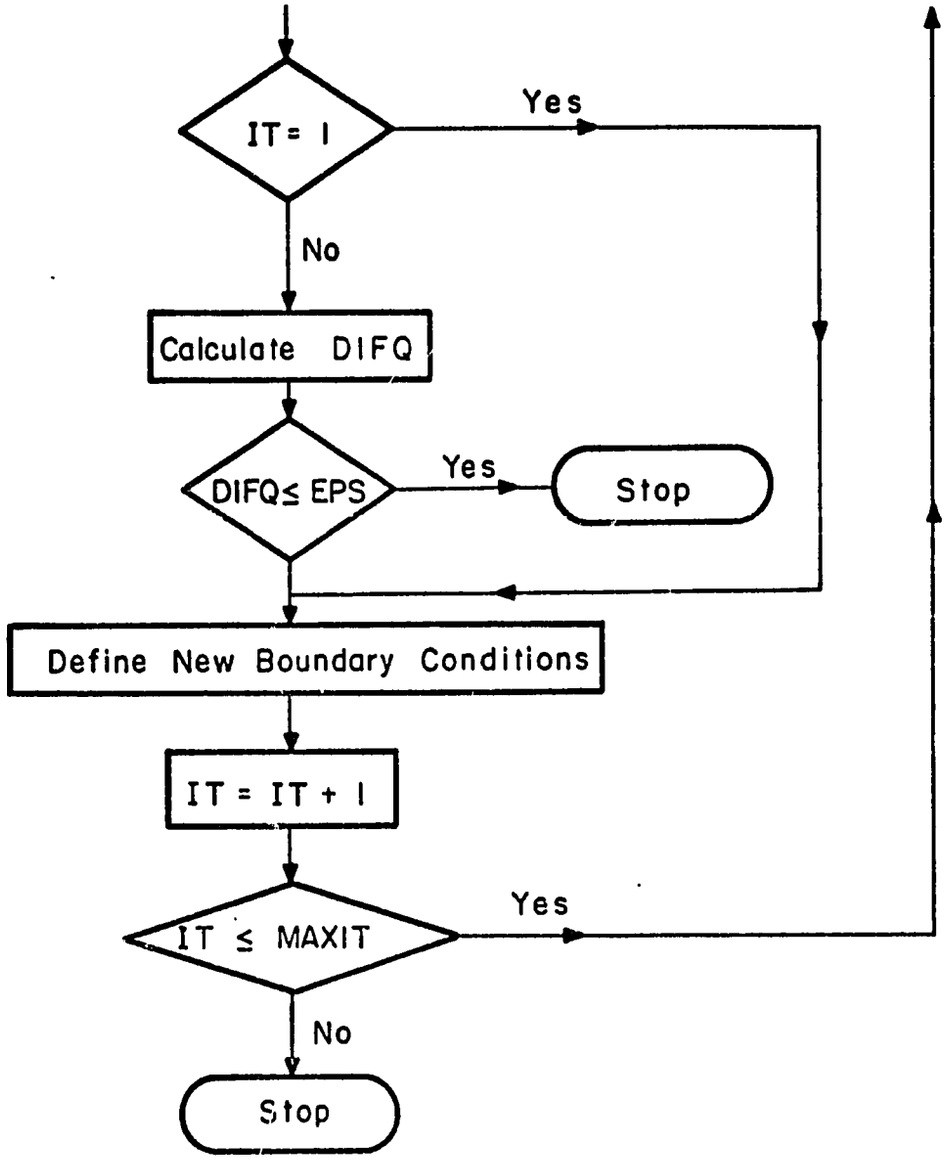

Figure 13. Flow chart (continued).

for two successive iterations was found to be about two orders of magnitude larger than the change in the H(I, J) values (on percentage basis). It was, therefore, convenient to select as a criterion for convergence of the solution, that DIFQ be less than or equal to EPS, a number so chosen that the discharge computation did not change by more than 0.005%.

The important steps involved in the above iterative procedure are illustrated by the flow chart in Figure 13. The mathematical model developed in this study is referred to as CONING. This computer program has been written in Fortran IV language. The CDC 6400 computer at Colorado State University was used for the analysis. The main program, CONING, together with its subroutines, TCOEF, TTCOEF, and SQSOLV is listed in its final form in Appendix A. The function of the subroutines TCOEF and TTCOEF is to compute the flow coefficients for the "useable grids" and store them in their proper locations in the Coefficient Matrix T. The set of simultaneous equations that were generated for the flow model by TCOEF were solved for head distribution by employing another subroutine called SQSOLV.

RESULTS AND DISCUSSION

Verification of Existing Analytic Solutions

In order to check the validity of the two existing analytic solutions, results of the analysis of six different cases made by using these solutions are presented here. These cases were also studied experimentally with the help of the physical model.

In using Wang's approach it has been assumed that the highest stable cone is one which just reaches the bottom of the well. The critical drawdown $\hat{D}_w$ is calculated from the formula

$$\hat{D}_w = \frac{\Delta\rho}{\rho_f} H_e (1 - \alpha) \tag{73}$$

The critical discharge, that is, the maximum discharge without entrainment of saline water, is then computed from the following formula for the case of lateral recharge

$$Q_w = \left[\frac{2\pi K H_e}{\ell n(r_e/r_w)}\right] \cdot \frac{\Delta\rho}{\rho_f} \alpha (1-\alpha) \left[1 + 7\left(\frac{r_w}{2\alpha H_e}\right)^{\frac{1}{2}} \cos\frac{\pi\alpha}{2}\right]. \tag{74}$$

Since this formula was used many times for computing Q_w for several cases, the calculations were made by using a short computer program called DISCHRG. A listing of this program is given in Appendix A.

In using Muskat's approach, his approximate formulas for potential distribution due to production of a partially penetrating well were employed to obtain $\Delta\phi/(\Delta\phi)_e$ vs. $\bar{z}/H_e$ curves. Muskat presented the following two formulas for potential distribution due to production from a partially penetrating well. These formulas were derived assuming that the sink-strength was uniform along the well; i.e., the flux density toward the well at all points was the same.

For small values of ρ

$$\phi = q \left\{ \ell n \frac{\Gamma(1+w+x)\Gamma(1-w+x)}{\Gamma(1-w-x)\Gamma(1+w-x)} - \ell n \frac{w+x+[\rho^2+(w+x)^2]^{\frac{1}{2}}}{w-x+[\rho^2+(w-x)^2]^{\frac{1}{2}}} \right.$$

$$+ \frac{1}{4}\rho^2 [\, \xi(2, 1-w-x) - \xi(2, 1-w+x) + \xi(2, 1+w-x)$$

$$\left. - \xi(2, 1+w+x)\,] + 0(\rho^4) \right\} \quad ; \tag{75}$$

and for large values of ρ (of the order of 1)

$$\phi = 4q \left[-\frac{1}{\pi} \sum_1^{\infty} \frac{1}{n} K_o(2n\pi\rho) \cos 2n\pi w \sin 2n\pi x + x \ell n \frac{2}{\rho} \right] \tag{76}$$

where,

q = uniform flux density at the well-face ,

H_e = thickness of the aquifer ,

w = $\bar{z}/2H_e$,

x = $PW/2H_e$,

ρ = $r/2H_e$,

$$\xi(s,y) = \sum_{n=0}^{\infty} \frac{1}{(n+y)^s} \quad , \text{ and}$$

K_o = Hankel function of order zero.

The potential in the well was calculated by taking $r = r_w$, and $\phi(0,\bar{z})$ by taking $r = 0$. In the former case, since $\rho_w = r_w/2H_e$ was a very small number, terms containing ρ^4 were neglected. In the latter case all the terms containing ρ vanish. In order to facilitate computations for several cases using Muskat's formula (3), a computer program called POTEN was written and is presented in Appendix A. The critical drawdown D_M was computed for each case using his graphical approach. The potential distribution data for the six cases is given in Tables B-1 through B-6 in Appendix B and the results of this analysis are presented in Figures 14 through 19. The slope of the tangent lines to the potential

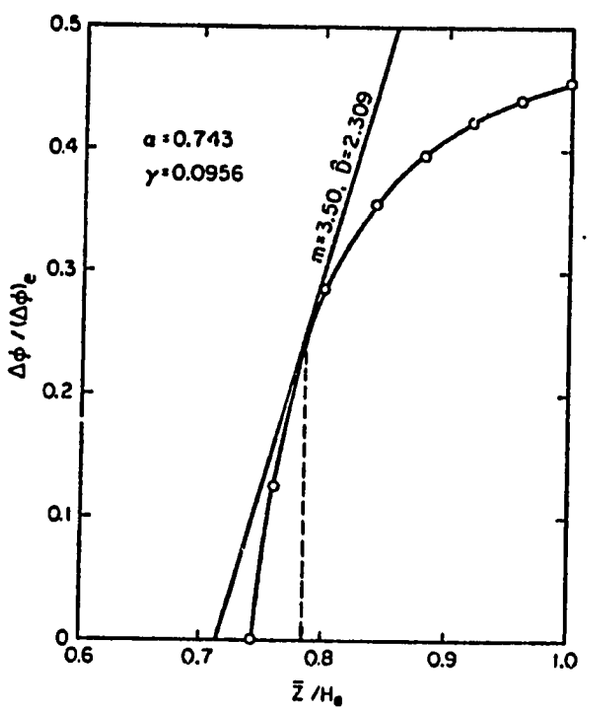

Figure 14. Muskat's analysis for Case 1.

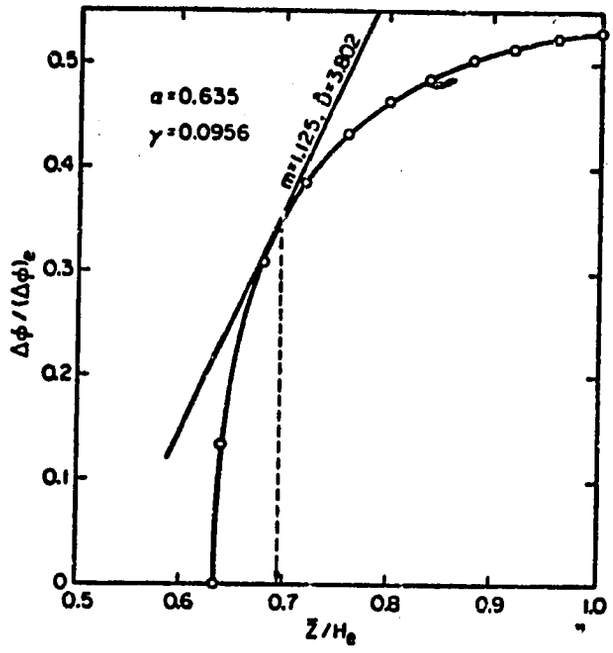

Figure 15. Muskat's analysis for Case 2.

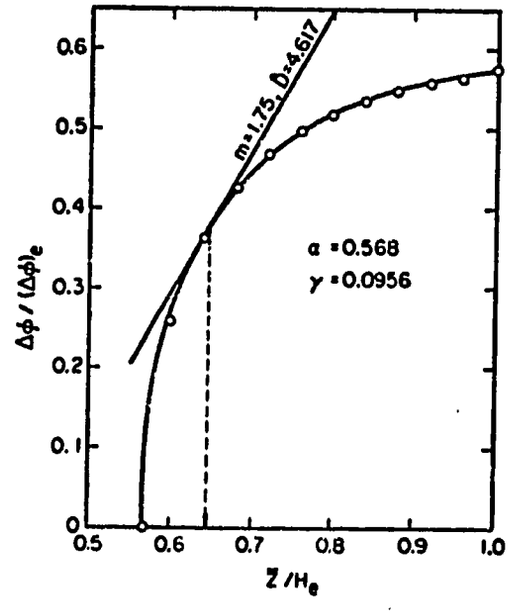

Figure 16. Muskat's analysis for Case 3.

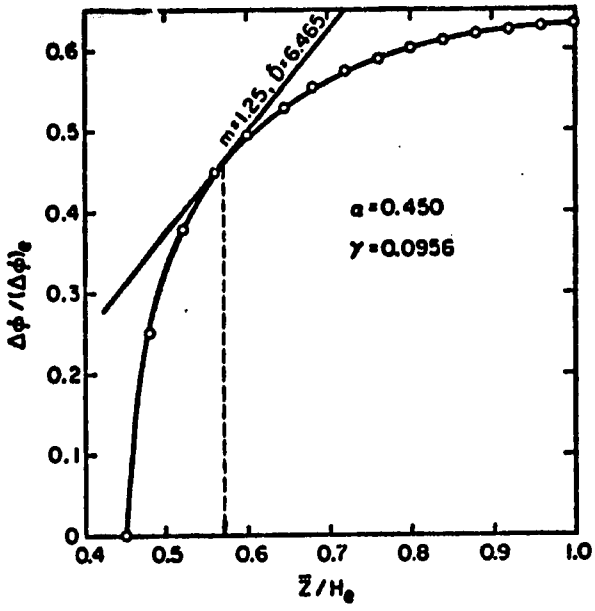

Figure 17. Muskat's analysis for Case 4.

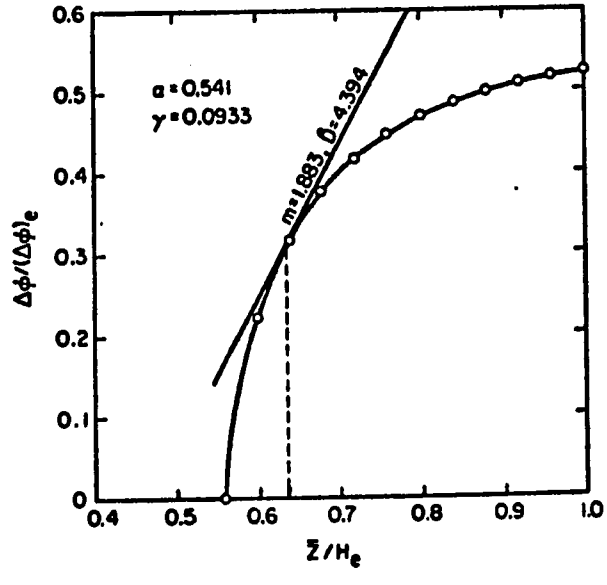

Figure 18. Muskat's analysis for Case 5.

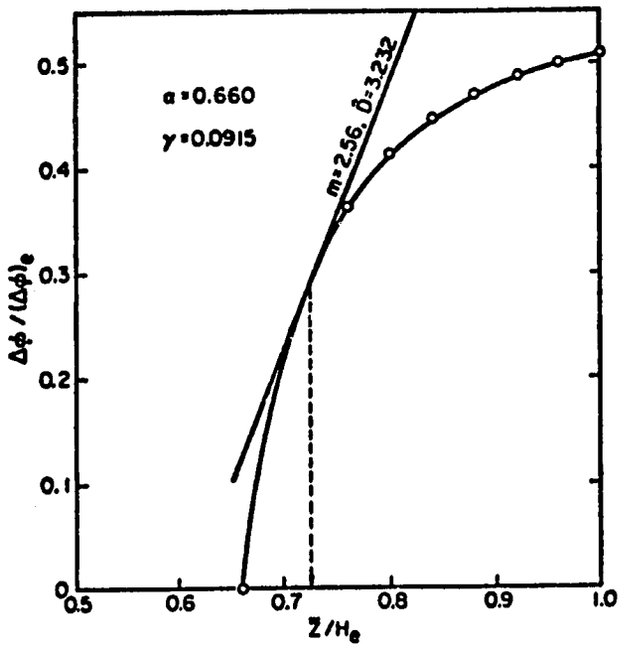

Figure 19. Muskat's analysis for Case 6.

distribution curves drawn through the point (1, 1) is used to compute the critical drawdown and the position of the apex of critical cone is determined by the point of tangency. Muskat's formula, or Kozeny's formula (a simpler version of the former), was not employed to compute critical discharge because it holds for the case of a confined aquifer without a second fluid and for which the lower boundary always remains horizontal and fixed. The discharge was, therefore, computed numerically, employing Muskat's potential distribution near the radius of influence of the well r_e. At this exterior radius the flow is essentially radial and, therefore, it is considered reasonable to compute the discharge as a summation of the flow rates for all grid rows.

The experimental results were obtained as explained in earlier sections. In Tables 1 through 3, $\hat{D}$, Q, and $\hat{C}$ denote respectively the critical drawdown, discharge and the amount of coning below the well. The suffixes E, W, and M designate the corresponding values obtained by using experimental data, Wang's approach, and Muskat's procedure, respectively. Figure 20 shows a comparison of the

Table 1. Experimental Results

Case #	α	γ	$\hat{D}_E$ cm	Q_E cc/sec	$\hat{C}_E$ cm	coning (%)
1	0.743	0.0956	1.60	7.50	6.10	95.31
2	0.635	0.0956	2.50	10.60	8.45	94.13
3	0.568	0.0956	3.15	11.50	9.74	90.48
4	0.450	0.0956	4.35	12.30	11.30	82.48
5	0.541	0.0933	4.60	11.50	9.90	84.61
6	0.660	0.0915	3.20	9.30	7.50	88.24

Table 2. Results from Wang's Theory

Case #	α	γ	$\hat{D}_W$ cm	Q_W cc/sec	$\hat{C}_W$ cm	coning (%)	Error in Q_W (%)
1	0.743	0.0956	2.067	10.592	6.40	100.00	41.23
2	0.635	0.0956	2.938	15.982	9.10	100.00	50.77
3	0.568	0.0956	3.487	18.968	10.80	100.00	64.94
4	0.450	0.0956	4.424	22.842	13.70	100.00	85.71
5	0.541	0.0933	3.778	16.123	11.70	100.00	40.20
6	0.660	0.0915	2.869	11.937	8.84	100.00	28.36

Table 3. Results from Muskat's Theory

Case #	α	γ	$\hat{D}_M$ cm	Q_M cc/sec	$\hat{C}_M$ cm	coning (%)	Error in Q_M (%)
1	0.743	0.0956	2.309	8.653	5.35	83.59	15.37
2	0.635	0.0956	3.802	12.752	7.60	83.46	20.30
3	0.568	0.0956	4.617	14.007	8.84	81.84	21.80
4	0.450	0.0956	6.465	15.863	10.71	68.20	28.97
5	0.541	0.0933	4.394	13.069	9.31	79.56	13.64
6	0.660	0.0915	3.232	11.564	7.15	83.32	24.34

critical discharge obtained by the three methods for cases 1 through 4. The comparison indicates the following points:

1) Wang's theory always overestimates the critical discharge. This departure from the experimental results is more conspicuous at smaller values of α than at larger values. Wang's theory, however, can be expected to predict a reasonable value of critical discharge at very large values of α. This can be explained as follows. Production from a well with a shallower penetration results in a steeper critical cone. When the brine cone is not too steep, the vertical flow components near the well are relatively less significant. In such a case, the Ghyben-Herzberg relation, which is the basis of Wang's theory, is not too serious an approximation. Therefore, the critical discharge computed by using Wang's skimming-well formula shows relatively better agreement with the experimental

values for wells with deeper penetration. On the other hand, in a case of shallow-well penetration, the cone beneath the well is relatively steep. The vertical flow components, especially in the immediate vicinity of the well, cannot be neglected in this case and the Ghyben-Herzberg approximation is no longer valid. The resistance to flow due to much stronger convergence toward the well affects the potential field in the flow region. This explains why a more conspicuous departure of Wang's predictions from the experimental results occurs at relatively smaller values of α.

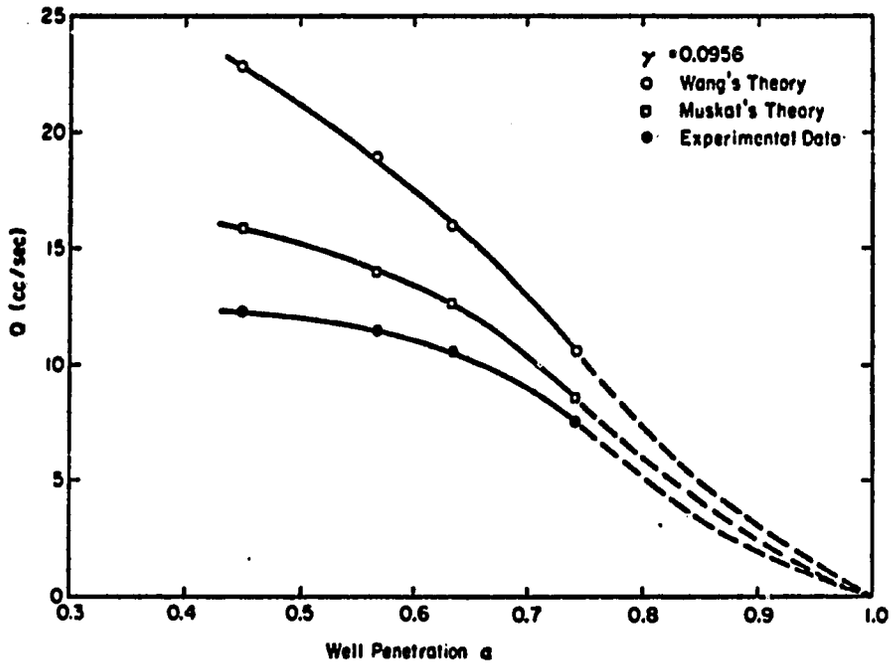

Figure 20. Comparison of theoretical critical discharge with the experimental results.

Further, it would seem possible to explain why Wang's theory always overestimates the critical discharge regardless of the value of α by the fact that Wang's analysis assumes that a stable brine cone could reach the

bottom of the well for a certain drawdown, called the critical drawdown, and remain there in static equilibrium. With this assumption, the critical drawdown is computed from the Ghyben-Herzberg relation as that drawdown for which the coning below the well is equal to the height of the bottom of the well above the original position of the interface. This value of drawdown is in turn used to calculate the critical discharge. Experiments have shown beyond doubt that, in fact, the cone does become unstable before it can rise to the bottom of the well. Therefore, one would expect that the value of the critical drawdown used in Wang's analysis should always be greater than the actual critical drawdown which in turn results in an overestimation of critical discharge by Wang's formula. However, this argument is not complete. It would be true only if the actual height of the cone was related to the drawdown exactly as predicted by equation (73). In reality this is not the case. In fact, it has been verified by experiments that the actual mounding is much less than that predicted by equation (73). As a result, even if it were physically possible for a stable cone to rise to the bottom of the well, the drawdown for that case would be much less than that calculated from equation (73). From Tables 1, 2, and 3, it is observed that each value of $\hat{D}_W$ is greater than the corresponding value of $\hat{D}_E$ but less than $\hat{D}_M$. Furthermore, the value of critical discharge Q_W is greater than Q_E and also Q_M for each case even though $\hat{D}_M$ is greater than $\hat{D}_W$. It

is concluded, therefore, that the use of Kozeny's formula for computing discharge in Wang's theory seems questionable. It is important to note that in the derivation of Kozeny's formula it was assumed that

1. the aquifer is confined,
2. the lower boundary is fixed and flat, so that the aquifer is of uniform thickness which remains constant, and
3. the aquifer is saturated with only one fluid throughout.

None of these conditions exist in the case which is the subject of investigation in Wang's analysis and the present study.

2) Muskat's analysis of the coning problem is also only an approximate one. The potential distribution in this technique is obtained from the formulas which assume that the lower boundary of the flow region is horizontal and remains fixed. Thus the perturbation in the potential field due to the rise of the interface is not taken into account. Further, these formulas also assume a uniform flux density at all points on the surface of a well partially penetrating into the aquifer. This is not true in the rigorous sense, However, Muskat's analysis does consider the important physical phenomenon of the instability of the rising cone beneath the well. This has been explained in detail in earlier sections. Table 3 shows that the height of the critical cone, that is, the highest stable cone beneath the well, as computed by Muskat's method, is always less than the height of the

bottom of the well. Also, the critical discharge calculated by this method is in much better agreement with the experimental values than are the results obtained from Wang's formula as illustrated by Figure 19.

Thus, both methods of analysis of the coning problem, namely those given by Wang and Muskat, are only approximate ones and both have their own limitations. Nevertheless, the results show that Muskat's analysis is more realistic than Wang's analysis.

Verification of the Results of Computer Analysis

As explained before, the basic difference between Muskat's analysis and the mathematical model developed in this study is that whereas in the former analysis the perturbation in the potential field resulting from the rise of the lower boundary cannot be taken into account, the latter does consider it by employing an iterative procedure. In that sense the analysis made by the present mathematical model continues from where Muskat's analysis stops. The fact that the theoretical model presented in this study does accomplish this objective is illustrated by the following two examples. Each case is analyzed by employing Muskat's approach, computer simulation, and the physical model.

Example 1. The aquifer properties and the well geometry studied in this example are the same as in Case 5 in Tables 1, 2, and 3.

In the computer analysis of this case, first some reasonable value for critical drawdown was assumed and the problem solved for the potential distribution by the iterative procedure as explained earlier. The graphical analysis was performed using the computed potential distribution for the assumed drawdown. If the line corresponding to this drawdown intersects the $\Delta H/(\Delta H)_e$ vs. $\bar{z}/H_e$ curve in two points, it means the drawdown assumed is subcritical for this case; if it is tangent to the curve the drawdown is critical; if it does not meet the curve at any point, the assumed value of drawdown is over-critical. If the critical condition was not arrived at in the first trial, the drawdown was changed and the procedure repeated. Generally four to five trials are sufficient to obtain the critical condition. For the sake of brevity only the results obtained for three drawdowns including the critical, one subcritical and one over-critical, are described here.

Tables C-1, C-2 and C-3 in Appendix C represent the computations for three drawdowns of 4.00 cm, 4.50 cm, and 4.65 cm respectively. Figures 21, 22, and 23 show the graphical analysis of these three conditions. The results of this analysis are presented in Table 4, where $\hat{D}_N$, Q_N, and $\hat{C}_N$ denote critical drawdown, discharge and coning, respectively. This analysis shows that a drawdown of 4.00 cm is subcritical and that of 4.65 cm is over-critical. The critical drawdown is 4.50 cm and the apex of the critical cone

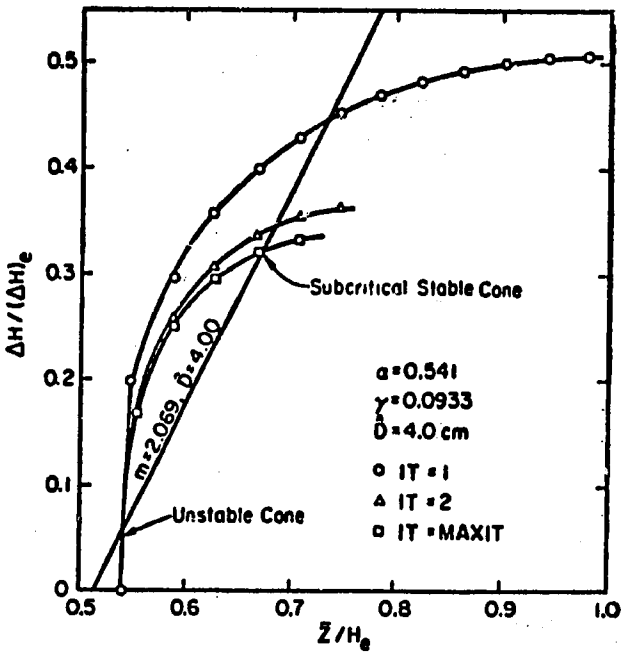

Figure 21. Numerical analysis for Case 5 (I).

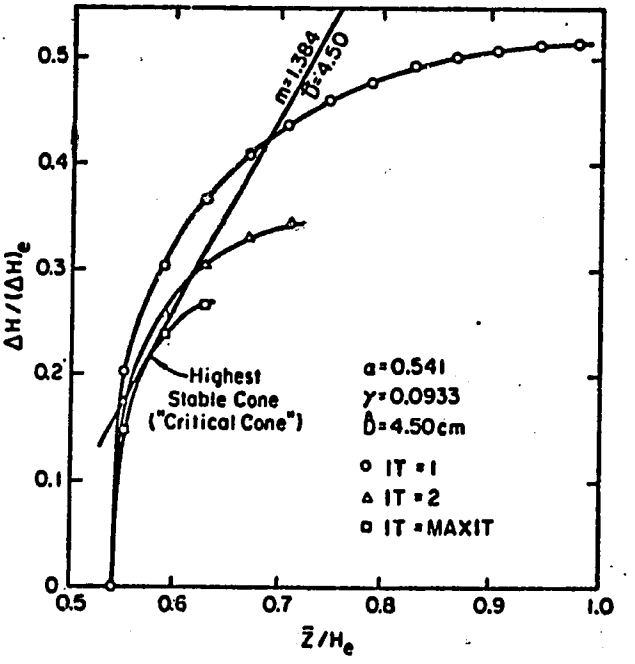

Figure 22. Numerical analysis for Case 5 (II).

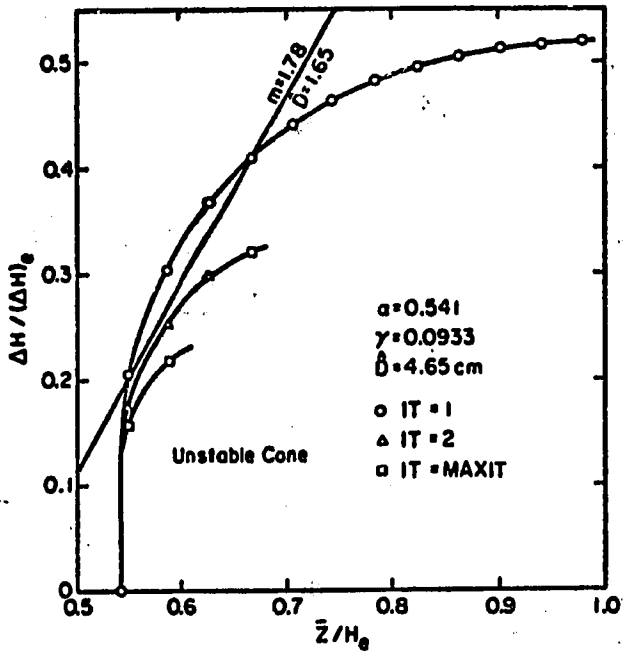

Figure 23. Numerical analysis for Case 5 (III).

is at a depth of 10.14 cm below the original free surface. The critical discharge is calculated at 12.38 cc/sec for the 15° sector of the entire flow region around the well. Experimentally, the depth of the highest stable cone was found to be 9.90 cm for a drawdown of 4.60 cm. The corresponding critical discharge of 12.38 cc/sec is different from the experimental value of 7.65%.

Table 4. Results from Numerical Model

Case #	α	γ	$\tilde{D}_N$ cm	Q_N cc/sec	$\hat{C}_N$ cm	coning %	Error in Q_N (%)
5	0.541	0.0933	4.50	12.379	10.14	86.67	7.65
6	0.660	0.0915	3.15	9.973	8.06	91.18	7.24

In order to get a composite picture, the position of the free surface and the interface were also computed at a number of distances from the well-axis. The data for the critical conditions are given in Table C-4 in Appendix C. The corresponding experimental data are given in Table D-1 in Appendix D. Figure 24 shows a comparison of the computed depths of the free surface and the interface with the experimental values.

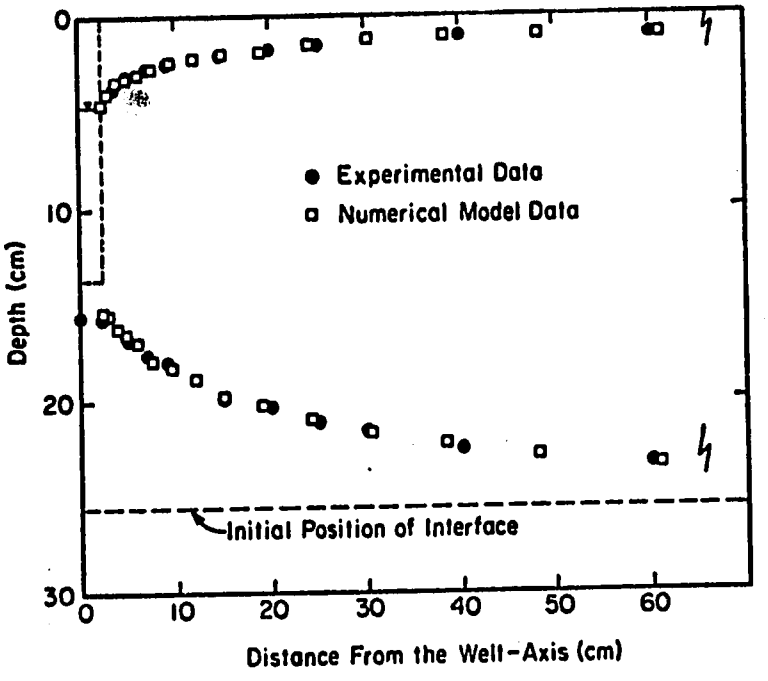

Figure 24. Location of free surface and interface for critical conditions in Case 5.

Example 2. The situation described here deals with case 6 studied in the physical model and also by Wang's and Muskat's methods. The same procedure was followed as in Example 1. The computations made by using Muskat's formula are given in Table 3 and the analysis thereof in Figure 19. According to this analysis the critical drawdown

should be 3.23 cm, the apex of the critical cone should be at a height of 7.15 cm above the initial position, and the discharge for this case should be 11.564 cm/sec. The potential distribution computed using the numerical model for three different values of drawdown is presented in Tables C-5, C-6 and C-7 and the corresponding graphical analyses in Figures 25, 26, and 27. This analysis predicts the location of the apex

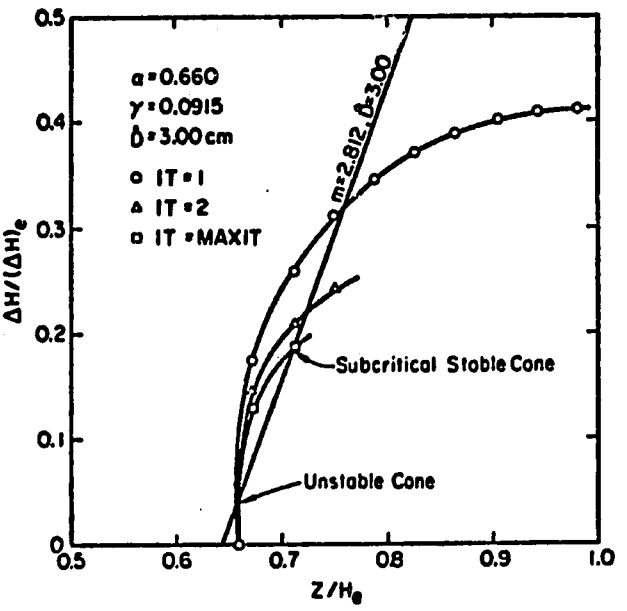

Figure 25. Numerical analysis for Case 6 (I).

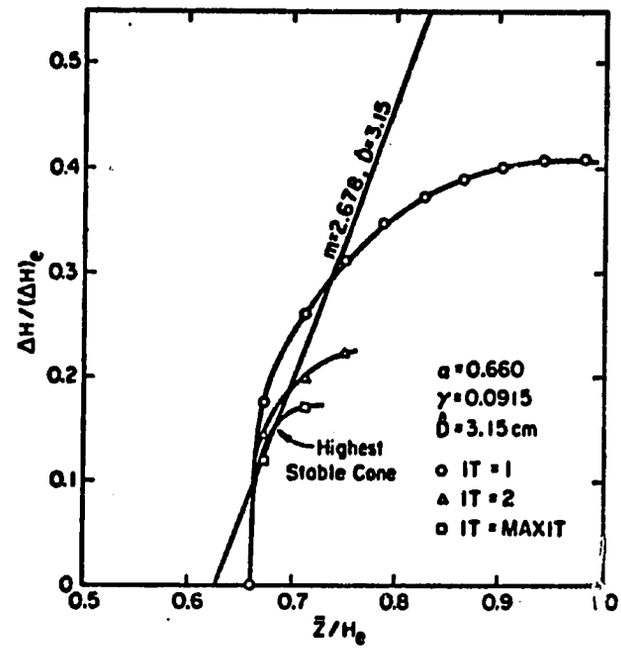

Figure 26. Numerical analysis for Case 6 (II)

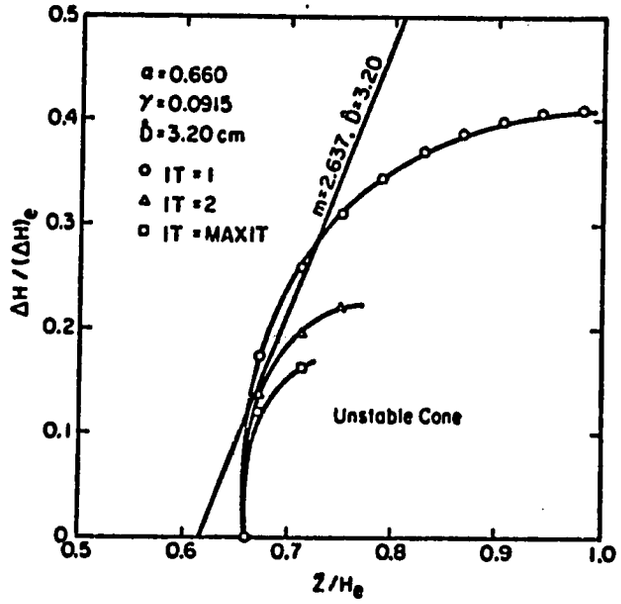

Figure 27. Numerical analysis for Case 6 (III).

of the critical cone at a height of 8.06 cm for a drawdown of 3.15 cm and the corresponding critical discharge of 9.973 cc/sec. The experiments showed an actual coning below the well under critical conditions of 7.50 cm for a drawdown of 3.20 cm and a discharge of 9.30 cc/sec. The computed value of critical discharge is thus in error by 7.24% for this case. A comparison of the location of the interface and the free surface as obtained from numerical data and experimental data for this case is shown in Figure 28.

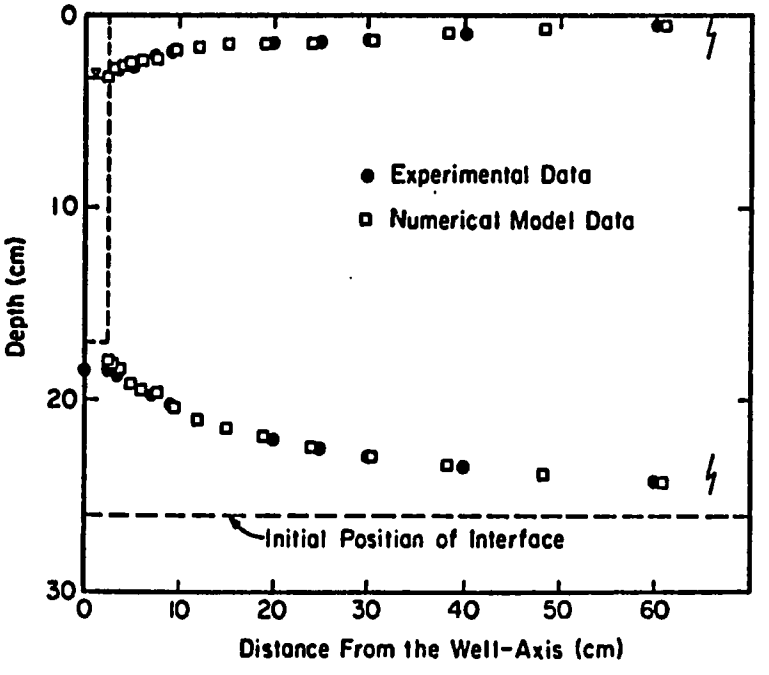

Figure 28. Location of free surface and interface for critical conditions in Case 6.

The above two examples show that the results obtained from the numerical model are in better agreement with the experimental results as compared to those obtained by following Muskat's approach, which in turn is more realistic than Wang's model. The mathematical model developed in this study, therefore, is expected to yield more accurate and realistic results as compared to the two existing theoretical models.

Application of the Mathematical Model

Having checked the validity of the model developed in this study, the model is then used to analyze a number of possible field situations with regard to:

1. thickness of the fresh-water zone,
2. hydraulic properties of the aquifer material,
3. densities of fresh water and saline water,
4. radius of the skimming well,
5. depth of penetration of the well, and
6. radius of influence of the well.

Twenty different situations have been studied. In each case the critical drawdown, position of the interface below the well, and the maximum fresh water production were determined using the procedure explained earlier. On the average, four trial runs were made for each case in order to arrive at the critical conditions.

The potential distribution data generated by each computer run for each case considered were analyzed graphically to check whether the drawdown for a particular case in question was critical or not. However, all the computations and graphical analyses for the entire set of all computer runs are not presented here. Instead, only the final results for the critical condition for each of the twenty cases are discussed.

In order to derive a more meaningful inference from the above results, all the important variables were transformed into dimensionless parameters and the results were expressed in the form of interrelationships among these dimensionless parameters. This has the advantage that the results would then not only apply to the twenty cases studied, but to a much wider range of field situations since a large variety of combinations of various variables involved could produce similar results in the dimensionless form. With this in view, the following dimensionless groups are selected:

1. well-penetration

$$\alpha = \frac{PW}{H_e} \tag{77}$$

2. well-slimness

$$\gamma = \frac{r_w}{H_e} \tag{78}$$

3. effective radius of influence

$$\dot{L} = \frac{r_e}{H_e} \tag{79}$$

4. drawdown at the well

$$\dot{D} = \frac{\rho_f (H_e - H_w)}{\Delta\rho \; H_e} \tag{80}$$

5. dimensionless discharge

$$\dot{Q} = \frac{\rho_f Q}{\Delta\rho \; H_e^2 \; K} \tag{81}$$

6. specific capacity

$$\dot{S} = \frac{Q}{K \; H_e \; (H_e - H_w)} \tag{82}$$

The reason for the choice of the first three parameters listed above is obvious. The dimensionless parameter for drawdown follows readily from equation (20) which is written in the dimensionless form. The dimensionless parameter for discharge listed above was arrived at as follows:

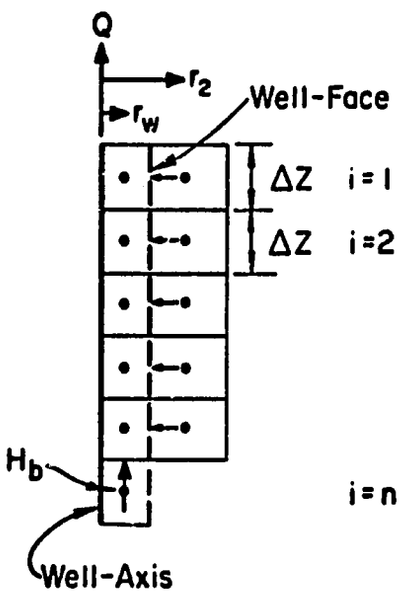

Figure 29. The producing well and the adjoining grids.

A consideration of flow into the well from all the grids surrounding the well such as in Figure 29, shows that by mass balance the total well discharge is given by

$$Q = \sum_{i=1}^{n} Q_{ri} + Q_z \tag{83}$$

where Q_{ri} is the radial flow crossing the well face from adjoining grid i and Q_z is the vertical upward flow into the well from the grid just below the well-bottom.

Applying Darcy's law at the well face, the total radial flow into the well is given by

$$Q_r = 2\pi K \int_{z_n}^{z_1} \left(\frac{\partial H}{\partial \ell nr}\right)_w dz \qquad (84)$$

where $(\partial H/\partial \ell nr)_w$ is the derivative of head with respect to the natural logarithm of radial distance evaluated at r_w; and z_n and z_1 are the elevations of the grids n and 1 respectively.

However, since it is difficult to evaluate the integral in equation (84), its approximate value $\sum_{i=1}^{n} Q_{ri}$ could be used which can be written as

$$Q_{ri} = 2\pi K \sum_{i=1}^{n} \frac{H_i - H_w}{\Delta \ell nr} \cdot \Delta z \qquad (85)$$

where H_i is the head in grid i and H_w that in the well, Δz is the thickness of grid i and $\Delta \ell nr = \ell nr_2 - \ell nr_w = \lambda$ (a dimensionless number).

Assuming Δz is the same for all grids, and since $\Delta \ell nr$ is a constant, equation (85) can be written as

$$Q = \frac{2\pi K}{\lambda} \Delta z \sum_{i=1}^{n} (H_i - H_w) + K\pi(2r_w)^2 \frac{H_b - H_w}{\Delta z}$$

$$= \frac{2\pi K}{\lambda} \Delta z (H_e - H_w) \sum_{i=1}^{n} \frac{H_i - H_w}{H_e - H_w} + 4\pi K r_w^2 \frac{(H_e - H_w)}{\Delta z} \frac{H_b - H_w}{H_e - H_w} . \qquad (86)$$

Multiplying the above equation through by $\rho_f/\Delta\rho \; H_e^2 K$ it becomes

$$\frac{\rho_f Q}{\Delta\rho\, H_e^2 K} = \frac{2\pi}{\lambda}\left(\frac{\Delta z}{H_e}\right)\left(\frac{H_e - H_w}{H_e}\right)\sum_{i=1}^{n}\frac{H_i - H_w}{h_o - h_w}$$

$$+ 4\pi\left(\frac{r_w}{H_e}\right)^2\left(\frac{H_e - H_w}{\Delta z}\right)\left(\frac{H_b - H_w}{H_e - H_w}\right) \qquad (87)$$

It is now readily seen that every term in equation (87) is in dimensionless form. Hence, a dimensionless parameter for discharge could be defined as

$$\dot{Q} = \frac{\rho_f Q}{\Delta\rho\, H_e^2 K}$$

The dimensionless parameter for specific capacity (i.e., discharge for unit drawdown) can be obtained as follows:

$$\dot{S} = \frac{\dot{Q}}{\dot{D}}$$

$$= \frac{\rho_f Q}{\Delta\rho\, H_e^2 K} \Bigg/ \frac{\rho_f (H_e - H_w)}{\Delta\rho\, H_e}$$

$$= \frac{Q}{K H_e (H_e - H_w)}$$

The results of the computer analysis of the twenty cases mentioned earlier are expressed in the form of the above dimensionless groups in Tables C-9 through C-12 in Appendix C. The interrelationships of these dimensionless variables are presented in Figures 30, 31, 33, and 34.

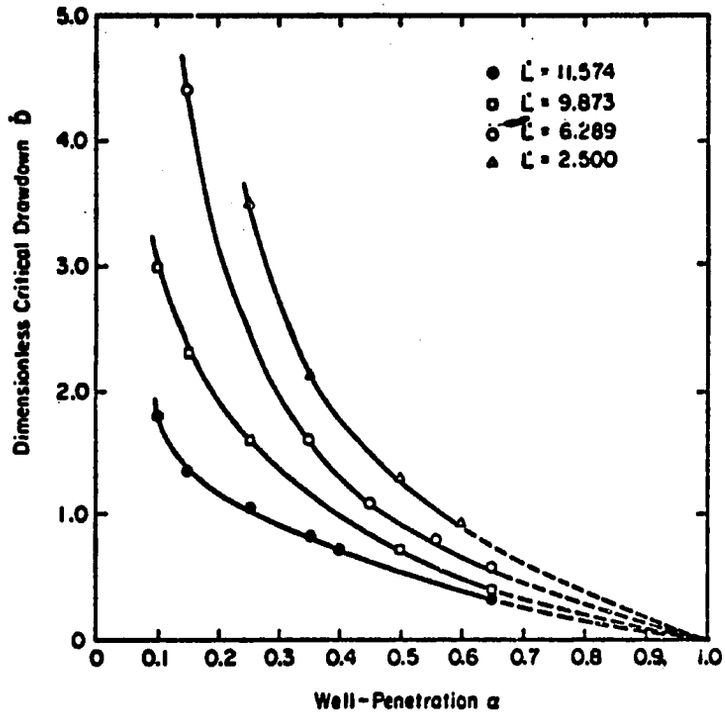

Figure 30. Variation of critical drawdown with well penetration.

The following inferences are drawn from the data shown in these figures:

1) For a given fresh-water thickness, the critical drawdown increases rapidly as the well penetration α becomes small, and the rate of this increase is much faster for greater fresh-water thickness H_e.

2) The critical drawdown becomes infinitesimal as α approaches 100%, that is, as the bottom of the producing well approaches the initial position of the interface. This implies that when the well penetrates very deep, even a small drawdown at the well is sufficient to produce unstable conditions causing the cone to break through the well.

3) The dimensionless critical drawdown $\dot{D}$ versus well-penetration α curves tend to become asymptotic at very small values of α depending on the $\dot{L}(=r_e/H_e)$ value. This means that at such small values of α the critical drawdown approaches infinity. Furthermore, the curves become asymptotic at relatively larger values of α for smaller values of $\dot{L}$. This implies that for a given set of conditions, as the well penetration α is continually decreased, eventually a situation arrives when the critical drawdown does not exist. In other words, no cone is critical regardless of the value of drawdown at the well. This finding is in agreement with the prediction of Muskat's theory.

4) It is also observed from Figure 31 that for a given value of α, the dimensionless critical drawdown $\dot{D}$ decreases as the ratio $\dot{L}$ increases and the rate of change in $\dot{D}$ becomes increasingly pronounced as α decreases, especially at very large values of $\dot{L}$.

5) Furthermore, it is interesting to note that for a given α, the analysis predicts a higher critical cone for larger values of $\dot{L}$ (Tables C-9 through C-12).

The physical meaning of the inferences 4 and 5 is explained as follows. Consider two situations referred to as case (a) and case (b) in Figure 32, where the fresh-water thickness, well-penetration, and all other conditions are the same except that in case (b), the radius of influence r_e is much greater than in case (a). Assume that

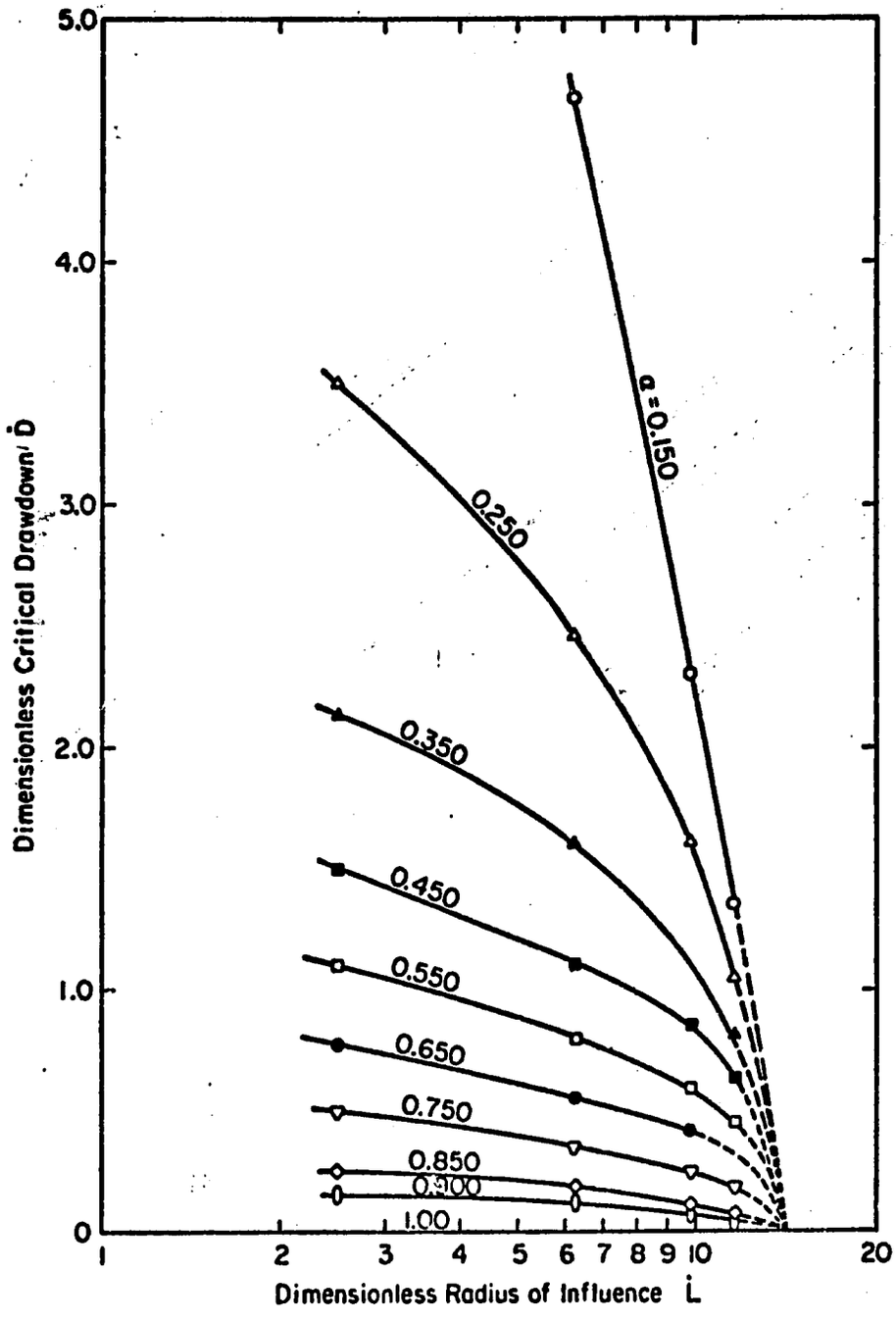

Figure 31. Dimensionless critical drawdown versus dimensionless radius of influence of the well.

the production rates are such that the height h_c of the stable cone below the well is the same in both cases. Obviously, the convergence of the

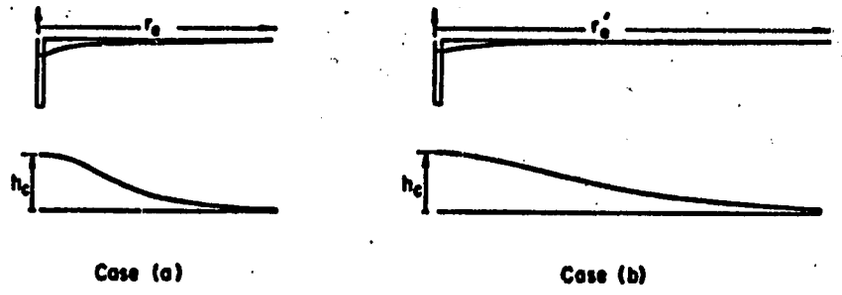

Figure 32. Explanation of the effect of radius of influence of the well on the critical drawdown and coning.

streamlines toward the well will be much stronger in case (a) than in case (b). This should result in a greater drawdown in case (a). Furthermore, if h_c were the critical cone height in case (b), then because of larger vertical pressure gradients in case (a), the cone beneath the well would become unstable before it could rise by an amount h_c. This explains why the critical drawdown is greater and the critical cone height smaller in a situation such as in case (a) than in a situation like case (b).

6) The above discussion leads to another important conclusion, that a greater drawdown at the well is not always necessarily accompanied by a greater cone-rise beneath the well. The Ghyben-Herzberg relation is, therefore, not always a conservative one with regard to the location of the interface as it is usually thought to be.

7) Another significant point brought out by Figure 31 is that all the $\dot{D}$ versus $\dot{L}$ curves for various values of α, on extrapolation seem to converge to the same point (0, 14.5). This implies that as r_e/H_e is increased, $\dot{D}$ continually decreases and approaches an infinitesimal value at about $r_e/H_e = 14.5$.

8) Figure 33 presents the variation of dimensionless critical discharge $\dot{Q}$ with well penetration for various values of r_e/H_e. A comparison of these curves leads to the conclusion that for a given α $\dot{Q}$ increases as $\dot{L}$ decreases and that this increase becomes more pronounced as $\dot{L}$ decreases. The nature of this variation is in general agreement with the findings of Bennett, et. al. (1).

It is also significant to note that the $\dot{Q}$ vs. α curves show maxima at small values of α (approximately 10 to 20%) depending on the value of $\dot{L}$. Furthermore, it does not seem possible that these curves pass through the origin as predicted by Wang's analysis. This becomes clear from the fact that at certain values of α, a $\dot{D}$ vs. α curve becomes asymptotic (Figure 30) and that for well penetration less than this value a critical condition does not exist. Therefore, the function $\dot{Q}$ does not exist and the $\dot{Q}$ vs. α curves cannot be continuous through the origin as predicted by Wang's theory.

It is also important to note that the critical discharge is not directly proportional to the drawdown as assumed by Wang's analysis.

Figure 34 represents the dimensionless critical specific capacity $\dot{S}$ versus well penetration α for various values of γ and $\dot{L}$. It shows

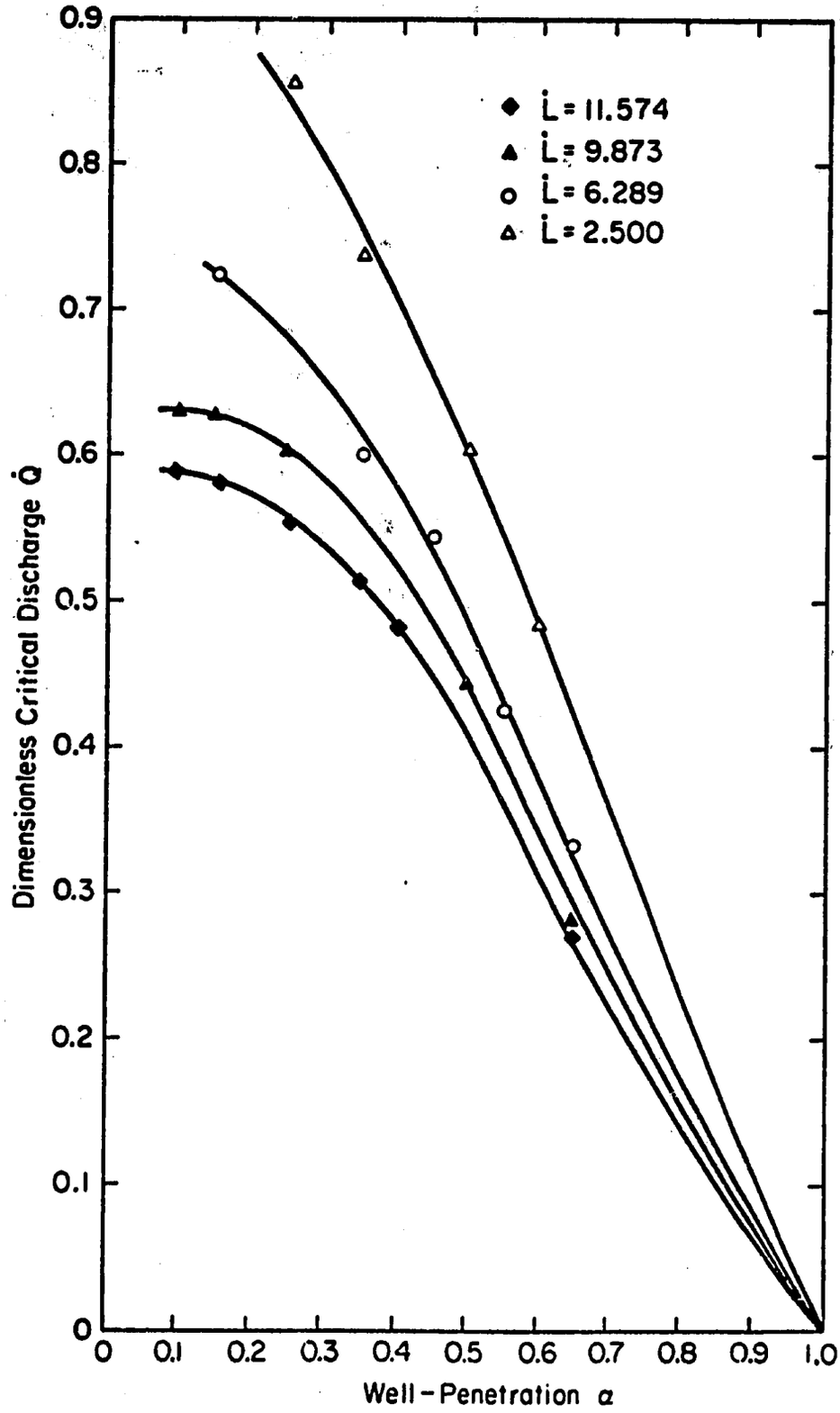

Figure 33. Dimensionless critical discharge versus well penetration.

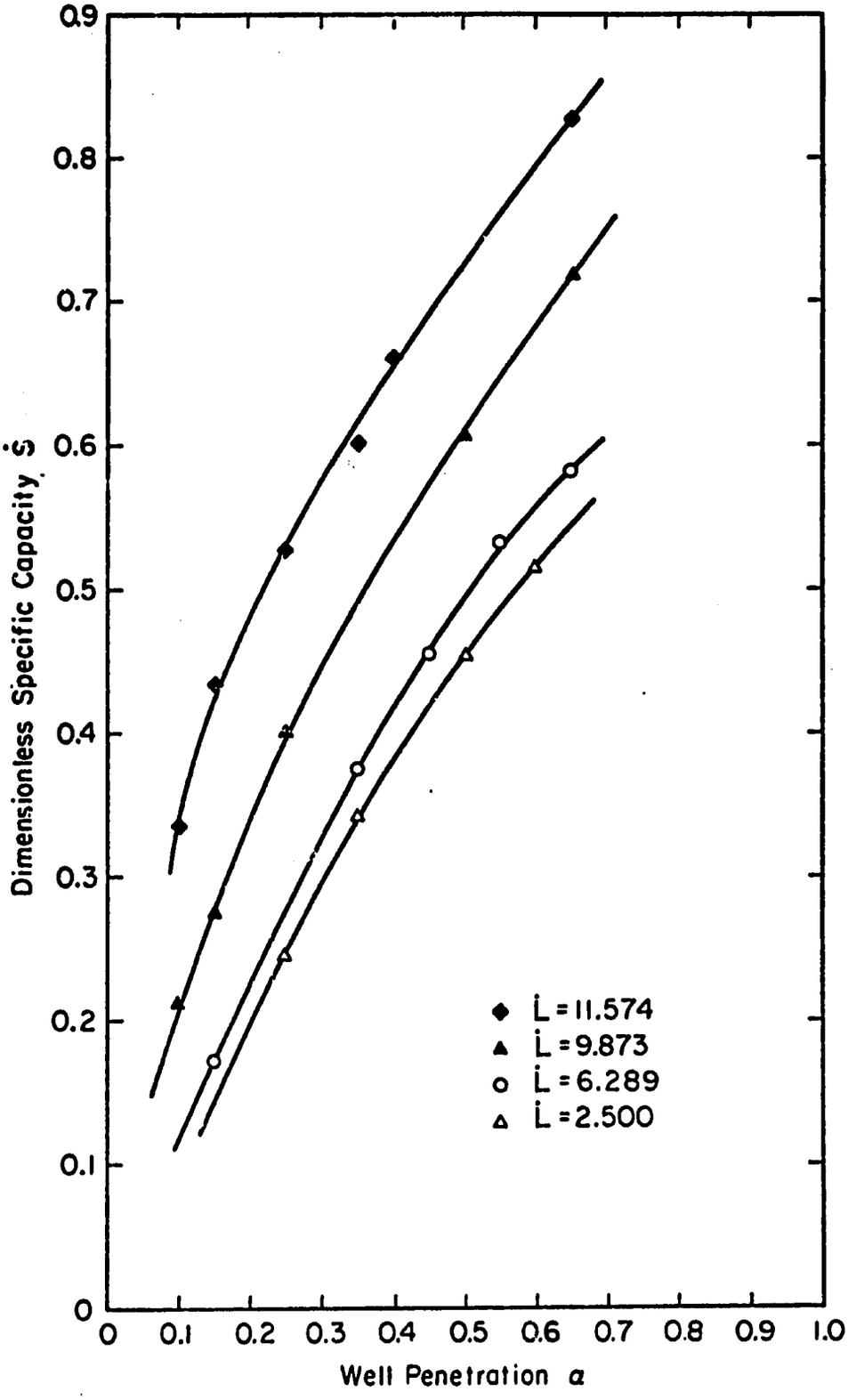

Figure 34. Dimensionless critical specific capacity versus well penetration.

that $\dot{S}$ increases as α increases and that at a given value of α, $\dot{S}$ increases as $\dot{L}$ increases.

Application of Results and their Limitations

The following example illustrates how the results of this study may be used to indicate the optimum practical conditions with regard to a skimming well in the field in order to get maximum fresh water without entrainment of salt water. Consider a case in which

H_e = 200 feet

r_e = 1250 feet

K = 0.002 cfs per sq. ft.

$\Delta\rho/\rho_f$ = 0.015

and it is desired to study the performance of a skimming well 0.7 foot in radius.

Using the nomograms in Figures (30) and (33), a dimensionless critical drawdown of about 4.425 feet and a dimensionless maximum permissible discharge of 0.75 are obtained at α = .150 for this case. Therefore,

$$\hat{D} = 4.425\ (\Delta\rho H_e)$$

$$= 13.28 \text{ feet}$$

and

$$Q = 0.75\ (H_e^2 K \Delta\rho)$$

$$= 0.90 \text{ cfs or } 403.9 \text{ gpm.}$$

The optimal depth of penetration in this case is 30 feet. Thus, the well should be screened from 13 to 30 feet below the water table. It should be noted that it has been assumed in this analysis that the recharge in the area is sufficient to result in a steady-state and that the "well-losses" are negligible. If the area under consideration does not have sufficient recharge, the well should be pumped at a smaller rate than suggested above in order to avoid depletion of the aquifer. The second assumption of negigible well-losses requires that the velocity of flow into and within the well be very small, which in turn may require a smaller pumping rate and a larger well radius than those in the present example.

Another important point that must be considered while using the results of the present study is that it has been assumed that a distinct interface exists at all times between the fresh water and the underlying saline water. The effects of diffusion and dispersion have been neglected. Therefore, it is possible that at a critical drawdown predicted by this study the well in the field may produce water with slight salinity, depending on the vertical thickness of the dispersion zone and the vertical gradient of salt concentration within this zone. It would, therefore, in general be safer to suggest a pumping rate somewhat lower than that predicted by this study. It should further be pointed out that the results of this study are applicable to homogeneous and isotropic aquifers.

Thus, some of the assumptions used in this study might place certain restrictions on the practical utility of the results. Nevertheless, the method appears to have considerable value in the sense that it is more realistic in approach than the existing analytic methods.

CONCLUSIONS AND REDOMMENDATIONS

The phenomenon of salt-water coning below a fresh-water skimming well was studied both theoretically and experimentally. The experimental part of the study gave a better insight into the physics of the phenomenon and helped check the validity of the existing analytic solutions and of the mathematical model developed in this study.

The following conclusions were drawn from the results of this work.

1. The salt water rises in the form of a cone in response to pumping of a skimming well with its apex vertically below the well. Under steady-state conditions the cone rises until its apex reaches a certain height depending on the drawdown at the well. However, in every field situation there is a drawdown, called "critical" in this study, at which the highest stable cone can occur. If the drawdown exceeds this value, the cone becomes unstable. As a result, the cone keeps rising and eventually the well starts producing saline water. This occurs when the production rate is such that the velocity of fresh water flow along the interface exceeds the maximum value $\Delta\rho K/\rho_f$ which can exist without flow in the underlying brine.

2. Regardless of the well geometry and the aquifer and fluid properties, the highest stable cone can never rise as high as the bottom of the well-screen. This is in agreement with Muskat's predictions and the findings of Bennett, et. al. (1) based on their electric analog studies. Thus, the phenomenon of instability of the rising cone is confirmed beyond doubt with the help of the electric analog and physical models as well as the mathematical model.

3. Both Wang's theory as well as Muskat's theory are based on assumptions some of which are questionable. The former assumes that

   (a) Ghyben-Herzberg relation is valid,

   (b) Kozeny's formula for discharge from a partially penetrating well in a confined aquifer with a fixed lower boundary can be used for the case of an unconfined aquifer with the interface between two fluids as its lower boundary,

   (c) discharge is directly proportional to drawdown,

   (d) maximum uncontaminated discharge occurs with the apex of the brine cone just at the bottom of the well.

The present study shows that none of these assumptions, particularly (d), is valid in the phenomenon of coning

beneath a skimming well. However, under certain limited conditions, for example, for very deep well-penetration, when the cone is not too steep, Wang's formulas can yield reasonably reliable predictions. Muskat's analysis is more realistic than Wang's in the sense that the former does consider the phenomenon of instability and, therefore, recognizes the fact that the highest stable cone always occurs with its apex at a lower elevation than the bottom of the well.

4. The mathematical model presented in this study takes into consideration the non-linearity of the boundary conditions. That is, it takes into account the fact that while the potential distribution depends on the position of the lower and upper boundaries, the positions of these boundaries in turn depend on the potential distribution. Hence, an iterative procedure was used to arrive at a solution. The validity of this mathematical model was checked by comparing the results obtained therefrom with the experimental results and those obtained by using Muskat's approach. The results of the mathematical model showed better agreement than Muskat's analysis with the experimental results. The results obtained by using this mathematical model are summarized as follows.

(a) For a given fresh-water thickness, the maximum permissible drawdown increases rapidly, especially for greater fresh-water thickness, as the well penetration decreases. At very small penetrations, the critical drawdown approaches infinity.

(b) For a given fresh-water thickness and well penetration, the critical drawdown decreases and the coning increases as the radius of influence of the well increases.

(c) For a given radius of influence of the well, the dimensionless critical discharge rapidly increases as well penetration decreases, especially at very shallow penetrations.

(d) The $\dot{Q}$ versus α curves show maxima in the neighborhood of 10% to 20% well penetration. For the same cases Wang's analysis shows maxima at well penetrations of about 33% to 41%. Also, the results of this study show that the dimensionless critical discharge versus well penetration curves tend to become flat at these maxima and do not pass through the origin, whereas, the maxima predicted by

Wang's theory are also the points of inflexion of the curves which pass through the origin. Physically, it implies that for given aquifer and fluid properties and well geometry, there exists a well penetration such that the critical conditions cannot occur at shallower penetrations than this value.

(e) The results of this analysis lead to some interferences which are of practical significance with regard to designing a skimming well procedure. It has been shown that under a given set of field conditions the maximum fresh water discharge is obtained with well penetrations much smaller than those predicted by analytical skimming well formulations available at present.

(f) Other conditions being equal, the critical conditions occur at greater production rates for smaller radii of influence of the wells. Furthermore, although it has been shown that the mounting is not directly proportional to the drawdown, nevertheless, smaller mounding occurs for smaller drawdown. Therefore, if

several wells are pumped together to give the same fresh water production collectively as could be obtained from a single well under critical conditions according to the results of this study, the mounding so produced will be less than critical. It is, therefore, possible to get more production of fresh water without getting salt water in the wells when a battery of larger number of wells is used. However, a quantitative inference to this effect could not be drawn from this analysis. When a group of skimming wells are operated with the help of a single suction pump, their closer spacing would be more economical even from the installation point of view.

It is suggested that while applying the results presented in this Dissertation to a field situation, their limitations should be taken into account. The "entrance losses" at the well and the thickness of the dispersion zone have been considered negligible in this analysis. Also, the results apply to homogeneous and isotropic aquifers and to steady-state conditions.

The results presented in this work are intended to indicate the conditions under which a stable cone can exist and the critical

conditions beyond which the cone becomes unstable. It has been shown that the maximum uncontaminated fresh water production occurs as the critical conditions are approached. However, it is not intended to suggest that this alone should be the objective in using skimming wells to pump fresh water. Sometimes it may be more economical and practical to pump at lower rates.

Also, in some situations an entrainment of some brine along with fresh water may not be as undesirable as in some other situations. If the underlyind saline water is not of very poor quality, it may be desirable to pump the well at a higher rate than critical as long as the quality of the water produced is within tolerable limits, depending on the use it is intended for. Hence, while making a decision with regard to the rate of pumping various factors such as water quality in the aquifer, the tolerable limits of salinity, amount of recharge available in the area, and economics of the operation must also be taken into account.

Further study is required to analyze several aspects of the phenomenon of coning. The utility of the nomograms presented in this Dissertation can be increased by considering a wider range of possible situations. It would be worth-while to study the effect of dispersion on the maximum fresh water production predicted in this study. Finally, the mathematical model presented here should be further generalized by considering the effects of heterogeneity and anisotropy with regard to the hydraulic properties of the aquifer.

REFERENCES

1. Bennett, G. D., Mundorff, M. J., and Hussain, S. Amjad, "Electric-analog studies of brine coning beneath fresh-water wells in the Punjab region, West Pakistan", U. S. Geol. Survey Water-Supply Paper 1608-J, 1968.

2. Botset, H. G., "The electrolytic model and its application to the study of recovery problems", Trans., AIME, Vol. 165, 15, 1946.

3. Bradley, H. B., Heller, J. P., and Odeh, A. S., "Potentiometric study of the effects of mobility ratio on reservoir flow pattern", Trans., AIME, Vol. 222, II-125, 1961.

4. Brooks, R. H., and Corey, A. T., "Hydraulic properties of porous media", Colorado State University, Fort Collins, Colorado, Hydrology Paper No. 3, March, 1964.

5. Bruce, W. A., "An electrical device for analyzing oil-reservoir behavior", Trans., AIME, Vol. 151, 318, 1943.

6. Carman, P. C., "Flow through granular beds", Trans., Inst. Chem. Eng., London, Vol. 15, 150, 1937.

7. Caudle, B. H., "Laboratory model of oil reservoirs produced by natural water drive", Ph.D. Dissertation, University of Texas, August, 1963.

8. Charmonman, S. C., "A solution of the pattern of fresh-water flow in an unconfined coastal aquifer", Jl. Geop. Res., Vol. 70, No. 12, 2813, 1965.

9. _____, "Effectiveness of an artificial fresh-water barrier in the alleviation of the effects of salt-water intrusion", Ph.D. Dissertation, Georgia Institute of Technology, Atlanta, 1964.

10. _____, "A numerical method of solution of free surface problems", Jl. Geop. Res., Vol. 71, No. 16, 3861, 1966.

11. Dagan, G., and Bear, J., "Solving the problem of local interfact upconing in a coastal aquifer by the method of small perturbations", Jl. Hydr. Res., Vol. 6, No. 1, 15, 1968.

12. Geertsma, J., Croes, G. A., and Schwartz, N., "Theory of dimensionally scaled models of petroleum reservoirs", Trans., AIME, Vol. 207, 118, 1956.

13. Henley, D. H., Owens, W. W., and Craig, F. F., "A scaled model study of bottom-water drives", Jl. of Pet. Tech., Vol. 13, 90, Jan., 1961.

14. Hubbert, M. K., "The theory of ground-water motion", Jl. of Geol., Vol. 48, 785, 1940.

15. Karp, J. C., Lowe, D. K., and Marusov, N., "Horizontal barriers for controlling water coning", Jl. of Pet. Tech. 14, 783, July, 1962.

16. Khan, A. R., "Scaled model studies of thin oil columns produced by natural water drive", Ph.D. Dissertation, University of Texas, Austin, January, 1968.

17. Letkeman, J. P., and Ridings, R. L., "A numerical coning model", Soc. Pet. Eng. Jl., Vol. 10, 418, Dec., 1970.

18. Linsley, R, K., Kohler, M. A., and Paulhus, J. L. H., Hydrology for Engineers, McGraw Hill Book Company, 1958.

19. MacDonald, R. C., and Coats, K. H., "Methods for numerical simulation of water and gas coning", Soc. Pet. Eng. Jl., Vol. 10, 425, 1970.

20. Meyer, H. L., and Gardner, A. O., "Mechanics of two immiscible fluids in porous media", Jl. of Appl. Phys., 1400, Nov., 1954.

21. Muskat, M. and Wyckoff, R. D., "An approximate theory of water-coning in oil production", Trans., AIME, Vol. 114, 144, 1935.

22. Muskat, M., Flow of Homogeneous Fluids, J. W. Edwards, Ann Arbor, Michigan, 1965.

23. _____, "Potential distribution in large cylindrical disks with partially penetrating electrodes", Physics, Vol. 2, 329, May, 1932.

24. _____, "The performance of bottom-water drive reservoirs", Trans., AIME, Vol. 170, 81, 1947.

25. _____, "Theory of potentiometric models", Trans., AIME, Vol., 179, 216, 1949.

26. Polubarinova-Kochina, P. Ya. (English translation from Russian by DeWiest, R. J. M.), Theory of Ground Water Movement, Princeton Univ. Press, Princeton, New Jersey, 1962.

27. Rapoport, L. A., "Scaling laws for use in design and operation of water-oil flow models", Trans., AIME, Vol. 204, 143, 1955.

28. Schmorak, S., and Mercado, A., "Upconing of fresh water-sea water interface below pumping wells, field study," Water Resources Research, Vol. 5, No. 6, 1290, 1969.

29. Smith, C. R., "Water coning control in oil wells by fluid injection", Ph.D. Dissertation, University of Texas, 1962.

30. Smith, C. R., and Pirson, S. J. "Water coning control in oil wells by fluid injection", Soc. Pet. Eng. Jl., Vol. 228, 314, 1963.

31. Sobocinski, D. P., and Cornelius, A. J., "A correlation for predicting water coning time", Jl. of Pet. Tech., Vol. 17, 594, May, 1965.

32. Soengkowo, I., "Model studies of water coning in petroleum reservoirs with natural water drive", Ph. D. Dissertation, University of Texas, Austin, 1969.

33. Stallman, R. W., "Electric analog of three-dimensional flow to wells and its application to unconfined aquifers", U. S. Geol. Survey Water-Supply Paper 1536-H, 1963.

34. Stephen, A. C., "A model study of bottom-water drive performance", M.S. Thesis, University of Texas, Austin, August, 1962.

35. Todd, D. K., Ground Water Hydrology, John Wiley & Sons, New York, Sixth Printing, 1966.

36. Walton, W. C., Groundwater Resources Evaluation, McGraw-Hill Book Company, 1970.

37. Wang, F. C., "Approximate theory for skimming well formulation in the Indus Plain of West Pakistan", Jl. Geop. Res., Vol. 70, No. 2, 5055, 1965.

38. West, T. S., "A gravel pack completion for exclusion of gas and water", Trans., AIME, Vol. 192, 183, 1951.

39. Wyllie, M. R. J., and Spangler, M. B., "Applications of electrical resistivity measurements to problems of flow in porous media", Bull., Am. Assoc. Pet. Geol., Vol. 36, 359, 1952.

40. Youngs, E. G., "Optimum pumping conditions for wells located in unconfined coastal aquifers", Jl. Hydrology, Vol. 13, 63, 1971.

41. _____, "Seepage through unconfined aquifers with lower boundaries of any shape", Water Resources Res., Vol. 7, No. 3, 624, June, 1971.

APPENDICES

APPENDIX A - COMPUTER PROGRAMS

```
      PROGRAM POTEN1 (INPUT,OUTPUT,TAPE5=INPUT,TAPE6=OUTPUT)

C        CALLING PROGRAM FOR SIMPSON'S RULE INTEGRATION
C        DEFINE INTEGRAND FOR SIMPSON'S RULE INTEGRATION
      DIMENSION W(30),A(30),B(30),C(30),D(30),YA(30),YAL(30),YB(30),
     1YBL(30),YC(30),YCL(30),YD(30),YDL(30),TSUM(30)

      COMMON CX
      EXTERNAL ARG
      READ (5,1)X
    1 FORMAT(F7.5)
      WRITE(6,4)
    4 FORMAT(1H1,3X,'W',7X,'TSUM')
      A(1)=1.+X
      B(1)=A(1)
      C(1)=1.-X
      D(1)=C(1)
      W(1)=0.00
      GL=0.00001
      DO 10 I=2,26
      K=I-1
      W(I)=W(K)+.02
      A(I)=A(K)+.02
      B(I)=B(K)-.02
      C(I)=C(K)-.02
      D(I)=D(K)+.02
   10 CONTINUE
      DO 20 I=1,26
      CX=A(I)
      YA(I)=SIMPSN(ARG,GL,999.,.0001)
      YAL(I)=ALOG(ABS(YA(I)))
      CX=B(I)
      YB(I)=SIMPSN(ARG,GL,999.,.0001)
      YBL(I)=ALOG(ABS(YB(I)))
      CX=C(I)
      YC(I)=SIMPSN(ARG,GL,999.,.0001)
      YCL(I)=ALOG(ABS(YC(I)))
      CX=D(I)
      YD(I)=SIMPSN(ARG,GL,999.,.0001)
      YDL(I)=ALOG(ABS(YD(I)))
      TSUM(I)=-YAL(I)-YBL(I)+YCL(I)+YDL(I)
      WRITE(6,2)(W(I),TSUM(I))
    2 FORMAT(1H0,1X,F4.2,2X,F10.5)
   20 CONTINUE
      CALL EXIT
      END
```

```
      FUNCTION ARG(X)
      COMMON C
      ARG=X**(C-1.)*EXP(-X)
      X2=EXP(-X)
      X1=X**(C-1.)
      RETURN
      END

      FUNCTION SIMPSN(ARG,Y1,Y2,FERR)
C     SIMPSN INTEGRATION ROUTINE WRITTEN AS FORTRAN IV FUNCTION
      DIMENSION F2T(20),FMT(20),F3T(20),F4T(20),FBT(20),
     1DXT(20),X1T(20),X2T(20),ART(20),EPST(20),ES2T(20),
     2ES3T(20),LEG(20),SUM1(20),SUM2(20)
      COMMON C
C     INITIAL SET-UP
      A=Y1
      EPS=FERR
      B=Y2
      DA=B-A
      FA=ARG(A)
      FM=4.*ARG((A+B)*.5)
      FB=ARG(B)
      AREA=1.0
      EST=1.0
      L=1
C     BEGIN SIMPSON
    1 DX=DA/3.
      X1=A+DX
      X2=X1+DX
      F1=4.*ARG(A+.5*DX)
      F2=ARG(X1)
      F3=ARG(X2)
      F4=4.*ARG(A+2.5*DX)
      DX6=DX/6.
      EST1=(FA+F1+F2)*DX6
      EST2=(F2+F4+F3)*DX6
      EST3=(F3+F4+FB)*DX6
      AREA=AREA-ABS(EST)+ABS(EST1)+ABS(EST2)+ABS(EST3)
      SUM=EST1+EST2+EST3
C     TEST FOR CONVERGENCE
      IF(ABS(EST-SUM)-EPS*AREA)2,2,3
    2 IF(EST-1.0)5,3,6
    3 IF(L-20)5,6,6
    5 L=L+1
      LEG(L)=3
C     STORE PARAMETERS FOR SIMPSON II AND III
      F2T(L)=F2
      FMT(L)=FM
      F3T(L)=F3
      F4T(L)=F4
      FBT(L)=FB
      DXT(L)=DX
      X1T(L)=X1
```

```
      X2T(L)=X2
      ART(L)=AREA
      EPST(L)=EPS/1.7
      ES2T(L)=EST2
      ES3T(L)=EST3
C     RETURN TO SIMPSON I
      DA=DX
      FM=F1
      FB=F2
      EST=EST1
      EPS=EPST(L)
      GO TO 1
    6 IF(LEG(L)-2)9,8,7
    7 SUM1(L)=SUM
      LEG(L)=2
C     RETURN TO SIMPSON II
      A=X1T(L)
      DA=DXT(L)
      FA=F2T(L)
      FM=FMT(L)
      FB=F3T(L)
      AREA=ART(L)
      EST=ES2T(L)
      EPS=EPST(L)
      GO TO 1
    8 SUM2(L)=SUM
      LEG(L)=1
C     RETURN TO SIMPSON III
      A=X2T(L)
      DA=DXT(L)
      FA=F3T(L)
      FM=F4T(L)
      FB=FBT(L)
      AREA=ART(L)
      EST=ES3T(L)
      EPS=EPST(L)
      GO TO 1
    9 SUM=SUM1(L)+SUM2(L)+SUM
      L=L-1
      IF(L-1)11,11,6
   11 SIMPSN = SUM
      RETURN
      END
```

```
      PROGRAM POTEN2 (INPUT,OUTPUT,TAPE5=INPUT,TAPE6=OUTPUT)

C     CALCULATION OF NATURAL LOG OF (A*C)/(B*D) WHERE A=W+X AND B=W-X
C     RO=RADIAL DISTANCE FROM THE WELL DIVIDED BY TWICE THE THIKNESS OF
C     FRESH WATER AT THE RADIUS OF INFLUENCE.
C     W=DEPTH FROM TOP DIVIDED BY TWICE THE THIKNESS OF FRESH WATER AT
C     THE RADIUS OF INFLUENCE.
C     X=DEPTH OF PENETRATION OF WELL DIVIDED BY TWICE THE THICKNESS OF
C     FRESH WATER AT THE RADIUS OF INFLUENCE.
      DIMENSION W(30),P(30)

      READ(5,1) RO,X
    1 FORMAT(2F10.5)
      ROS=RO**2.0
      MAXLIN=24
      IMAX=26
      I=1
    5 WRITE(6,2)
    2 FORMAT(1H1/)
      WRITE(6,3)
   10 Y=FLOAT(I)
      W(I)=Y*.02-.02
      A=W(I)+X
      B=W(I)-X
      C=SQRT(ROS+A**2.0)
      D=SQRT(ROS+(ABS(B))**2.0)
      E=(A*C)/(B*D)
      P(I)=ALOG(ABS(E))
      WRITE(6,4)W(I),P(I)
      I=I+1
      IF(I.GT.IMAX) GO TO 20
      IF (I.GE.MAXLIN) GO TO 5
      GO TO 10
    3 FORMAT(1H0,3X,*W*,9X,*P*)
    4 FORMAT(1H0,1X,F4.2,4X,F8.4)
   20 CALL EXIT
      END
```

```
      PROGRAM POTEN3 (INPUT,OUTPUT,TAPE5=INPUT,TAPE6=OUTPUT)

      DIMENSION W(30)
      READ(5,6) RO,X
    6 FORMAT(2F10.5)
      ROS=RO**2.0
      READ(5,1) N
    1 FORMAT(I5)
      READ(5,2) (W(I),I=1,26)
    2 FORMAT(8F10.2)
      DO 3 I=1,26
      SUM=0.0
      W1=W(I)
      IF(W1.GT.X) GO TO 3
      DO 4 J=1,N
      DN=J-1
      A=1.0/(DN+1.0-X-W(I))**2
      B=1.0/(DN+1.+X-W(I))**2
      C=1.0/(DN+1.0-X+W(I))**2
      D=1.0/(DN+1.+X+W(I))**2
    4 SUM=SUM-A+B-C+D
      TSUM=SUM
      TSUM1=TSUM*0.25*ROS
      WRITE(6,5) I,TSUM,TSUM1
    5 FORMAT(//10X,I2,F15.5,5X,F15.7)
    3 CONTINUE
      END
```

```
      PROGRAM DISCHRG (INPUT,OUTPUT,TAPE5=INPUT,TAPE6=OUTPUT)

C     COND IS CONDUCTIVITY OF THE AQUIFER MATERIAL TO THE FLUID
C       BEING SKIMMED (L/T).
C     D1 IS THE DRAWDOWN AT THE WELL (L).
C     RW IS THE RADIUS OF THE WELL (L).
C     HE IS THE THICKNESS OF THE FLOW REGION ABOVE THE INTERFACE
C       PRIOR TO PUMPING (L).
C     PW IS THE WELL PENETRATION (L).
C     Q IS WELL DISCHARGE FOR A 15 DEGREE SEGMENT OF THE ENTIRE
C       FLOW REGION AND IS 1/24 OF THE TOTAL DISCHARGE (VOL./TIME).

      READ (5,1) COND,RW,RE,HE,PW,D1
    1 FORMAT(6F10.3)
      ALPHA=PW/HE
      BETA=SQRT(RW/(2.*HE*ALPHA))
      GAMMA=RW/HE
      XMU=5.2832*COND*HE*ALPHA*D1
      XNU=COS(1.5708*ALPHA)
      XI=ALOG(RE/PW)
      Q=(XMU*(1.+7.*BETA*XNU))/(24.*XI)
      WRITE(6,2) ALPHA,GAMMA,Q
    2 FORMAT(1H ,5X,*ALPHA=*,F6.4,5X,*GAMMA=*,E10.4,5X,
     1*DISCHARGE=*,F10.3)
      CALL EXIT
      END
```

```
      PROGRAM CONING (INPUT,OUTPUT,TAPE5=INPUT,TAPE6=OUTPUT)
      DIMENSION P(33,20), JIN(19), ZETA(33,19), JS(19), ZW(19), H(33,20)
     1, OSU4(5,19), DIFQ(5,19)
      COMMON T(532,19),RHS(532),KBOUN(33,20),COND(33,20),R(33,20),DELR2,
     1HF,HW,NC,NCWEL,JP3,JP1,CONST,NR1,NC1,DELZ(33,20),NU,NCW,Z(33,20),D
     2EL71,DELZ2
      INTEGER ETA
      REAL JIN
      NRJ=532
      NCT=19
      J=2
      I=2
      READ (5,65) PB,ETA,RHOF,RHOS,CONDS,NC
      READ (5,66) RW,RE,Z1,HE,HW,NR
      READ (5,67) D1,PW,JD1,JP1,NCWEL,RJEX
      READ (5,68) IC,MAXIT,EPS,DELZ1,DELZ2
      JD3=JD1+1
      JP3=JP1+1
      NCW=NCWEL+1
      NCW2=NCWFL+2
      NCW3=NCWEL+3
      PI=3.1416
      NC1=NC+1
      NR1=NR+1
      NC2=NC1+1
      DO 1 I=2,NR1
    1 READ (5,69) (KBOUN(I,J),J=2,NC2)
      RALPHA=PW/HE
      GAMA=RW/HE
C     ...  PRINT INPUT DATA.
      WRITE (6,70) PB,ETA,RHOF,RHOS,CONDS,NC,RW,RE,Z1,HE,HW,NR,D1,PW,JD1
     1,JP1,NCWEL,RJEX,IC,DELZ1,DELZ2,ALPHA,GAMA,MAXIT,EPS
C
C     CALCULATION OF HORIZONTAL DISTANCE OF GRIDS.
C     RADIUS MEASURED TO THE BOUNDARIES OF THE GRIDS.
C     CONST=RADIUS OF THE FIRST COLUMN.
      CONST=RW
      I=2
      R(I,2)=CONST
      R(I,NC1)=RE
      RLN=ALOG(CONST)
      TC=NC1
      DRLN=(ALOG(RE)-ALOG(CONST))/(TC-2.0)
      DO 2 I=3,NC2
      RLN=RLN+DRLN
    2 R(I,J)=EXP(RLN)
```

```
      DO 3 I=3,NR1
      DO 3 J=2,NC2
    3 R(I,J)=R(I-1,J)
      WRITE (6,71) ((R(I,J),J=2,NC2),I=2,NR1)
C     DELR1=DISTANCE BET. COLS. J=NC AND J=NC1.
C     DELR2=DISTANCE BET. COLS. J=NC1 AND J=NC2.
      DELR1=R(2,NC1)-R(2,NC)
      DELR2=R(2,NC2)-R(2,NC1)
C
C
C     COMPUTE THE ELEVATION Z(I,J) OF THE CENTER OF GRID(I,J).
      J=2
      Z(2,J)=Z1
      IC1=IC+1
      DO 7 I=3,NR1
      IF (I.GT.IC) GO TO 4
      Z(I,J)=Z(I-1,J)-DELZ1
      GO TO 7
    4 IF (I.EQ.IC1) GO TO 5
      GO TO 6
    5 Z(I,J)=Z(I-1,J)-(DELZ1+DELZ2)*0.5
      GO TO 7
    6 Z(I,J)=Z(I-1,J)-DELZ2
    7 CONTINUE
      DO 8 J=3,NC1
      DO 8 I=2,NR1
    8 Z(I,J)=Z(I,J-1)
      WRITE (6,72) ((Z(I,J),J=2,NC1),I=2,NR1)
C
C
C     INITIALISE THE PRESSURE HEAD AND CONDUCTIVITY IN EACH GRID. IT IS
C     ASSUMED THAT PRIOR TO PUMPING TOTAL HEAD IS SAME EVERYWHERE AND
C     EQUAL TO HE.
      DO 10 I=2,NR1
      DO 10 J=2,NC1
      H(I,J)=HE
      P(I,J)=H(I,J)-Z(I,J)
      IF (P(I,J).LT.PB) GO TO 9
      COND(I,J)=CONDS
      GO TO 10
    9 COND(I,J)=CONDS*((PB/P(I,J))**ETA)
   10 CONTINUE
C
C
C     COMPUTE FLOW COEFFICIENTS USING MOST RECENTLY CALCULATED VALUES
C       OF CONDUCTIVITY.
C
      IT=1
C
      KITN=NP1
   11 CALL TCOEF
C
C
      N=NU
      NCOF=NC1
      NCM=NC
C
C
      CALL SOSOLV (T,RHS,N,NCOF,NCM,DET,QUAD,ISUM,EPS,IPRNT1,IPRNT2,IREA
     1D,NRJ,NCT)
C
C
      WRITE (6,73)
      IF=0
      DO 17 I=2,NR1
      DO 17 J=2,NC2
```

```
      KB=KBOUN(I,J)
      GO TO (12,13,14,15), KB
   12 H(I,J)=0.0
      GO TO 16
   13 H(I,J)=HE
      GO TO 16
   14 H(I,J)=HW
      GO TO 16
   15 IK=IK+1
      H(I,J)=RHS(IK)
   16 CONTINUE
   17 CONTINUE
      WRITE (6,74) ((H(I,J),J=2,NC2),I=2,NR1)
C
C     .... CALCULATE PRESSURE DISTRIBUTION.
      DO 21 J=2,NC1
      DO 20 I=2,NR1
      P(I,J)=HE
      IF (J.LE.NCW.AND.I.LE.JD1) GO TO 18
      GO TO 19
   18 P(I,J)=0.0
      GO TO 20
   19 P(I,J)=H(I,J)-Z(I,J)
   20 CONTINUE
   21 CONTINUE
C
C     ... LOCATE FREE SURFACE.
      DO 27 J=2,NC1
      DO 26 I=2,JD3
      IF (J.LE.NCW) GO TO 22
      GO TO 23
   22 JS(J)=JD1
      WRITE (6,75) J,JS(J)
      GO TO 27
   23 IF (P(I-1,J).LE.0.0.AND.P(I,J).GE.0.0) GO TO 24
      GO TO 26
   24 IF (ABS(P(I-1,J)).GT.ABS(P(I,J))) GO TO 25
      JS(J)=I-1
      WRITE (6,75) J,JS(J)
      GO TO 27
   25 JS(J)=I
      WRITE (6,75) J,JS(J)
      GO TO 27
   26 CONTINUE
   27 CONTINUE
C
      DO 33 J=2,NC1
      IF (J.LE.NCW) GO TO 28
      GO TO 29
   28 ZW(J)=HW
      GO TO 33
   29 IF (P(I,J).NE.0.0) GO TO 30
      ZW(J)=Z(I,J)
      GO TO 33
   30 DO 32 I=2,JD3
      IF (P(I,J).LT.0.0) GO TO 32
      IF (P(I,J).GT.0.0.AND.P(I-1,J).LT.0.0) GO TO 31
      GO TO 32
   31 DELP=P(I,J)-P(I-1,J)
      ZW(J)=Z(I,J)+(P(I,J)*DELZ(I,J)/DELP)
      GO TO 33
   32 CONTINUE
   33 CONTINUE
      IF (IT.EQ.MAXIT) WRITE (6,76) (ZW(J),J=2,NC1)
```

```
C
C     ...  CALCULATE THE POSITION OF THE INTERFACE ON THE BASIS OF HOST
C      RECENT HEAD DISTRIBUTION.JIN IS THE NUMBER OF THE ROW IN WHICH
C      THE INTERFACE FALLS IN COLUMN J AND ZETA IS THE EXACT ELEVATION
C      OF THE INTERFACE.
C
      WRITE (6,77)
      WRITE (6,78)
      J=2
      IF (IT.EQ.1) GO TO 34
      GO TO 35
   34 RN1=NR1
      JIN(J)=RN1
      GO TO 36
   35 KJIN=JIN(J)
      RN1=KJIN
      JIN(J)=RN1
   36 I1=JS(J)
      IZETA=0
      DO 40 II=I1,KJIN
      I=KJIN+I1-II
      ZETA(I,J)=(RHOF/(RHOS-RHOF))*(HE-H(I,J))
      DZETA=ZETA(I,J)
      IF (ZETA(I,J).LE.Z(I-1,J).AND.ZETA(I,J).GE.Z(I,J)) GO TO 37
      GO TO 40
   37 IF (ZETA(I,J).NE.Z(I,J)) GO TO 38
      JIN(J)=FLOAT(I)
      IZETA=1
      GO TO 41
   38 IF (ZETA(I,J).NE.Z(I-1,J)) GO TO 39
      JIN(J)=FLOAT(I)-1.0
      IZETA=1
      GO TO 41
   39 JIN(J)=NR1-((ZETA(I,J)-Z(NR1,J))/DELZ(I,J))
      IZETA=1
      GO TO 41
   40 CONTINUE
   41 CONTINUE
      IF (IZETA.EQ.1) WRITE (6,79) J,JIN(J),DZETA
      IF ((IZETA.EQ.0).AND.(JIN(J).EQ.RN1)) WRITE (6,79) J,JIN(J),DZETA
      J=J+1
      IF (J.GT.NC1) GO TO 42
      IF (IT.GT.1) GO TO 35
      GO TO 34
   42 CONTINUE
C
C     ROUND THE NUMBRS. IN JIN. IF JIN IS EVEN ROUND IT TO THE LOWER
C      INTEGER, IF ODD, ROUND IT TO NEXT HIGHER NUMBER. INT AND AINT
C      ARE SYSTEM SUBROUTINES FOR TRUNCATION.
      DO 45 J1=2,NC1
      D=JIN(J1)
      N=INT(D)
      IF ((D).GE.0.0).AND.(D.LE.0.50)) GO TO 44
      IF (D.LT.0.0) GO TO 44
      RN1=AINT(D)
      R1=D-RN1
      IF (MOD(N,2).NE.0) GO TO 43
      IF (R1.GT.0.50) N=N+1
      GO TO 44
   43 IF (R1.GE.0.50) N=N+1
   44 JIN(J1)=N
      WRITE (6,80) D,JIN(J1)
   45 CONTINUE
C
```

```
C
C     ... CALCULATE CONDUCTIVITY BASED ON NEW PRESSURE DISTRIBUTION.
C
C       FIRST SET CONDUCTIVITY IN ALL GRIDS BELOW THE INTERFACE EQUAL
C      TO ZERO.
      J=2
   46 KJIN=JIN(J)
      KJN1=KJIN+1
      IF (KJIN.EQ.NR1) GO TO 48
      DO 47 IK=KJN1,NR1
   47 COND(IK,J)=0.0
   48 J=J+1
      IF (J.GT.NC1) GO TO 49
      GO TO 46
   49 CONTINUE
C
      DO 55 J=2,NC1
      KJIN=JIN(J)
      DO 54 I=2,KJIN
      IF (J.LE.NCW.AND.I.LT.JD1) GO TO 51
      IF (J.LE.NCW.AND.I.EQ.JD1) GO TO 50
      GO TO 52
   50 COND(I,J)=CONDS
      GO TO 54
   51 COND(I,J)=0.0
      GO TO 54
   52 IF (P(I,J).LT.PB) GO TO 53
      COND(I,J)=CONDS
      GO TO 54
   53 COND(I,J)=CONDS*((PB/P(I,J))**ETA)
   54 CONTINUE
   55 CONTINUE
C
C     ... DISCHARGE COMPUTATION.
      J=NC1
      KJIN=JIN(J)
      NJIN=KJIN-1
      QSUM(IT,J)=0.0
      DO 56 I=2,NJIN
      AVCOND=(COND(I,NC1)+COND(I,NC))/2.0
      AVR=R(I,NC)+0.5*DELR1
      Q=2.0*PI*AVR*DELZ(I,J)*AVCOND*((H(I,NC1)-H(I,NC))/DELR1)
      QSUM(IT,J)=QSUM(IT,J)+Q
   56 CONTINUE
      QSUM1=QSUM(IT,J)
      WRITE (6,81) IT,QSUM1
      IF (IT.EQ.1) GO TO 57
      DIFQ(IT,J)=ABS(QSUM(IT,J)-QSUM(IT-1,J))
      DIFQ1=DIFQ(IT,J)
      IF (DIFQ1.LE.EPS) GO TO 64
      GO TO 57
C
C     ... DEFINE THE NEW BOUNDARY CONDITIONS SUCH THAT HYDRAULICALLY DE
C      GRIDS ABOVE THE FREE SURFACE AND BELOW THE INTERFACE ARE
C      PROPERLY SIMULATED.
   57 DO 59 J1=2,NC1
      KJ1=JIN(J1)+1.0
      IF (KJ1.GT.NR1) GO TO 59
      DO 58 I1=KJ1,NR1
```

```
   58 KHOUN(I1,J1)=1
   59 CONTINUE
C
      J=NC1
      I1=JIN(J)
      IF (KHOUN(I1,J-1).NE.4) GO TO 60
      GO TO 61
   60 KHOUN(I1,J)=2
   61 CONTINUE
C
      RJEXM=RJEX-1.0
      DO 63 J1=2,NC1
      JSM=JS(J1)-1
      IF (JSM.LE.RJEXM) GO TO 63
      DO 62 I1=2,JSM
   62 KHOUN(I1,J1)=1
   63 CONTINUE
C
C     ... REPEAT THE CYCLE. IT DENOTES THE ITERATION NUMBER.
      IT=IT+1
      IF (IT.LE.MAXIT) GO TO 11
      GO TO 64
      QSUM1=QSUM(IT,J)
      WRITE (6,81) IT,QSUM1
   64 CONTINUE
      CALL EXIT
C
   65 FORMAT (F10.3,I10,3F10.3,I10)
   66 FORMAT (5F10.3,I10)
   67 FORMAT (2F10.3,3I10,F10.3)
   68 FORMAT (2I10,3F10.3)
   69 FORMAT (8I10)
   70 FORMAT (1H ,5X, 3HPB=,F10.3,3X, 4HETA=,I10,3X, 5HRHOF=,F10.3,3X
     1, 5HPHOS=,F10.3,3X, 6HCONDS=,F10.3,/,3X, 3HNC=,I10,3X, 3HRW=,F
     210.3,3X, 3HRE=,F10.3,3X, 3HZ1=,F10.3,3X, 3HHE=,F10.3,3X, 3HHW=
     3,F10.3,3X, 3HNR=,I10,/1X, 3HD1=,F10.3,3X, 3HPW=,F10.3,3X, 4HJD
     41=,I10,3X, 4HJP1=,I10,3X, 6HNCWEL=,I10,3X,/,3X, 5HRJEX=,F10.3,3
     5X, 3HIC=,I10,3X, 6HDELZ1=,F10.3,3X, 6HDELZ2=,F10.3,2X, 6HALPHA
     6=,F10.3,2X, 5HGAMA=,E10.3,2X, 6HMAXIT=,I10,2X, 4HEPS=,F10.5)
   71 FORMAT (10X,10F10.3)
   72 FORMAT (10X,10F10.3)
   73 FORMAT (1H0,5X, 17HHEAD DISTRIBUTION)
   74 FORMAT (1H0,5X,10F12.6)
   75 FORMAT (15X,2I15)
   76 FORMAT (1H ,5X,10F12.4)
   77 FORMAT (1H0,10X, 34HLOCATION OF INTERFACE IN THE MODEL)
   78 FORMAT (1H0,8X, 4HCOL.,10X, 3HROW,11X, 18HELEV. OF INTERFACE)
   79 FORMAT (1H0,I10,5X,E17.8,5X,E17.8)
   80 FORMAT (10X,2F20.3)
   81 FORMAT (1H0,10X, 3HIT=,I3,10X, 10HDISCHARGE=,E20.10)
      END
      SUBROUTINE TCOEF
      COMMON T(532,19),RHS(532),KHOUN(33,20),COND(33,20),R(33,20),DELR2,
     1HE,HW,NC,NCWEL,JP3,JP1,CONST,NR1,NC1,DELZ(33,20),NU,NCW,Z(33,20),D
     2ELZ1,DELZ2
C     ... INITIALISE THE COEFFICIENT MATRIX TO ZERO.
C     .. KOL IS THE NUMBER OF COLUMNS IN THE T MATRIX.
C
```

```
C
      IR=0
      NCOL=NC1
      DO 2 I=2,NR1
      DO 2 J=2,NC1
      IF (KBOUN(I,J).NE.4) GO TO 2
      IR=IR+1
      DO 1 KOL=1,NCOL
      RHS(IR)=0.0
    1 T(IR,KOL)=0.0
    2 CONTINUE
C
      IR=0
      DO 19 I=2,NR1
      DO 19 J=2,NC1
C
      Z(1,J)=Z(2,J)+DELZ1
      COND(1,J)=0.0
      R(1,J)=R(2,J)
      KBOUN(1,J)=1
      NR2=NR1+1
      Z(NR2,J)=-DELZ2*0.5
      R(NR2,J)=R(NR1,J)
      COND(NR2,J)=0.0
      KBOUN(NR2,J)=1
      Z(I,1)=Z(I,2)
      COND(I,1)=0.0
      R(I,1)=-CONST
      KBOUN(I,1)=1
      NC2=NC1+1
      Z(I,NC2)=Z(I,NC1)
      COND(I,NC2)=COND(I,NC1)
      KB=KBOUN(I,J)
      IF (KB.NE.4) GO TO 19
      A=0.0
      B=0.0
      C=0.0
      D=0.0
      E=0.0
      RHSIDE=0.0
      IR=IR+1
      JP1=J+1
      JM1=J-1
      IP1=I+1
      IM1=I-1
      DEL1=DELZ(I,J)
      DEL2=Z(I-1,J)-Z(I,J)
      DEL3=DELZ(I,J)
      DEL4=Z(I,J)-Z(I+1,J)
      C0=COND(I,J)
      C1=COND(I,JP1)
      C2=COND(IM1,J)
      C3=COND(I,JM1)
      C4=COND(IP1,J)
      R0=R(I,J)
      R1=R(I,JP1)
      R2=R(IM1,J)
      R3=R(I,JM1)
      R4=R(IP1,J)
      KB1=KBOUN(I,JP1)
      KB2=KBOUN(IM1,J)
```

```
      KB3=KBOUN(I,JM1)
      KB4=KBOUN(IP1,J)
C     ..
      IF (J.NE.2) GO TO 3
C
      R3=-CONST
      IF (I.EQ.IP3) C2=C0
      GO TO 4
    3 IF (J.NE.NC1) GO TO 4
      R1=R0+DEL2
      C1=C0
    4 CONTINUE
C     ..
C     ..... CALCULATE COEFFICIENT B BETWEEN GRIDS I,J AND I,J+1
      GO TO (7,5,7,6), KB1
    5 CONTINUE
C     ... CALCULATE COEFFICIENT B IF GRID I,J+1 IS A CONSTANT HEAD BOUN
      B=TTCOEF(C0,C1,C2,C3,C4,DEL1,DEL2,DEL3,DEL4,R0,R1,R2,R3,R4,1)
      RHSIDE=RHSIDE+B*HE
      E=E+B
      B=0.0
      GO TO 7
    6 CONTINUE
C     ... CALCULATE COEFFICIENT B IF GRID I,J+1 IS A USEABLE GRID.
      B=TTCOEF(C0,C1,C2,C3,C4,DEL1,DEL2,DEL3,DEL4,R0,R1,R2,R3,R4,1)
      E=E+B
      B=-B
    7 CONTINUE
C
C     ... CALCULATE COEFFICIENT C BETWEEN GRID I,J AND I-1,J.
      IF (I.EQ.2) GO TO 10
      IF (J.EQ.NC1.AND.KB3.EQ.1) GO TO 10
      GO TO (1 ,8,8,9), KB2
    8 CONTINUE
C     ... CALCULATE COEFFICIENT C IF GRID I-1,J IS A CONSTANT HEAD BOUN
      C=TTCOEF(C0,C1,C2,C3,C4,DEL1,DEL2,DEL3,DEL4,R0,R1,R2,R3,R4,2)
      RHSIDE=RHSIDE+C*HW
      E=E+C
      C=0.0
      GO TO 10
    9 CONTINUE
C     ... CALCULATE COEFFICIENT C IF GRID I-1,J IS A USEABLE GRID.
      C=TTCOEF(C0,C1,C2,C3,C4,DEL1,DEL2,DEL3,DEL4,R0,R1,R2,R3,R4,2)
      E=E+C
      C=-C
   10 CONTINUE
C
C     ... CALCULATE COEFFICIENT A BETWEEN GRIDS I,J AND I,J-1.
      IF (J.EQ.2) GO TO 13
      GO TO (12,11,11,12), KB3
   11 CONTINUE
C     ... CALCULATE COEFFICIENT A IF GRIDS I,J-1 IS A CONSTANT HEAD BOU
      A=TTCOEF(C0,C1,C2,C3,C4,DEL1,DEL2,DEL3,DEL4,R0,R1,R2,R3,R4,3)
      RHSIDE=RHSIDE+A*HW
      E=E+A
      A=0.0
      GO TO 13
   12 CONTINUE
C     ... CALCULATE COEFFICIENT A IF GRID I,J-1 IS A USEABLE GRID.
      A=TTCOEF(C0,C1,C2,C3,C4,DEL1,DEL2,DEL3,DEL4,R0,R1,R2,R3,R4,3)
      E=E+A
```

```
      A=-A
   13 CONTINUE
C     ... CALCULATE COEFFICIENT D BETWEEN GRIDS I,J AND I+1,J.
      IF (I.EQ.NR1) GO TO 15
      GO TO (15,15,15,14), KB4
   14 CONTINUE
C     ... CALCULATE COEFFICIENT D IF GRID I+1,J IS A USEABLE GRID.
      D=TTCOEF(C0,C1,C2,C3,C4,DEL1,DEL2,DEL3,DEL4,R0,R1,R2,R3,R4,4)
      E=E+D
      D=-D
   15 CONTINUE
C
C     .... STORE COEFFICIENTS IN THE COEFFICIENT MATRIX T.
C
C     ... STORE COEF.D
      III=I+1
      IF (III.GT.NR1) GO TO 18
      IF (KBOUN(III,J).NE.4) GO TO 18
      JUSE=NC1-J+1
      DO 16 JJ1=2,J
      IF (KBOUN(III,JJ1).NE.4) GO TO 16
      JUSE=JUSE+1
   16 CONTINUE
      JP2=JUSE
      IF (JP2.GT.2) GO TO 17
      GO TO 18
   17 T(IR,JP2)=D
   18 CONTINUE
      T(IR,1)=E
      T(IR,2)=R
      RHS(IR)=RHSIDE
   19 CONTINUE
C
      NU=IR
C     ... THE ABOVE VALUE OF NU IS THE NO. OF USEABLE GRIDS FOR THIS IT
      RETURN
C
      END
      FUNCTION TTCOEF(C0,C1,C2,C3,C4,DEL1,DEL2,DEL3,DEL4,R0,R1,R2,R3,R4,
     1ICOF)
C     ... CALCULATE THE COEFFICIENTS B,C,A,AND D FOR SUBROUTINE TCOEF.
C     ... NOTE THAT R3 WILL BE NEGATIVE FOR GRID- CLMN. J=2.
      PI=3.14159
      GO TO (1,2,3,4), ICOF
    1 TTCOEF=PI*(C1+C0)*DEL3/ALOG(R1/R0)
      RETURN
    2 TTCOEF=PI*(R1**2-R0**2)*(C2+C0)*0.5/DEL2
      RETURN
    3 TTCOEF=PI*(C3+C0)*DEL1/ALOG(ABS(R0/R3))
      RETURN
    4 TTCOEF=PI*(R1**2-R0**2)*(C4+C0)*0.5/DEL4
      RETURN
      END
      SUBROUTINE SOSOLV (T,RHS,N,NCOF,NCM,DET,QUAD,ISUM,EPS,IPRNT1,IPRNT
     12,IREAD,NRJ,NCT)
C
C     ...USE THE SQUARE ROOT METHOD TO SOLVE A SET OF
C        SIMULTANEOUS LINEAR EQUATION.
C
```

```
C
C                T = N BY NCOF REDUCED COEFFICIENT MATRIX.
C              RHS = N BY 1 RIGHT-HAND SIDE VECTOR.  THE SOLUTION VECTO
C                    IS STORED IN THIS VECTOR BEFORE RETURNING TO THE
C                    CALLING PROGRAM.
C                N = TOTAL NO. OF USABLE GRIDS (DOES NOT INCLUDE
C                    BOUNDARY GRIDS) IN THE MODEL FOR WHICH THE FLOW
C                    EQUATIONS ARE WRITTEN.
C             NCOF = NO. OF COLUMNS IN MATRIX T.
C              NCM = MAX. NO. OF USABLE COLUMN GRIDS.
C              DET = VALUE OF THE DETERMINANT FOR THE ORIGINAL
C                    COEFFICIENT MATRIX COMPUTED IN THIS SUBROUTINE.
C             QUAD = VALUE OF THE QUADRATIC FORM FOR THE ORIGINAL
C                    COEFFICIENT MATRIX B COMPUTED IN THIS SUBROUTINE.
C                    IF X IS THE SOLUTION VECTOR AND XA IS THE TRANSPOS
C                    OF X, THEN QUAD = XA*B*X.
C             ISUM = CODE 0 IF THE ORIGINAL COEFFICIENT MATRIX IS TRI-
C                    DIAGONAL OR IF THE SUMMATION TERM USED TO COMPUTE
C                    THE NEW OFF-DIAGONAL ELEMENTS IS ZERO (CODE 0 FOR
C                    THE TWO-DIMENSIONAL GROUND-WATER FLOW PROBLEM).
C                    OTHERWISE, CODE ISUM=1.
C              EPS = TOLERANCE VALUE FOR THE DIAGONAL ELEMENT (SUGGEST
C                    1.0E-5 AS A MAXIMUM VALUE).  IF THE DIAGONAL
C                    ELEMENT IN EITHER THE ORIGINAL T-MATRIX OR THE NEW
C                    T-MATRIX IS LESS THAN EPS, AN ERROR MESSAGE IS
C                    PRINTED AND PROGRAM EXECUTION IS TERMINATED (CALL
C                    EXIT).
C
      DOUBLE PRECISION TEMP1,TEMP2,T1,DETER,SUM1,T2,ROUAD
C     DOUBLE PRECISION T,RHS
C
      DIMENSION T(NRJ,NCT), RHS(NRJ)
C
C          ------------------------------------------------------
C
      IPRNT1=0
      IPPNT2=0
      KRUG1=IPRNT1
      KRUG2=IPPNT2
      IREAD=0
      ISUM=1
      EPS=.00001
      QUAD=0.0
      IQUAD=1
      DETER=0.0
      IDET=1
C
      IF (KRUG1.NE.0.OR.KBUG2.NE.0) WRITE (6,21)
C
      IF (KRUG2.NE.0) WRITE (6,22)
C
      IF (IREAD.EQ.0) GO TO 2
      READ (5,23) N,NCOF,NCM,ISUM,EPS
      DO 1 I=1,N
      READ (5,24) RHS(I),(T(I,J),J=1,NCOF)
    1 CONTINUE
    2 IF (KRUG2.EQ.0) GO TO 4
      WRITE (6,25) N,NCOF,NCM,ISUM,EPS
      DO 3 I=1,N
    3 WRITE (6,26) I,RHS(I),(T(I,J),J=1,NCOF)
C
```

```
C
C       ...CALCULATE NEW ELEMENTS FOR THE FIRST ROW OF THE UPPER
C       ...REWIND SCRATCH TAPE.
C          READ FIRST ROW OF BOTH MATRIX T AND THE RIGHT-HAND SIDE FROM
C          SCRATCH TAPE.
C
    4   ID=1
        IF (T(1,1).LT.EPS) GO TO 18
C       IF(T(1,1).LT.EPS) WRITE(6,8860) ID
        T1=T(1,1)
        T1=DSQRT(T1)
        IF (KHUG1.NE.0) WRITE (6,27) T1,T(1,1)
        T(1,1)=T1
C
        DO 5 J=2,NCOF
        TEMP1=T(1,J)
        T(1,J)=TEMP1/T1
        IF (KHUG1.NE.0) WRITE (6,28) J,TEMP1,T(1,J)
    5   CONTINUE
        TEMP1=RHS(1)
        RHS(1)=TEMP1/T1
        IF (KHUG1.NE.0) WRITE (6,29) TEMP1,RHS(1)
C
C       ...UPDATE DETERMINANT VALUE.
        DETER=T1
C
C            ------------------------------------------------------
C
C       ...CALCULATE NEW ELEMENTS FOR ROWS 2 TO N IN THE UPPER TRIANGULAR
C          MATRIX T AND THE RIGHT-HAND SIDE.
C
        DO 12 I1=2,N
        ID=I1
        NUM1=I1-1
C       ...CALCULATE THE NEW DIAGONAL ELEMENT FOR ROW I1 IN MATRIX T.
        SUM1=0.
C       ...REWIND THE SCRATCH TAPE
C       ...READ ELEMENTS IN ROW I1 FROM SCRATCH TAPE AND SAVE THEM FOR USE
C          THROUGH STATEMENT NO. 250.
C          REWIND THE SCRATCH TAPE.
        DO 6 I2=1,NUM1
C       ...READ ELEMENTS IN ROW I2 FROM SCRATCH TAPE.
        IF (I1.GT.(I2+NCM1)) GO TO 6
        J1=I1-I2+1
        TEMP1=T(I2,J1)
        SUM1=SUM1+TEMP1*TEMP1
        IF (KHUG1.NE.0) WRITE (6,30) I2,J1,TEMP1,SUM1
    6   CONTINUE
        T1=T(I1,1)
        IF (T(I1,1).LT.EPS) GO TO 18
        IF (T1.LE.SUM1) GO TO 19
C       IF(T1.LE.SUM1) WRITE(6,8870) ID
        T1=DSQRT(T1-SUM1)
        IF (IDET.EQ.0) DETER=DETER*T1
        IF (KHUG1.NE.0) WRITE (6,31) I1,T(I1,1),T1,DETER
        T(I1,1)=T1
C
        IF (T(I1,1).LT.EPS) GO TO 20
C       IF(T(I1,1).LT.EPS) WRITE(6,8880) ID
```

```
C
C       ...CALCULATE THE NEW OFF-DIAGONAL ELEMENTS FOR ROW I1 IN MATRIX T.
C          NOTE THAT THE SUMMATION TERM (PRECEDES STATEMENT NO. 160) WILL
C          BE ZERO FOR SYMMETRIC TRI-DIAGONAL MATRICES.  IN THIS CASE,
C          THE COMPUTATIONAL EFFORT REQUIRED FOR DETERMINING THE NEW OFF-
C          DIAGONAL ELEMENTS CAN BE REDUCED BY SETTING ISUM=0.
C
      IF (I1.EQ.N) GO TO 10
      IF (ISUM.NE.0) GO TO 7
C
      J1=2
      T2=T(I1,J1)
      T(I1,J1)=T2/T1
      IF (KBUG1.NE.0) WRITE (6,32) I1,J1,T1,T2,T(I1,J1)
      GO TO 10
C
    7 J2=I1
      DO 9 J1=2,NCOF
      J2=J2+1
      SUM1=0.
      IF (J2.GT.N) GO TO 10
C     ...REWIND SCRATCH TAPE.
      DO 8 I2=1,NUM1
C     ...READ ELEMENTS OF ROW I2 FROM SCRATCH TAPE.
      IF (J2.GT.(I2+NCM1)) GO TO 8
      J3=I1-I2+1
      J4=I1-I2+J1
      TEMP1=T(I2,J3)
      TEMP2=T(I2,J4)
      SUM1=SUM1+TEMP1*TEMP2
      IF (KBUG1.NE.0) WRITE (6,33) I2,J3,J4,TEMP1,TEMP2,SUM1
    8 CONTINUE
      T2=T(I1,J1)
      T(I1,J1)=(T2-SUM1)/T1
      IF (KBUG1.NE.0) WRITE (6,34) I1,J1,T1,T2,SUM1,T(I1,J1)
    9 CONTINUE
C
C       ...CALCULATE THE NEW ELEMENT IN ROW I1 OF THE RIGHT-HAND SIDE
C          VECTOR RHS.
   10 SUM1=0.
C     ...REWIND SCRATCH TAPE.
      DO 11 I2=1,NUM1
C     ...READ ELEMENTS OF ROW I2 FROM SCRATCH TAPE.
      IF (I1.GT.(I2+NCM1)) GO TO 11
      J1=I1-I2+1
      TEMP1=T(I2,J1)
      TEMP2=RHS(I2)
      SUM1=SUM1+TEMP1*TEMP2
      IF (KBUG1.NE.0) WRITE (6,35) I2,J1,TEMP1,TEMP2,SUM1
   11 CONTINUE
      TEMP1=RHS(I1)
      RHS(I1)=(TEMP1-SUM1)/T1
      IF (KBUG1.NE.0) WRITE (6,36) I1,TEMP1,T1,RHS(I1)
   12 CONTINUE
C
      DETER=DETER*DETER
      DET=DETER
C
```

```
C
C     ...CALCULATE THE VALUE OF THE QUADRATIC FORM FOR MATRIX T.
C     ...REWIND SCRATCH TAPE.
C        READ VECTOR RHS FROM SCRATCH TAPE AND STORE.
C        LEAVE TAPE ON THE N-TH RECORD.
      IF (IQUAD.NE.0) GO TO 14
      RQUAD=0.
      DO 13 I1=1,N
      TEMP1=RHS(I1)
   13 RQUAD=RQUAD+TEMP1*TEMP1
      QUAD=RQUAD
      IF (KBUG1.NE.0) WRITE (6,37) QUAD
C
C          ------------------------------------------------------
C
C     ...BACK SUBSTITUTE INTO MATRIX T AND SOLVE FOR THE UNKNOWN
C        VARIABLES.  STORE THE UNKNOWNS IN VECTOR RHS.
C
C     ...READ ELEMENTS OF ROW N IN MATRIX T FROM SCRATCH TAPE.
C        BACKSPACE SCRATCH TAPE TO BEGINNING OF N-TH RECORD.
   14 CONTINUE
      TEMP1=RHS(N)
      T1=T(N,1)
      RHS(N)=TEMP1/T1
      IF (KBUG1.NE.0) WRITE (6,38) N,TEMP1,T1,RHS(N)
      JP=N+1
      DO 17 I1=2,N
      JP=JP-1
      IRHS=JP-1
      SUM1=0.
C     ...BACKSPACE SCRATCH TAPE 1 RECORD.
C        READ ELEMENTS IN ROW IH OF MATRIX T.
C        BACKSPACE SCRATCH TAPE 1 RECORD.
      DO 15 I2=JP,N
      IF (I2.GT.(IRHS+NCM)) GO TO 16
      J1=I2-IRHS+1
      TEMP1=T(IRHS,J1)
      TEMP2=RHS(I2)
      SUM1=SUM1+TEMP1*TEMP2
      IF (KBUG1.NE.0) WRITE (6,39) IRHS,J1,I2,TEMP1,TEMP2,SUM1
   15 CONTINUE
   16 TEMP1=RHS(IRHS)
      T1=T(IRHS,1)
      RHS(IRHS)=(TEMP1-SUM1)/T1
C     ...SAVE ALL NEW VALUES OF RHS.
      IF (KBUG1.NE.0) WRITE (6,40) IRHS,TEMP1,T1,RHS(IRHS)
   17 CONTINUE
C
      IF (KBUG1.NE.0.OR.KBUG2.NE.0) WRITE (6,41)
      RETURN
C
C
```

```
C
   18 WRITE (6,42) ID
      CALL EXIT
C
   19 WRITE (6,43) ID
      CALL EXIT
C
   20 WRITE (6,44) ID
      CALL EXIT
C
C          ------------------------------------------------------
C
C
   21 FORMAT (1H1/31X,35(1H*)/31X,35HBEGIN OUTPUT FROM SUBROUTINE SOSOLV
     1/31X,35(1H*))
   22 FORMAT (1H0/2X, 17HORIGINAL DATA ARE)
   23 FORMAT (4I5,F10.0)
   24 FORMAT (8F10.0)
   25 FORMAT (1H0/5X, 2HN=,I3, 8H  NCOF=,I3, 7H  NCM=,I3, 8H  ISU
     1M=,I3, 7H  EPS=,E13.5)
   26 FORMAT (1H0/5X, 3HROW,I3/7X,E13.5,(/7X,8E13.5))
   27 FORMAT (1H0//2X, 3HT1=,D13.5, 10H  T(1,1)=,E13.5)
   28 FORMAT (1H0,1X, 2HJ=,I3, 9H  TEMP1=,D13.5, 10H  T(I,J)=,E13.5)
   29 FORMAT (1H0,1X, 6HTEMP1=,D13.5, 8H RHS(1)=,E13.5)
   30 FORMAT (1H0//2X, 3HI2=,I3, 6H  J1=,I3, 9H  TEMP1=,D13.5, 8H
     1  SUM1=,D13.5)
   31 FORMAT (1H0,1X, 3HI1=,I3, 11H  T(I1,1)=,E13.5, 6H  T1=,D13.5,
     1 9H  DETER=,D13.5)
   32 FORMAT (1H0/2X, 3HI1=,I3, 6H  J1=,I3, 6H  T1=,D13.5, 6H  T2
     1=,D13.5, 12H  T(I1,J1)=,D13.5)
   33 FORMAT (1H0//2X, 3HI2=,I3, 6H  J3=,I3, 6H  J4=,I3/2X, 6HTEMP
     11=,D13.5, 9H  TEMP2=,D13.5, 7H  SUM1=,D13.5)
   34 FORMAT (1H0,1X, 3HI1=,I3, 5H  J1=,I3, 6H  T1=,D13.5, 6H  T2=
     1,D13.5/2X, 5HSUM1=,D13.5, 12H  T(I1,J1)=,E13.5)
   35 FORMAT (1H0//2X, 3HI2=,I3, 6H  J1=,I3, 9H  TEMP1=,D13.5, 9H
     1  TEMP2=,D13.5, 8H  SUM1=,D13.5)
   36 FORMAT (1H0,1X, 3HI1=,I3, 8H  TEMP1=,D13.5, 6H  T1=,D13.5, 9H
     1 RHS(I1)=,E13.5)
   37 FORMAT (1H0//2X, 5HQUAD=,E13.5)
   38 FORMAT (1H0/2X, 2HN=,I3, 9H  TEMP1=,D13.5, 6H  T1=,D13.5, 10H
     1  RHS(N)=,E13.5)
   39 FORMAT (1H0//2X, 5HIRHS=,I3, 6H  J1=,I3, 6H  I2=,I3/2X, 6HTE
     1MP1=,D13.5, 9H  TEMP2=,D13.5, 8H  SUM1=,D13.5)
   40 FORMAT (1H0,1X, 5HIRHS=,I3, 9H  TEMP1=,D13.5, 6H  T1=,D13.5,
     1134  RHS(IRHS)=,E13.5)
   41 FORMAT (1H0/31X,36(1H*)/31X,36HEND OF OUTPUT FROM SUBROUTINE SOSOL
     1V/31X,36(1H*))
   42 FORMAT (1H0,39(1H*)/2X,37HERROR DETECTED IN SUBROUTINE SOSOLV--//2
     1X,27HTHE DIAGONAL ELEMENT IN ROW,I4,33H OF THE ORIGINAL T-MATRIX I
     2S .LT. EPS./2X,9HCALL EXIT/1X,39(1H*))
   43 FORMAT (1H0,51(1H*)/2X,37HERROR DETECTED IN SUBROUTINE SOSOLV--//2
     1X,54HT1 IS .LE. SUM1 FOR CALCULATING THE DIAGONAL ELEMENT IN ROW,I
     24/2X,9HCALL EXIT/1X,51(1H*))
   44 FORMAT (1H0,39(1H*)/2X,37HERROR DETECTED IN SUBROUTINE SOSOLV--//2
     1X,27HTHE DIAGONAL ELEMENT IN ROW,I4,33H OF THE NEW T-MATRIX IS .LT
     2. EPS./2X,9HCALL EXIT/1X,39(1H*))
      END
```

APPENDIX B - DATA FOR MUSKAT'S ANALYSIS

TABLE B-1. POTENTIAL DISTRIBUTION FOR CASE 1 USING MUSKAT'S FORMULA

$\bar{z}/H_e$	$-\phi(0,\bar{z})$ *	$\Delta\phi(0,\bar{z})/(\Delta\phi)_e$
0.743	6.426	0.0
0.76	5.619	0.126
0.80	4.590	0.286
0.84	4.151	0.354
0.88	3.889	0.395
0.92	3.715	0.422
0.96	3.594	0.441
1.00	3.510	0.454

*In tables B-1 through B-6, $\phi_e = 0.0$ (reference).

TABLE B-2. POTENTIAL DISTRIBUTION FOR CASE 2 USING MUSKAT'S FORMULA

$\bar{z}/H_e$	$-\phi(0,\bar{z})$	$\Delta\phi(0,\bar{z})/(\Delta\phi)_e$
0.635	5.922	0.0
0.64	5.128	0.134
0.68	4.089	0.309
0.72	3.639	0.386
0.76	3.364	0.432
0.80	3.177	0.464
0.84	3.042	0.486
0.88	2.943	0.503
0.92	2.870	0.516
0.96	2.816	0.524
1.00	2.779	0.531

TABLE B-3. POTENTIAL DISTRIBUTION FOR CASE 3 USING MUSKAT'S FORMULA

$\bar{z}/H'_e$	$-\phi(0,\bar{z})$	$\Delta\phi(0,z)/(\Delta\phi)_e$
0.568	5.628	0.0
0.60	4.211	0.252
0.64	3.574	0.365
0.68	3.225	0.427
0.72	2.996	0.468
0.76	2.832	0.497
0.80	2.710	0.519
0.84	2.618	0.535
0.88	2.548	0.547
0.92	2.495	0.557
0.96	2.457	0.563
1.00	2.388	0.576

TABLE B-4. POTENTIAL DISTRIBUTION FOR CASE 4 USING MUSKAT'S FORMULA

$\bar{z}/H_e$	$-\phi(0,\bar{z})$	$\Delta\phi(0,z)/(\Delta\phi)_e$
0.45	4.999	0.0
0.48	3.744	0.251
0.52	3.106	0.379
0.56	2.756	0.449
0.60	2.523	0.495
0.64	2.354	0.529
0.68	2.227	0.555
0.72	2.128	0.574
0.76	2.049	0.590
0.80	1.988	0.602
0.84	1.939	0.612
0.88	1.901	0.620
0.92	1.873	0.625
0.96	1.853	0.629
1.00	1.840	0.632

TABLE B-5. POTENTIAL DISTRIBUTION FOR CASE 5 USING MUSKAT'S FORMULA

$\bar{z}/H_e$	$-\phi(0,\bar{z})$	$\Delta\phi(0,z)/(\Delta\phi)_e$
0.56	4.865	0.0
0.60	3.764	0.223
0.64	3.300	0.319
0.68	3.017	0.378
0.72	2.821	0.418
0.76	2.677	0.448
0.80	2.568	0.470
0.84	2.485	0.487
0.88	2.421	0.500
0.92	2.373	0.510
0.96	2.338	0.518
1.00	2.314	0.523

TABLE B-6. POTENTIAL DISTRIBUTION FOR CASE 6 USING MUSKAT'S FORMULA

$\bar{z}/H_e$	$-\phi(0,\bar{z})$	$\Delta\phi(0,\bar{z})/(\Delta\phi)_e$
0.68	6.225	0.0
0.72	4.510	0.276
0.76	3.957	0.364
0.80	3.644	0.415
0.84	3.437	0.448
0.88	3.292	0.471
0.92	3.188	0.488
0.96	3.112	0.500
1.00	3.059	0.509

APPENDIX C - RESULTS OF NUMERICAL ANALYSIS

TABLE C-1. RESULTS OF NUMERICAL ANALYSIS - CASE 5: (I)

$\alpha = 0.541$ $\gamma = 0.0933$ $\rho_f = 0.755$ gm cm^{-3}

$H_e = 25.5$ cm $H_w = 21.5$ cm $\Delta\rho = 0.245$ gm cm^{-3}

$\bar{z}/H_e$	$\Delta H/(\Delta H)_e$		
	IT = 1	IT = 2	IT = MAXIT
0.541	0.000	0.000	0.000
0.549	0.199	0.175	0.171
0.588	0.297	0.259	0.252
0.627	0.358	0.307	0.297
0.667	0.400	0.337	0.322
0.706	0.430	0.355	0.333
0.745	0.453	0.363	
0.784	0.470		
0.824	0.483		
0.863	0.493		
0.902	0.500		
0.941	0.505		
0.980	0.507		

TABLE C-2. RESULTS OF NUMERICAL ANALYSIS - CASE 5: (II)

$\alpha = 0.541$ $\quad \gamma = 0.0933$ $\quad \rho_f = 0.755$ gm cm^{-3}

$H_e = 25.5$ cm $\quad H_w = 21.0$ cm $\quad \Delta\rho = 0.245$ gm cm^{-3}

$\bar{z}/H_e$	$\Delta H/(\Delta H)_e$		
	IT = 1	IT = 2	IT = MAXIT
0.541	0.000	0.000	0.000
0.549	0.205	0.176	0.152
0.588	0.306	0.260	0.239
0.627	0.368	0.306	0.269
0.667	0.410	0.332	
0.706	0.441	0.345	
0.745	0.464		
0.784	0.482		
0.824	0.495		
0.863	0.505		
0.902	0.512		
0.941	0.517		
0.980	0.519		

TABLE C-3. RESULTS OF NUMERICAL ANALYSIS - CASE 5: (III)

$\alpha = 0.541$ $\gamma = 0.9033$ $\rho_f = 0.755$ gm cm^{-3}

$H_e = 25.5$ cm $H_w = 20.85$ cm $\Delta\rho = 0.245$ gm cm^{-3}

$\bar{z}/H_e$	$\Delta H/(\Delta H)_e$		
	IT = 1	IT = 2	IT = MAXIT
0.541	0.000	0.000	0.000
0.549	0.205	0.173	0.157
0.588	0.306	0.254	0.218
0.627	0.368	0.299	
0.667	0.410	0.321	
0.706	0.441		
0.745	0.464		
0.784	0.482		
0.824	0.495		
0.863	0.505		
0.902	0.512		
0.941	0.517		
0.980	0.519		

TABLE C-4. FREE SURFACE AND INTERFACE LOCATION FOR CASE 5 UNDER CRITICAL CONDITIONS (NUMERICAL ANALYSIS)

Distance from Well-Axis cm	Depth of Free Surface cm	Interface Depth cm
2.38	4.50	15.36
3.00	3.98	15.53
3.78	3.34	16.23
4.77	3.17	16.52
6.01	3.00	16.99
7.58	2.82	17.88
9.54	2.37	18.25
12.04	2.16	18.86
15.17	2.00	19.85
19.13	1.99	20.29
24.11	1.45	21.03
30.39	1.26	21.68
38.31	1.07	22.21
48.29	1.00	22.83
60.87	0.99	23.36
76.73	0.98	23.94
96.72	0.33	24.47
121.92	0.17	24.98

TABLE C-5. RESULTS OF NUMERICAL ANALYSIS - CASE 6: (I)

$\alpha = 0.660$ $\gamma = 0.0915$ $\rho_f = 0.755$ gm cm^{-3}

$H_e = 26.0$ cm $H_w = 23.0$ cm $\Delta\rho = 0.245$ gm cm^{-3}

$\bar{z}/H_e$	$\Delta H/(\Delta H)_e$		
	IT = 1	IT = 2	IT = MAXIT
0.660	0.000	0.000	0.000
0.673	0.174	0.145	0.134
0.712	0.260	0.210	0.187
0.750	0.312	0.241	
0.788	0.347		
0.827	0.372		
0.865	0.389		
0.904	0.401		
0.942	0.409		
0.981	0.412		

TABLE C-6. RESULTS OF NUMERICAL ANALYSIS - CASE 6: (II)

$\alpha = 0.660$ $\gamma = 0.0915$ $\rho_f = 0.755$ gm cm^{-3}

$H_e = 26.0$ cm $H_w = 22.85$ cm $\Delta\rho = 0.245$ gm cm^{-3}

$\bar{z}/H_e$	$\Delta H/(\Delta H)_e$		
	IT = 1	IT = 2	IT = MAXIT
0.660	0.000	0.000	0.000
0.673	0.174	0.139	0.120
0.712	0.260	0.197	0.172
0.750	0.312	0.221	
0.788	0.347		
0.827	0.372		
0.865	0.389		
0.904	0.401		
0.942	0.409		
0.981	0.412		

TABLE C-7. RESULTS OF NUMERICAL ANALYSIS - CASE 6: (III)

$\alpha = 0.660$ $\quad \gamma = 0.0915$ $\quad \rho_f = 0.755$ gm cm^{-3}

$H_e = 26.0$ cm $\quad H_w = 22.80$ cm $\quad \Delta\rho = 0.245$ gm cm^{-3}

$\bar{z}/H_e$	$\Delta H/(\Delta H)_e$		
	IT = 1	IT = 2	IT = MAXIT
0.660	0.000	0.000	0.000
0.673	0.174	0.138	0.121
0.712	0.260	0.197	0.163
0.750	0.312	0.221	
0.788	0.347		
0.827	0.372		
0.865	0.389		
0.904	0.401		
0.942	0.409		
0.981	0.412		

TABLE C-8. FREE SURFACE AND INTERFACE LOCATION FOR CASE 6 UNDER CRITICAL CONDITIONS (NUMERICAL ANALYSIS)

Distance from Well-Axis cm	Depth of Free Surface cm	Interface Depth cm
2.38	3.15	17.93
3.00	2.73	18.10
3.78	2.60	18.44
4.77	2.50	19.16
6.01	2.49	19.47
7.58	2.25	19.66
9.54	1.83	20.39
12.04	1.68	21.08
15.17	1.51	21.46
19.13	1.49	21.87
24.11	1.49	22.47
30.39	1.48	22.90
38.31	0.84	23.42
48.29	0.70	23.85
60.87	0.55	24.31
76.73	0.50	24.73
96.72	0.45	25.17
121.92	0.20	25.58

TABLE C-9. RESULTS OF NUMERICAL ANALYSIS OF SET 1

$\gamma = 0.00865$ $\quad\quad$ $\dot{r} = 2.890 \times 10^{3}$

$\dot{L} = 2.500$ $\quad\quad$ $K = 53.42$ ft/day

α	$\Delta\rho$ ($gm\,cm^{-3}$)	$\hat{D}$ (ft)	$\frac{\rho_f \hat{D}}{\Delta\rho H_e}$	Q (cfd)	Q (cfs)	$\frac{Q}{H_e K \hat{D}}$	$\frac{Q}{H_e^2 K \Delta\rho}$	$\dot{\bar{z}}$
0.250	0.012	13.10	3.495	5.343×10^{4}	0.618	0.2450	0.8562	0.395
0.350	0.012	8.00	2.140	4.590×10^{4}	0.531	0.3443	0.7356	0.462
0.500	0.025	10.40	1.333	7.874×10^{4}	0.911	0.4543	0.6057	0.590
0.600	0.030	8.80	0.940	7.568×10^{4}	0.876	0.5160	0.4851	0.665

TABLE C-10. RESULTS OF NUMERICAL ANALYSIS OF SET 2

$\gamma = 0.00217$ $\quad\quad$ $\dot{r} = 2.890 \times 10^{3}$

$\dot{L} = 6.2893$ $\quad\quad$ $K = 53.42$ ft/day

α	$\Delta\rho$ ($gm\,cm^{-3}$)	$\hat{D}$ (ft)	$\frac{\rho_f \hat{D}}{\Delta\rho H_e}$	Q (cfd)	Q (cfs)	$\frac{Q}{H_e K \hat{D}}$	$\frac{Q}{H_e^2 K \Delta\rho}$	$\dot{\bar{z}}$
0.150	0.020	28.00	4.425	8.309×10^{4}	0.962	0.1725	0.7250	0.348
0.352	0.025	12.88	1.600	8.309×10^{4}	0.962	0.3750	0.6000	0.450
0.450	0.025	9.66	1.200	7.560×10^{4}	0.875	0.4550	0.5460	0.510
0.550	0.025	6.40	0.795	5.885×10^{4}	0.681	0.5346	0.4250	0.620
0.650	0.025	4.60	0.571	4.613×10^{4}	0.534	0.5831	0.3332	0.695

TABLE C-11. RESULTS OF NUMERICAL ANALYSIS OF SET 3.

$\gamma = 0.0150$ $\quad \dot{r} = 6.583 \times 10^{2}$

$\dot{L} = 9.8736$ $\quad K = 53.42$ ft/day

α	$\Delta\rho$ (gm cm^{-3})	$\hat{D}$ (ft)	$\frac{\rho_f \hat{D}}{\Delta\rho H_e}$	Q (cfd)	Q (cfs)	$\frac{Q}{H_e K \hat{D}}$	$\frac{Q}{H_e^2 K \Delta\rho}$	$\dot{\bar{z}}$
0.100	0.020	11.90	2.975	2.707×10^{4}	0.313	0.2147	0.6334	0.323
0.150	0.021	9.60	2.286	2.820×10^{4}	0.326	0.2749	0.6284	0.328
0.250	0.025	7.55	1.510	3.238×10^{4}	0.375	0.4014	0.6061	0.370
0.500	0.075	11.00	0.733	7.110×10^{4}	0.823	0.6050	0.6050	0.560
0.650	0.075	5.76	0.384	4.441×10^{4}	0.514	0.7217	0.2771	0.700

TABLE C-12. RESULTS OF NUMERICAL ANALYSIS OF SET 4

$\gamma = 0.050$ $\quad \dot{r} = 2.315 \times 10^{2}$

$\dot{L} = 11.574$ $\quad K = 133.69$ ft/day

α	$\Delta\rho$ (gm cm^{-3})	$\hat{D}$ (ft)	$\frac{\rho_f \hat{D}}{\Delta\rho H_e}$	Q (cfd)	Q (cfs)	$\frac{Q}{H_e K \hat{D}}$	$\frac{Q}{H_e^2 K \Delta\rho}$	$\dot{\bar{z}}$
0.100	0.027	4.72	1.802	2.049×10^{4}	0.237	0.3347	0.5949	0.310
0.150	0.050	6.49	1.338	3.597×10^{4}	0.416	0.4274	0.5720	0.320
0.250	0.059	5.09	1.050	3.482×10^{4}	0.403	0.5275	0.5536	0.360
0.350	0.050	4.18	0.862	3.246×10^{4}	0.376	0.5988	0.5160	0.420
0.400	0.050	3.51	0.725	3.033×10^{4}	0.351	0.6627	0.4822	0.465
0.650	0.109	3.45	0.326	3.702×10^{4}	0.428	0.8275	0.2700	0.690

APPENDIX D - EXPERIMENTAL DATA FOR LOCATION OF FREE SURFACE AND INTERFACE

TABLE D-1. FREE SURFACE AND INTERFACE LOCATION FOR CASE 5 UNDER CRITICAL CONDITIONS (EXPERIMENTAL DATA)

Distance from Well-Axis cm	Depth of Free Surface cm	Depth of Interface cm
0.0	4.60	16.10
2.5	4.60	16.20
3.5	3.75	--
5.0	3.00	16.75
7.0	2.55	17.60
9.0	2.40	18.00
15.0	2.00	20.10
20.0	1.75	20.40
25.0	1.50	21.20
30.0	--	22.15
40.0	1.10	22.50
60.0	0.80	23.30
80.0	0.50	24.10
100.0	0.25	24.60
119.0	0.15	25.40

TABLE D-2. FREE SURFACE AND INTERFACE LOCATION FOR CASE 6 UNDER CRITICAL CONDITIONS (EXPERIMENTAL DATA)

Distance from Well-Axis cm	Depth of Free Surface cm	Depth of Interface cm
0.0	3.20	18.50
2.5	3.20	18.50
3.5	2.70	18.80
5.0	2.50	--
7.0	2.20	19.70
9.0	1.80	20.30
15.0	1.50	21.50
20.0	1.40	22.10
25.0	1.35	22.60
30.0	1.30	22.90
40.0	1.00	23.50
60.0	0.65	24.30
80.0	0.50	24.80
100.0	0.35	25.30
119.0	0.20	25.80

APPENDIX E - PHYSICAL PROPERTIES OF SOLTROL "C"

TABLE E-1. PHYSICAL PROPERTIES OF SOLTROL "C"

Temperature °C	Density gram/cc	Viscosity Poise
20.0	0.5782	0.10589
21.0	0.7576	0.01555
22.0	0.7569	0.01524
23.0	0.7562	0.01494
24.0	0.7556	0.01468
25.0	0.7549	0.01440
26.0	0.7542	0.01414
27.0	0.7536	0.01388
28.0	0.7529	0.01362
29.0	0.7522	0.01337
30.0	0.7515	0.01315